Multifunctional Drug Carriers with Programmable Properties

by

Sahar Rahmani

A dissertation submitted in partial fulfillment
of the requirements for the degree of
Doctor of Philosophy
(Biomedical Engineering)
in the University of Michigan
2015

Doctoral Committee:

Professor Joerg Lahann, Chair
Assistant Professor Lola Eniola-Adefeso
Assistant Professor Sunitha Nagrath
Professor Lonnie D. Shea

To Aziz, My Grandmother

ACKNOWLEDGEMENTS

The work in this dissertation would not have been possible without the help, support, and dedication of a number of people. To begin, I would like to thank my PhD advisor, Professor Joerg Lahann, for all of his help and support during the past several years. He has taught me everything I know about being a scientist and conducting research successfully, and I owe any scientific achievement I have to him. In addition to this, he has taught me how to work with others and bring them together to form a team, and to always keep the bigger picture in mind, regardless of specific aspects that may not have worked. In short, I could have never asked, or hoped, for a better advisor. I would also like to thank my committee members, Professor Eniola, Professor Nagrath, and Professor Shea for all of their help during my PhD. Whether it's been through a class I've taken with them, a joint collaboration we've had, or questions they've thought important for me to address, they have shaped my dissertation immensely and I would like to thank them for it. I would also like to thank our collaborators, especially Professor Muzykantov, Professor Altschuler, Professor Nagrath, and Professor Mitragotri's groups. I have learned a great deal from each of their collaborations and I would like to thank them for the opportunity and their help along the way.

I would especially like to thank each and every one of my labmates for their tremendous help, and more importantly their friendships, during these past few years. I would like to specifically thank Dr. Jaewon Yoon for being first my mentor, then my best friend, and for teaching me everything I know about jetting. I would also like to particularly thank Dr. Asish Misra, who started his PhD with me and has been there during the entire journey, as well as Stacy Ramcharan, Kenneth Cheng, Jake Jordahl, Ramya Kumar, Hyesun Jun, Dr. Aftin Ross, and Gokcen Ukuser, for always being there when I've needed them. When I first joined our lab, I knew very little about chemistry, material science, or medicine and I have always been able to rely on our post doctoral researchers Drs. Sampa Saha, Tae-Hong Park, Kyung-Jin Lee, Hakan Durmaz, Luis Solorio, Brad Plummer, Xiaopei Deng, and Kathleen McEnnis for their generous help and mentorship. I would also like to thank the undergraduate and high school students I have had the opportunity to work with during these past few years: Alessandro Donini, Natalie Nagpal, Frederick Kuo, Vincent Lai, Krishna Mahajan, Charnelle Michel, Acacia Dishman, Chris Yu, Patrick Lown, Marika Grabowski, Luke Roggenkamp, and Melissa Cadena. They are a great team of brilliant students and I can only say that my work would not have been possible without their hard work and dedication. I would also like to thank our group in Karlsruhe Institute of Technology, especially Dr. Ekaterina Sokoloviskaya and Artak Shahnas, for their help in synthetic chemistry. Finally, I would like to thank the staff members in the Biomedical Engineering Department, Chemical Engineering Department, and the Biointerfaces Institute for all of their tremendous help these past few years. I would like to especially thank Mrs. Julie Gales and Mrs. Lisa Moran; there

have been times that I have bothered them on a daily basis and they have always been there to help.

On a more personal note, I would like to thank God for everything he has given me during my life and for guiding me along the way. I would also like to thank my family for their support and their unending love. First, I would like to thank my parents, Reza and Ellen Rahmani for everything they do for us and their many sacrifices for our family. They have always told us that we can do whatever we set our minds to, even when we haven't believed it ourselves, and they have always expected nothing less than the very best from us. In the end, they have shaped who we are as people, and for this, I can never thank them enough. I would also like to thank my husband, Amirmasoud Hedayati, for all of his support during the past few years. We got married during my first year in graduate school and he has always been there for me for all of it. I would not have been able to succeed if it had not been for his encouragement and dedication. Additionally, I would like to thank my siblings and their families: my brothers Justin Mohammad, Hameid, Amir, and Mehdi; and my sisters, Zainab and, especially, Samantha for always being there when I've needed them. Whether it's been reading my papers, looking at my figures to see if they made sense, or just listening, they have been there. I know I can always rely on them for anything, and I would not change that for the world. Lastly, I would like to thank my grandmother, Aziz, to whom this thesis is dedicated to, and my Aunts Zahra and Mitra, for their unending support and for never having a doubt in their minds that I would succeed.

TABLE OF CONTENTS

LIST OF FIGURES

LIST OF APPENDICES

ABSTRACT

In recent decades, drug-loaded carrier systems have become a viable option to replace or augment current, unsuccessful therapies that address a myriad of disease conditions. In this area, a successful therapy needs to address the following parameters: specificity, long circulation, biocompatibility/biodegradability, desired pharmacokinetics of single & multiple therapeutics, carrier-cell interactions, and potential imaging capabilities. While various formulations have tackled some of these characteristics, a concrete methodology to design multifunctional particles addressing all parameters is currently lacking.

Herein, the method of electrohydrodynamic (EHD) co-jetting and downstream processing are used to design multifunctional particles with tunable characteristics that could be used to address all desired parameters. Specifically, each of the chapters address (i) the development of carriers with selective and orthogonal surface modifications using functional polymers incorporated into individual compartments for the addition of stealth, targeting, or therapeutic capabilities; (ii) the development of carriers with programmable physical properties such as shape, size, porosity, roughness, and charge that can determine the fate of a particle in the body, and the testing of nanoparticles in animal models to determine their biodistribution; (iii) the development of particles with complex degradation and release kinetics of therapeutics using rapidly degrading or stimuli-responsive (pH, light, & oxidative stress) polymers; (iv) the design of multifunctional particles loaded with multiple therapeutics for cochlear delivery and their testing to determine the therapeutics' release kinetics, the particles' persistence & biodistribution in the cochlea, and the general biocompatibility of the system. Accordingly, this dissertation suggests the potential establishment of a toolbox that can be used for the design of particles with programmable properties for individual applications in the effective delivery of therapeutics.

CHAPTER 1

Introduction

The material in this chapter has been adapted with minor modifications from the following articles:

(1) S. Rahmani, J. Lahann, "Recent Progress with Multicompartmental Nanoparticles", *MRS Bull.*, **2014**, 39 (03), 251-257.

(2) S. Rahmani, T.-H. Park, A. F. Dishman, J. Lahann, "Multimodal Delivery of Irinotecan from Microparticles with Two Distinct Compartments", *J. Control. Release,* **2013**, 172, 239-245.

1.1 Goals & Challenges of Drug Delivery

The advent of new technologies and the discovery of numerous life-saving therapeutics in the last several decades have drastically changed the field of medicine and have greatly increased the life expectancy and living conditions of patients suffering from a myriad of health related issues.[1-3] While the medical and pharmaceutical fields have come a long way in diagnosing disease states and in finding therapeutics that can address them, the delivery of such therapeutics to the correct sites in the body and with the desired pharmacokinetics is not yet optimal.[4, 5] This has posed significant hurdles in the

treatment of patients, especially when the therapeutics are potent and any delivery to undesired sites in the body can lead to severe toxicities and low therapeutics indices.[2, 6]

Among the main challenges faced by current therapy methods, including the most common routes of oral consumption and injection of therapeutics, are their i) non-targeted nature; ii) short circulation times; iii) requirement for repeated intake/injections to achieve appropriate pharmacokinetics; iv) their tendency towards cellular resistance; and v) observed severe toxicities which together lead to patient compliance issues and overall lower treatment outcomes.[1] This is especially true in the case of cancer therapeutics (potent drugs designed for the destruction of cancerous tissue), where the side effects can be debilitating.[7-10] On the other hand, biological therapeutics, such as growth factors and nucleic acids, have very short lifetimes within the body, and it is a challenge to achieve therapeutic efficacy with these molecules, especially since some have severe side-effects at higher doses.[11-13]

The use of drug delivery carriers can provide an alternative for the administration of therapeutics since particles have the potential to initially protect the encapsulated therapeutic, circulate in the blood stream, specifically deliver the therapeutic to the targeted site in the body, and release the drug in a manner that can ideally be adjusted to the pharmacokinetics of the selected therapeutic (**Figure 1-1**).[14] In addition, such carriers can be biocompatible and/or biodegradable and intrinsically harmless to the body. These carriers can also contain contrast-imaging agents that can enable the tracking of such particles using various imaging systems (MRI, PET, CT, etc.), or, alternatively, be used for diagnostic applications.[15, 16] Most contrast-imaging agents are potentially toxic and

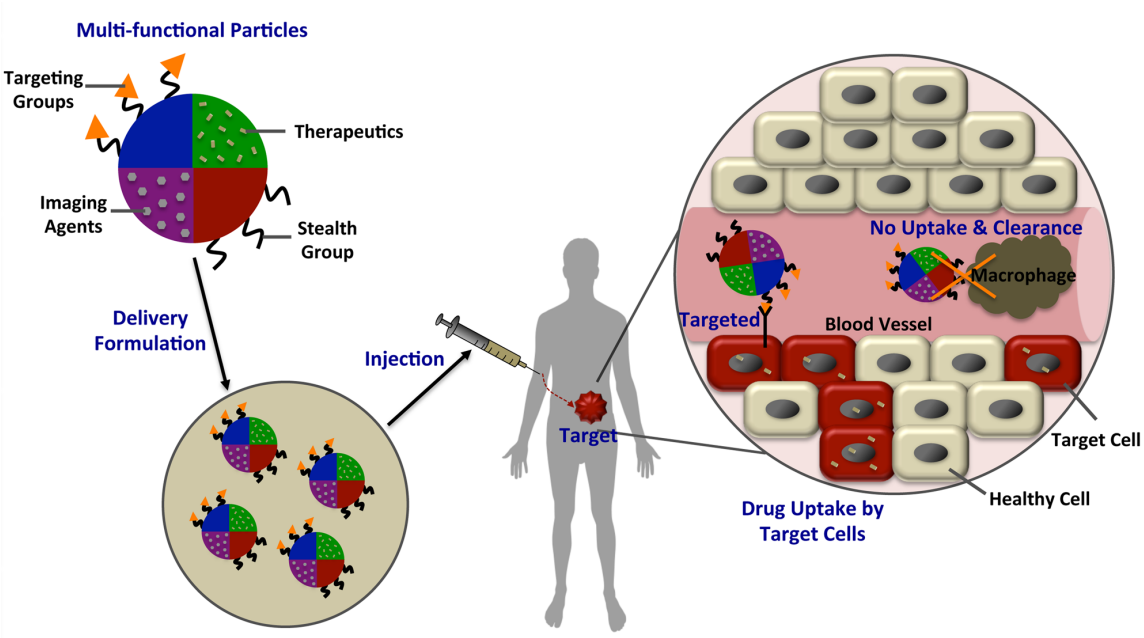

Figure 1-1: The capabilities of a multifunctional carrier. Multifunctional particles should be able to encapsulate and protect therapeutics; circulate in the blood stream and avoid uptake and clearance; specifically deliver and release the therapeutic to the targeted site in the body; and provide imaging capabilities for potential tracking of the nanoparticles and for diagnostic applications.

are typically not targeted, and their incorporation into nanoparticles can result in the reduction of their toxic side effects and improve on their targeting capabilities.

First formulations of drug delivery carriers have been evaluated in clinical trials and some have already been turned into pharmaceutical products.[17, 18] While these early formulations have demonstrated the clinical potential of prolonged release formulations, these carriers are still far from optimal and lack important aspects, such as active targeting, prolonged circulation, and tailored release kinetics.[19]

1.2 Multifunctional Nanoparticle Formulations

Nano- and micro-particles have demonstrated exceptional potential in a variety of areas, such as diagnostics and therapeutics.[20] Recent improvements in particle fabrication methods, such as the expansion of compositional flexibility and physical as well as

chemical tunability, have resulted in increased functional versatility of colloidal particles. In particular, precise engineering of shape, size, surface structures, and mechanical properties has been accomplished by several processes.[21-23] Beyond the current state of the art, the complementary control of internal (bulk) and external (surface) features has emerged as an important design parameter for multifunctional particles, where the bulk and surface of each particle is no longer isotropic in its functionality and characteristic. These anisotropic particles may feature two or more distinct compartments, controlled interfacial patterns, or compositionally distinct materials domains in a single particulate entity.[24-34] Novel self-assembled particles, such as the multifunctional particles, may find diverse applications in multiplexed bioassays,[35] vehicles for multiple therapeutic modalities,[36] biohybrid materials,[37] or microactuators.[38, 39]

Compositional bulk anisotropy may enable unique particle properties. Here, a particle configuration that features materials compartmentalized within a monolithic particle can impart entirely new properties and may be a decisive functional parameter, being similarly as important as the actual chemical makeup.[23] On the other hand, anisotropic surface functionalization can be realized in the form of patchy particles, where different surface patches are associated with different chemically or functionally orthogonal surface properties. Particles with this type of surface anisotropy can exhibit bipolar characteristics, such as particles that are simultaneously hydrophilic and hydrophobic, or can be used for self-assembly and drug delivery.[40-42] Independent control of the composition of individual compartments of the same particle allows for inclusion of materials with highly dissimilar sets of properties. This approach forms the foundation for the controlled release of multiple drugs with independent release kinetics (provided

that each drug is loaded in a separate compartment) or a combination of fully decoupled modalities for combined imaging and therapy (theranostics).[43] Current carrier systems that are loaded with multiple therapeutics in a single isotropic particle lack this characteristic and may even promote antagonistic cross-interactions between drugs.[19, 44-46]

Compartmentalized particles can be fabricated by a range of different methods. In particular, the self-assembly of block copolymers[47, 48] or the use of intended phase separation during seeded polymerizations (where two non-miscible solvents are used to create an emulsion, at the interface of which two different polymer brushes are grown on the same nucleation seed), are widely pursued approaches toward anisotropic nanoparticles.[49, 50] More recently, lithographic and template-assisted methods have attracted wider attention for their great flexibility in constructing non-spherical Janus particles, such as disks, rods, cubes, etc.[51-53] Recently, droplet-based strategies have found use for the preparation of multifunctional particles. In some instances, microfluidic techniques were combined with photolithographic methods to prepare particles with uniform size and shape. In some examples, this approach resulted in particles with impressive complexity of inner and outer geometries.[54-56] However, a narrow choice of materials is available for these rather specialized approached, and relatively large particle sizes are prepared. Further progress is needed to ensure diversification of materials choices and to augment the establishment of widely applicable processing methods.

1.3 Electrohydrodynamic Co-Jetting

Arguably, one of the most versatile approaches toward anisotropic particles, cylinders, fibers, and fiber scaffolds is based on electrohydrodynamic (EHD) co-jetting; a technology pioneered in the Lahann Lab at the University of Michigan.[23] This technology has been used for the fabrication of organic and inorganic nanoparticles.[57, 58] This research has been inspired by work done by Loscertales, *et al*., where coaxial, electrified liquid jets were used to fabricate nano- and micro-droplets with a core-shell structure, and built upon pioneering work done by Gupta, *et al.*, where side-by-side electrospinning was used to create multifunctional, but not multicompartmental, nanofibrous meshes.[59-63]

Electrospraying and electrospining processes have been applied to polymer solutions to establish straightforward methods for the preparation of nano-/microparticles using high electrical voltages as driving forces for the transport of polymer solutions. Importantly, the precise control of critical polymer solution properties such as material selection, concentration, viscosity, and conductivity can result in a diverse range of sizes and shapes in the nanometer and micron range.[64] Building on these well-established methods, EHD co-jetting now involves the use of two or more flows that are run through parallel capillary nee[61]dles in a side-by-side configuration. Thus, there is no convective mixing, and a very stable interface can be established between the two jetting solutions. Application of an electric field to the compound droplet, which forms at the outlet of the two capillary needles, results in distortion of the droplet into a stable cone and subsequent formation of an electrified polymer jet. The rapid acceleration of the viscoelastic jet with velocities on the order of 250 m/s, comparable to a rocket launch, can lead to a reduction

in jet diameter by several orders of magnitude and a simultaneous increase in surface area. This induces instantaneous evaporation of the solvents and results in solidification of the non-volatile components. Because solidification is extremely fast, surface energy driven reorientation of the polymers into a thermodynamically more stable core–shell configuration is restricted, and the initial flow-determined configuration can be maintained. Thus EHD co-jetting uses relatively simple manipulation of liquid geometries followed by rapid solidification to provide access to solid nano- and microfibers with architectures that would be otherwise impossible, or at least extremely difficult, to achieve. As a result, the particles are trapped in the initial, flow-determined compartmentalized geometry, rather than taking on the energetically most favorable constellation, which is in almost all cases a core–shell particle. Not surprisingly, however, the preparation of bicompartmental polymer particles via EHD co-jetting requires delicate control of several competing factors.

Initial work with EHD co-jetting has been focused on water-soluble polymers because water-based jetting systems typically exhibit lower toxicity, which is a critical factor for biomedical applications.[59] The preparation of bicompartmental particles using the EHD co-jetting approach was first demonstrated with aqueous solutions of polyacrylic acid (PAA) or poly(ethylene glycol) (PEG).[65] The relatively high free surface energy of water results in the formation of a nearly spherical droplet, where the biphasic flow interface is maintained, and a stable cone is formed (**Figure 1-2**). The compartmentalization is due to the particular manipulation of the liquid phases. However, the use of water-soluble polymers for the fabrication of particles also requires post-fabrication modification to ensure stability under physiological conditions. In the case of

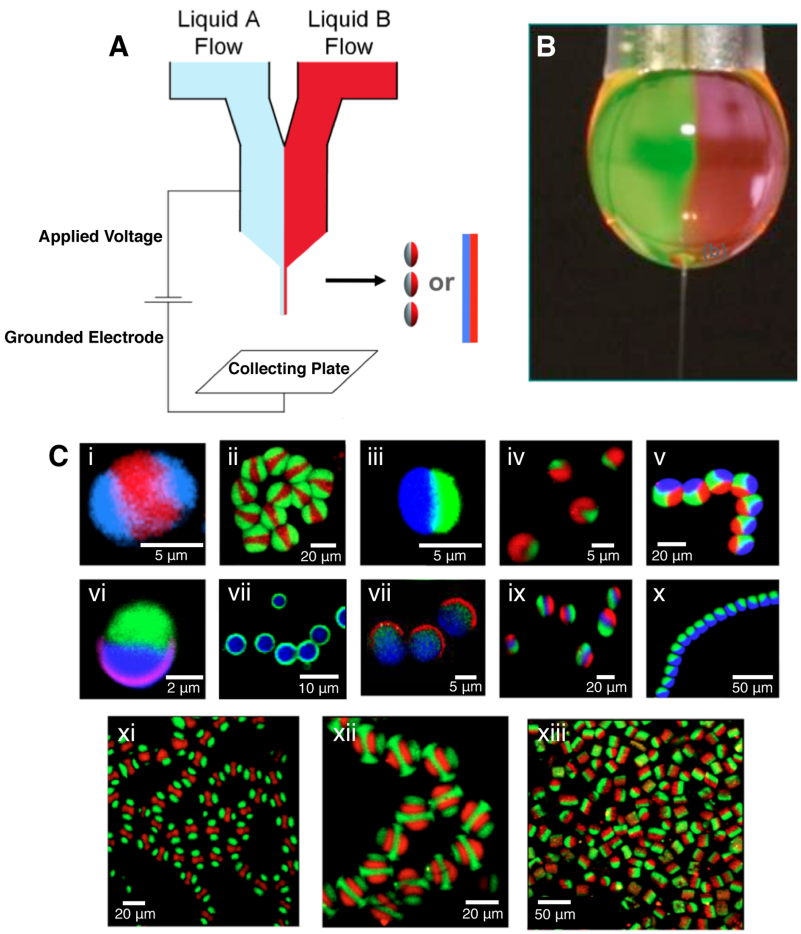

Figure 1-2: (A) Schematic description of the electrohydrodynamic (EHD) co-jetting process, which can lead to either particles (electrospraying) or fibers (electrospinning). (B) A photograph of a typical Taylor cone and jet ejection during EHD co-jetting. The interface between the two aligned polymer solutions is clearly observed. (C) Examples of particles and fibers obtained from the EHD co-jetting. Particles were composed of poly(lactic- co-glycolic acid) polymers, and a different dye was incorporated into each compartment to display their anisotropic nature. Imaging was done with a confocal laser scanning microscope.[31]

the above-mentioned poly(acrylamide-*co*-acrylic acid) (P(AAm-*co*-PAA)) particles, thermal imidization of carboxylic acid and amide groups provided sufficient particle stability and resulted in controllable swelling in water.[66]

More recently, EHD co-jetting of organic-soluble polymers has been demonstrated to yield anisotropic micro- and nano-particles. In particular, the EHD co-jetting of organic solution of poly(lactic-*co*-glycolic acid) (PLGA) has resulted in

bicompartmental particles and fibers.[67] Because of their biodegradability, these particles may constitute promising building blocks for drug delivery and tissue engineering.[68]

Systematic analysis of the EHD co-jetting system reveals that both solution and process parameters have to be controlled to achieve a particular compartmentalization, shape, and size.[68, 69] In addition, EHD co-jetting can be affected by a number of environmental factors, such as temperature, pressure, and humidity. Subtle alteration of these variables may lead to significant variation in particle size, shape, surface, morphology, and porosity. A wide range of PLGA particle characteristics has been achieved through variation of polymer concentration and flow rate of PLGA fluids as control parameters.[68] The viscosity of a polymer solution, a direct consequence of polymer concentration and molecular weight, significantly influences jet atomization and evaporation rates as well. For example, fiber architectures are preferentially prepared at higher concentrations and low flow rates, because more viscous solutions can resist the breakup of the jet.

Because the capillary needle configuration primarily determines the compartment geometry of particles and fibers fabricated by the EHD co-jetting process, an increase in the number of capillaries can provide access to particles with more than two compartments.[69, 70] The EHD co-jetting of aqueous P(AAm-*co*-PAA) solutions with a three-needle setup resulted in tricompartmental particles with diameters between hundreds of nanometers and a few micrometers.[69] On the other hand, multicompartmental fibers with as many as seven distinct compartments can be prepared by the EHD co-jetting of PLGA solution (**Figure 1-3**).[70] Combined with low flow rates and high solvent volatility, highly viscous PLGA solutions contribute to the formation of a very stable and

continuous jet, which results in fibers with multiple compartments only minimally affected by the perturbations during EHD co-jetting, such as humidity, air flow, charge build-up, and temperature fluctuations.[70] Moreover, the flow arrangement as well as the nozzle geometry can influence the orientation of compartments. For example, three parallel-aligned needles in a side-by-side configuration yield sandwiched compartments, which can show all possible "isomers" of tricompartmental fibers (Figure 1-3 a-c). On the other hand, a concentric side-by-side three-needle configuration realizes three pie-shaped

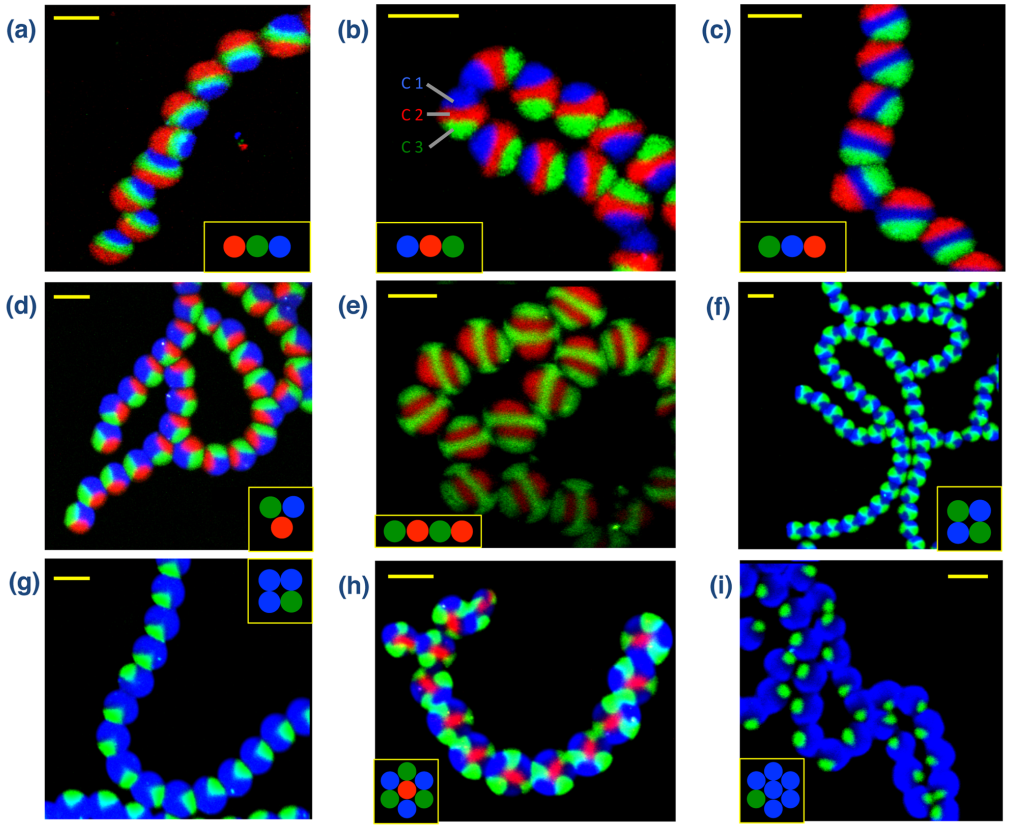

Figure 1-3: Confocal laser scanning microscope images of the cross-sectional view of multicompartmental microfiber bundles with two to seven compartments. The colored circles in the small inset boxes represent the number of compartments, their orientation, and the dyes used in each. In (A–C), tricompartmental microfibers with a side-by-side geometry are shown where the dye in each compartment has been switched to display the versatility of the fabrication method. In (B), the individual compartments in one fiber have been outlined, where "C" represents "Compartment." (D) Tricompartmental microfibers with a pie-shaped structure. (E–G) Tetra-compartmental microfibers, where the internal geometry of the fibers (side-by-side in (e) and pie-shaped in (f–g)) and their compartment size ((F) versus (G)) are compared. (H–I) Seven-compartmental microfibers and their respective compartment size. The scale bars represent 20 mm for all figures.[75]

compartments (Figure 1-3 d). When the jetting solutions were arranged in an alternating sequence, scaffolds consisting of striped microfibers with four distinguishable compartments in series were prepared (Figure 1-3 e). Similarly, more complicated rosettes consisting of seven compartments were prepared (Figure 1-3 h-i). Importantly, these multicompartmental microfibers can be used as platforms to transfer the well-defined anisotropic structures to cylindrical colloids by microsectioning.[71]

Differential reactivity of individual compartments within a compositionally anisotropic particle provides access to interesting particle architectures that would be otherwise impossible, or at least extremely difficult, to achieve. PLGA microdisks were prepared, which were composed of a quarter compartment containing a mixture of poly(*N*-isopropyl acrylamide) (PNIPAM) and PLGA. Selective removal of the PNIPAM compartment by exposure to water led to "Pac-Man"-like particles (**Figure 1-4**).[71] Spatially controlled photo-cross-linking reactions of poly(vinyl cinnamate) (PVCi) containing compartments of bicompartmental PLGA microparticles led to novel types of particles with respect to degradation rates, solvent resistance, and mechanical properties.[3] In addition to being used in biomedical applications such as selective release of therapeutics, such particles can be used for on-demand self-assembly of anisotropic particles. Treatment with chloroform yielded semicapsules manifesting small pores on their surface (Figure 1-4).[3] Such pores can be used to accelerate the selective degradation, or the release of therapeutics, from one compartment.

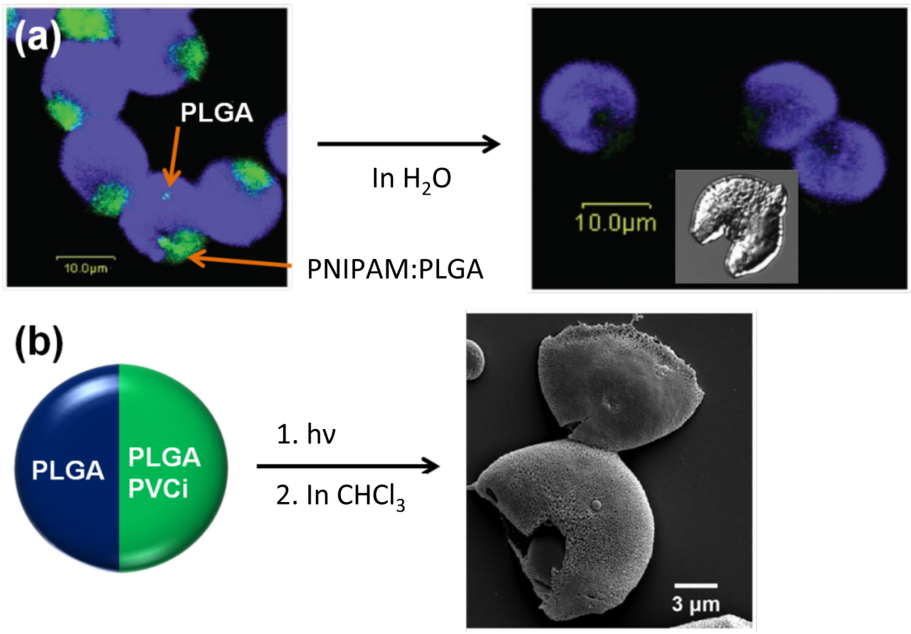

Figure 1-4: (A) A confocal laser scanning microscope image of bicompartmental poly(lacticco-glycolic acid) (PLGA) microdisks prepared by electrohydrodynamic co-jetting and subsequent microsectioning. The smaller one-quarter compartment (green) comprises a water-soluble polymer (PNIPAM, left), which was selectively removed to yield "Pac-Man"-like particles (right, scale bar: 10.0 μm for both the fluorescent and differential interference contrast images). (B) Porous hemicapsules obtained from spatially controlled photo-cross-linking and subsequent solvent treatment of bicompartmental PLGA particles containing poly(vinyl cinnamate) (PVCi) in one compartment. Note: h, Planck's constant; ν, frequency; PNIPAM, poly(N-isopropyl acrylamide).[3,76]

Anisotropic surface modification is one of the simplest methods to prepare Janus particles with different surface patches. The surface properties of these particles can be controlled effectively. Therefore, the selective surface functionalization of compartmentalized particles may offer novel properties, because distinctive functions can be given to external as well as internal design aspects in an independently controllable manner. Adding functionalized polymers into different jetting solutions used in the EHD co-jetting process allows for selective modification of certain parts of the particle. Ultimately, it may even be possible to simultaneously present multiple chemical moieties on parts of the particle surface. In one specific case, the EHD co-jetting of P(AAm-*co*-

AA) solutions was used to incorporate biotin- and acetylene-modified P(AAm-*co*-AA) in bicompartmental particles. In addition, surface modification of the entire surface area with PEG was necessary to minimize non-specific binding. Selectively functionalized particles had significantly higher binding as compared to PEG-containing particles.[37]

In another case, selectively acetylene-functionalized bicompartmental particles were prepared from the EHD co-jetting of PLGA solutions, where one of the solutions further contained poly[lactide-*co*-propagylglycolide]. Importantly, the addition of the acetylene-modified PLGA did not disturb the co-jetting process.[66] The mapping of the vibrational signature via confocal Raman spectromicroscopy confirmed the anisotropic distribution of the acetylene groups. The latter are characterized by a strong Raman band at 2100–2020 cm^{-1}.[72] Finally, the click reaction with azide-PEG-amine confirmed the selective modification of one hemisphere. Similarly, spatioselectively modified PLGA particles showed directional self-assembly of bicompartmental particles onto substrates.[72]

In a straightforward extension of the microfiber work, we were able to create microcylinders with multicompartmental architectures through a semi-automated microsectioning process.[71] The critical engineering advance was the preparation of perfectly aligned fiber scaffolds. This was achieved by jetting the microfibers on a spinning wheel where the spinning frequency was matched to the jetting velocity. **Figure 1-5** shows examples of different types of microcylinders that were prepared following this procedure. Variation of the microscectioning amplitude results in multicompartmental microcylinders with different aspect ratios. The improved understanding of the influence of different jetting parameters has allowed for varying the diameter of the microcylinders/microfibers from tens of microns to hundreds of

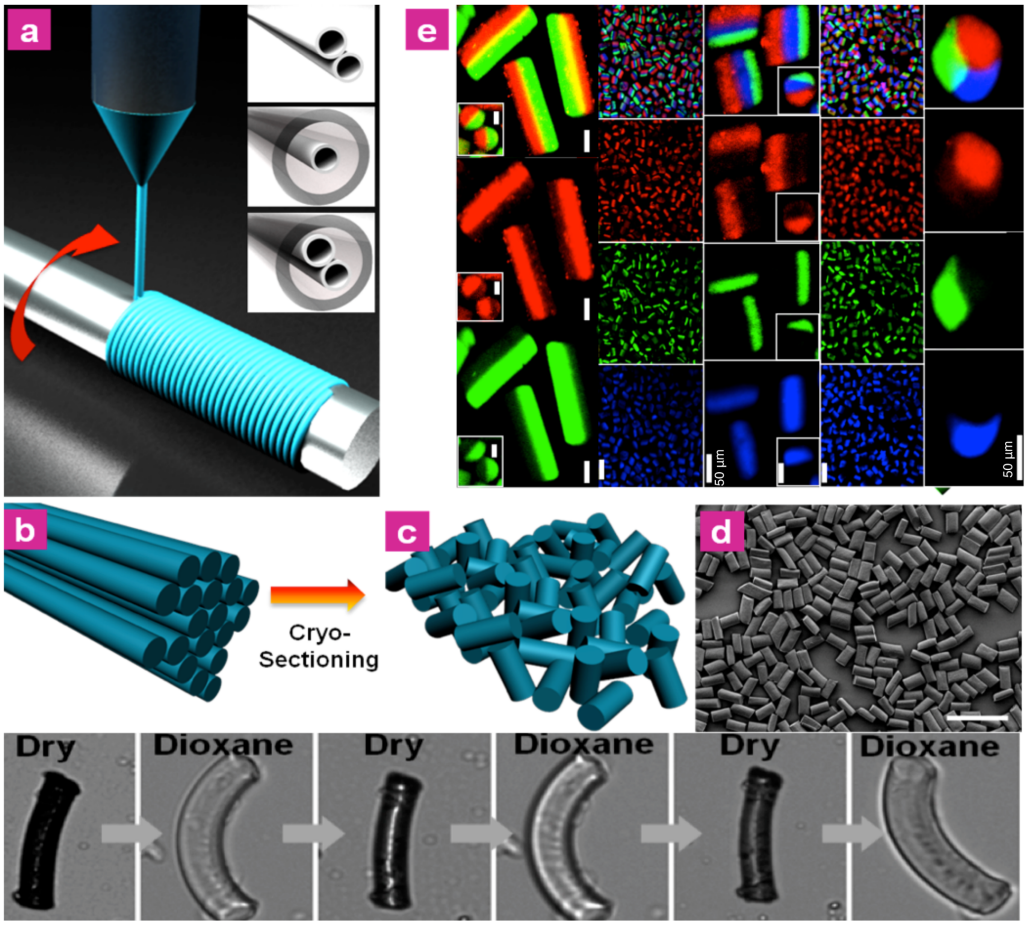

Figure 1-5: Fabrication of bicompartmental fibers and microcylinders based on electrohydrodynamic co-jetting. In (A–D), the fabrication of microcylinders from microfibers is shown: (A) the electrospinning method, types of needles used, and the collecting wheel used for microfiber fabrication; (B–C) the cryosectioning procedure used to process the microfibers into uniformly sized microcylinders; and (D) a scanning electron microscope image of uniformly sized microcylinders fabricated through this process (scale bar is 100 mm). In (E), the top square in each column represents the overlay confocal laser scanning microscope (CLSM) image of the particles, while each subsequent lower square displays the individual CLSM channels representing a single compartment. Scale bars are 10 µm unless otherwise noted; the scale bar in the bottom row of each column is the same for the entire column. (F) Bicompartmental microcylinders composed of a hydrogel/organogel that can undergo reversible, autonomous switching. Microcylinders are about 20 microns in size for imaging reasons but can be prepared with submicron diameters. [75,78]

nanometers. The fact that multiple, distinct compartments can be realized within the same microcylinder can give rise to asymmetric properties within the same microcylinder. For instance, two (or more) compartments may have very distinct mechanical properties. In this case, the multicompartmental architecture will be profoundly distinct from a simple blending of the individual polymers.[73]

While electrospraying and electrospinning can utilize a wide range of polymers, electrohydrodynamic (EHD) co-jetting has so far been accomplished with a limited set of polymers that have similar solution properties. The formation of a stable cone during EHD co-jetting is typically easier to achieve when key solution parameters of the jetting solutions, such as conductivity, viscosity, and density are similar for the different jetting flows. Beyond the expansion of the EHD co-jetting process to increasingly different sets of polymers, such as water–organic swelling polymers and thermoresponsive/ photoresponsive polymers, further modification of the jetting process, including the use of novel needle configurations, different combinations of solvents, and sacrificial templating, may allow for exotic types of multifunctional compartmental particles with dissimilar properties.

Nanometer- and micron-scale control of biodegradable materials is essential for many biomedical applications, including controlled drug delivery, regenerative medicine, or simultaneous imaging and diagnosis applications. The anisotropic surface functionalization of multicompartmental poly (lactic-*co*-glycolic) acid particles has the potential to satisfy such important criteria.

1.4 Objectives of This Work

The major objectives of this dissertation have focused on the development of a toolbox for the fabrication of multifunctional carriers, capable of programming desired properties for a given application. The engineering of multifunctional microparticles for cochlear delivery using this toolbox is demonstrated. Specifically, the following aims were established (**Figure 1-6**).

Aim 1: To develop carriers with selective & orthogonal surface modifications. Here, we have focused on the synthesis and selective incorporation of functional polymers in individual compartments and their use for the creation of orthogonal patches on the particles. Such patches can be used for the incorporation of stealth, targeting, or therapeutic capabilities.

Aim 2: To develop carriers with programmable physical properties. Given the importance of a particle's physical characteristics in determining its fate in the body, here the control over these properties were explored. Particles with various properties such as different shapes, sizes, porosities, textures, and charges were fabricated and characterized. Additionally, nanoparticles were synthesized in high yields and their separation into uniform fractions using centrifugation was demonstrated. Nanoparticles were also tested in animal models to determine their biodistribution and circulation times.

Aim 3: To develop particles with complex release kinetics of therapeutics. A major factor in determining the success of a drug-loaded particle is dependent on the precise control over the release kinetics of therapeutics incorporated within it. Here we demonstrated the controlled and stimuli responsive degradation and release of therapeutics from particles by changing the functional polymers used in their bulk.

Aim 4: To design particles for delivery of therapeutics to the cochlea. The prolonged release of multiple factors within the cochlea can potentially result in the survival of hair cells and thereby enhance the level of hearing for individuals suffering from severe hearing loss. Here, we have demonstrated the design of particles loaded with piribedil (small molecule therapeutic) and GDNF (Glial Derived Neurotrophic Factor), and their respective release from the particles for future use in this application. The survival and distribution of the particles over a seven-day period and the general biocompatibility of the particles in the cochlea is also demonstrated.

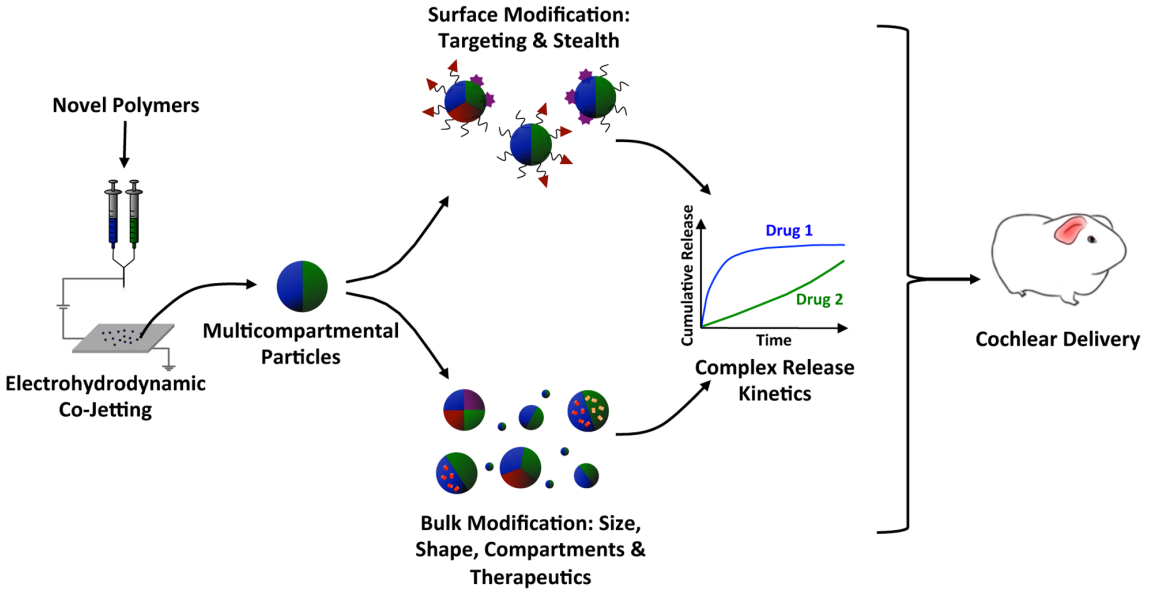

Figure 1-6: Schematic illustration of the aims addressed in this dissertation. (A) Distinct surface patches on the particles. (B) Programmable physical properties. (C) Complex release kinetics. (D) Design of multifunctional particles for cochlear delivery.

CHAPTER 2

Fabrication of Chemically Orthogonal Multi-Patch Particles

The material in this chapter has been adapted with minor modifications from the following articles:

(1) S. Rahmani, S. Saha*, H. Durmaz*, A. Donini, A. C Misra, J. Yoon, J. Lahann, "Chemically Orthogonal Three-Patch Microparticles", *Angew. Chem. Int. Ed.*, **2014**, 53, 2332-2338.

(2) S. Rahmani, S. Hwang, S. Saha, H. Durmaz, P. S. Lown, J. Lahann, "Self Assembly of Multicompartmental Disks Using Selective Surface Modifications", *In preparation*.

2.1 Motivation and Background

The directionally controlled presentation of chemical ligands on the surface of particles defines critical materials processes, such as three-dimensional gelation,[74, 75] directed self-assembly,[24, 76-81] or the controlled interaction of particles with biological cells.[82, 83] While the spatially controlled presentation of chemical and biological ligands is well established for two-dimensional substrates,[84-89] very few methodologies exist for the spatially controlled decoration of three-dimensional objects, such as microparticles.[80, 90-94]

Many of the patterning methods for two-dimensional substrates including photolithography, microcontact printing, dip-pen nanolithography or block copolymer micelle nanolithography,[87, 95-97] are not easily extendable to the three-dimensional surfaces of microparticles. Thus, there is a clear need for efficient microstructuring methodologies for meso-scale particles and some of the more promising strategies include microfluidic and microforming techniques,[92, 98-102] template-assisted polymerizations,[103-108] electrohydrodynamic co-jetting,[37, 64-67, 72, 109, 110] or the use of pickering emulsions.[111-113] With the requirement for spatially controlled immobilization of ligands also comes an increased need for the parallel immobilization of multiple, chemically distinct ligand on defined and independent interfacial patches of the same object. While most multi-ligand strategies have relied on statistical attachment of ligand mixtures,[114-119] several studies have emphasized the need for the independent attachment of two or more ligands on the same surface via orthogonal immobilization strategies.[120-122] In this case, an important prerequisite is the compatibility with the biological "reaction" environment. Bertozzi *et al*. coined the term bio-orthogonal ligation to express the need for chemical selectivity relative to (i) the biological environment and (ii) the different types of ligands to be co-presented on different surface patches.[123-125] Typically, different orthogonal immobilization schemes take advantage of click-type reactions and, in case of two-dimensional substrates, have been well-established,[126] including "double-click" strategies.[127, 128] Recent work has revealed the potential of particles with multiple surface patches, however, the orthogonal functionalization of different surface locations poses significant challenges.[129-134] In this chapter, we now report the spatially controlled immobilization of three chemically distinct patches on the same microparticle via

orthogonal surface reactions. Combining electrohydrodynamic co-jetting with synthetic polymer chemistry, we were able to create two- and three-patch microparticles displaying chemically orthogonal anchor groups on three distinct surface patches of the same particle. Using this technique, the attachment of stealth and targeting ligands on separate patches of particles and potential applications in self-assembly of unique structures were explored.

2.2 Experimental Methods

2.2.1 Materials

O-benzyl-L-serine was purchased from Alfa Aesar and diethyl ether was purchased from Acros Organics. Triethyl amine, bromoacetyl bromide, dimethyl amino pyridine, benzyl alcohol, l-lactide, tin (II) ethyl hexanoate, anhydrous toluene, palladium 10% wt. on activated carbon, anhydrous tetrahydrofuran (THF), 4-methylbenzophenone, carbon tetrachloride, N-Bromosuccinimide, benzoyl peroxide, sodium cyanide, hydrochloric acid, tetraethylammonium chloride, palladium acetate, diphenylphosphine, 1-methyl-2-aminoterephthalate, potassium iodide sodium sulfite, sodium sulfate, sodium chloride, sodium methoxide, dimethylsulfoxide, ethyl acetate, magnesium sulfate, silver perchlorate, methyl glycolate, potassium *tert* butoxide, bromoform, hexane, cycloheptene, poly(lactide-co-glycolide) (PLGA) 85:15, azide-PEGm, azide-PEG-azide, chloroform, dimethylformamide (DMF), MEHPV (polymeric dye), methanol, Tween 20,

phosphate buffered saline (PBS), and *N*-(3-Dimethylaminopropyl)-*N*'-ehtylcarbodiimide hydrochloride (EDC) were purchased from Sigma-Aldrich, USA. Sulfuric acid, acetonitrile, sodium nitrite, dichloromethane, sodium carbonate, acetone, Optimal Cutting Temperature (OCT) compound, and *N*-(hydroxysulfosuccinimide) (Sulfo-NHS) were purchased from Fisher Scientific, USA. Hydrogen was provided by Cryogenic Gases. Carboxyl-PEG-Folic acid molecular weight 5 kDa, amine-PEG-FITC molecular weight 5 kDa, azide-PEG-FITC molecular weight 3.4 kDa, amine-PEG-Rhodamine molecular weight 3.4 kDa, and carboxyl-PEG-rhodamine molecular weight 3.4 kDa were purchased from Nanocs, USA. Albumin from Bovine Serum (BSA), Tetramethylrhodamine conjugate, TRITC-Streptavidin™, and Alexa Fluor ® 647 Streptavidin™ were purchased from Life Technologies-Invitrogen, USA. Amine-dPEG23-biotin molecular weight 1.3 kDa and azide-dPEG47-biotin molecular weight 2.4 kDa were purchased from Quanta Biodesign, Ltd., USA. Thiol-iRGD-FITC was generously provided by the Professor Ruoslahti's laboratory at Sanford-Burnham Medical Research Institute.

2.2.2 Synthesis & Characterization of Functional Poly (Lactide -*co*-Glycolides)

The synthesis and full characterization of functional polymers used in this chapter were graciously done by Dr. Sampa Saha and Dr. Hakan Durmaz and are included in Appendix A.

2.2.3 Fabrication of Microparticles & Their Characterization

Microparticles were fabricated as described previously by Bhaskar, *et al.*[71] The jetting solutions were composed of PLGA 85:15 at 30% w/v in a 97:03 ratio of chloroform to DMF. For microparticles containing polymers **1-5**, the functional polymers were added as an additive at 25% weight of the PLGA 85:15, with an exception to the polymer **5** used for the bicompartmental microparticles. In this case, the polymer **5** used had a molecular weight of approximately 70 kDa and was used as 25% w/w of the PLGA 85:15 and not as an additive. To fabricate the fibers, the polymer solutions were flown through syringes tipped with 26 gauge metal needles at 0.03-0.05 ml/hr. The EHD conditions were a distance of 5-10 cm, RT, and a voltage of 10-12 kV. A rotating cylinder wrapped with aluminum foil and coated with OCT was used as the collector. Once jetted, the collector was placed in vacuumed to dry the fibers and then embedded in a mold filled with OCT for cryosectioning.[73] A HISTO-550 Cryostat at the Microscopy & Imaging Laboratory facilities at the University of Michigan was used to section the embedded fibers at 5 μm. Once sectioned, the microparticles were washed several times with deionized (DI) water and 1% Tween 20 to remove the excess OCT. The microparticles were filtered with 40 and 10 μm filters to remove larger aggregates before use. The microparticle's characterizations were done with CLSM (Confocal Laser Scanning Microscopy) using an Olympus Confocal Microscope and an Amray SEM (Scanning Electron Microscopy) at Microscopy & Imaging Laboratory facilities at the University of Michigan. For Raman-Confocal imaging, the microparticles were

lyophilized to remove excess water, deposited on glass slides, and characterized via the Raman-Confocal microscope using a 532 nm laser and an integration time of 0.5 seconds.

2.2.4 Creation of Orthogonal Patches on Particles

For EDC/Sulfo-NHS chemistry with polymer **1**, microparticles were incubated with 0.33 mg of EDC in 0.33 ml of buffer for 10 min, followed with 10 minutes incubation with 0.03 mg of sulfo-NHS in 0.33 ml of buffer to activate the carboxyl groups. Once activated, 1 mg of amine-PEG-Rhodamine, 0.22 mg of amine-PEG-biotin, or 1 mg of amine-PEG-FITC in 0.33 ml of buffer were added to the solution and incubated for 2 hours. The microparticles were then washed numerous times to remove unreacted material. Microparticles reacted with amine-PEG-biotin were further incubated with 100 μg of Alexa Fluor ® 647 Streptavidin™ in 1 ml of buffer for 3 hours to label the biotin before being washed and imaged with CLSM. The buffer used was PBS with 1% v/v Tween 20 and all reactions were done at RT on a rotator.

For EDC/Sulfo-NHS chemistry with polymer **2**, 0.33 mg of EDC in 0.33 ml of buffer was added to 1-1.5 mg of carboxyl-PEG-Rhodamine or carboxyl-PEG-folic acid for 10 min, followed with 10 minutes incubation with 0.033 mg of sulfo-NHS in 0.33 ml of buffer to activate the carboxyl groups. Once activated, the microparticles containing polymer **2** in 0.33 ml of buffer were added to the mixture and incubated for 2-3 hours. The microparticles were washed numerous times before imaging with CLSM. For the particles labeled with folic acid, they were incubated in primary and secondary antibodies

for 3 hours each, respectively. The particles were washed in between each step and numerous times after the final step before imaging with CLSM. The buffer used was PBS with 1% v/v Tween 20 and all reactions were done at RT on a rotator.

For Staudinger ligation with polymer **3**, microparticles were incubated overnight with 20 mg of azide-PEG-biotin in 1 ml of buffer. The microparticles were then washed numerous times to remove unreacted material. Once washed, the microparticles were incubated with 100 μg of TRITC-Streptavidin™ to label the biotin before washing again to remove unreacted material and imaging with CLSM. The buffer used was DI water with 1% v/v Tween 20 and all reactions were done at RT on a rotator.

For photoreactive chemistry with polymer **4**, the microparticles were incubated with 0.4-1 mg of BSA-tetramethylrhodamine conjugate in 1 ml of buffer for 1.5-2.5 hours before UV'ing at 365 nm for 30 minutes with a handheld UV lamp from Ultra Violet Products, Ltd. The microparticles were then washed to remove unreacted material before imaging via CLSM. The buffer used was PBS with 1% v/v Tween 20 and all reactions were done at RT.

For copper free click chemistry with polymer **5**, microparticles were incubated overnight with 20 mg of azide-PEG-biotin or 10 mg of azide-PEG-FITC in 1 ml of buffer. The microparticles were then washed numerous times to remove unreacted material. Microparticles reacted with azide-PEG-biotin were incubated with 100 μg of Alexa Fluor ® 647 Streptavidin™ to label the biotin. The microparticles were washed again to remove unreacted material before imaging with CLSM. The buffer used was DI water with 1% v/v Tween 20 and all reactions were done at RT on a rotator.

For copper click chemistry with polymer **6** or **7**, disks were incubated overnight with 1.33 mg of copper sulfate pentahydrate, 5.33 ascorbic acid, and 20 mg of azide-PEG-biotin or 10 mg of azide-PEG-FITC in 1 ml of buffer. For complete PEG-ylation of disks (needed for drug delivery), 90-180 mg of azide-PEGm (5 kDa) was used, while for the self-assembly particles 10 mg of azide-PEG-azide was used to covalently link the disks together. The disks were then washed numerous times to remove unreacted material. If unreacted copper was present, the disks were incubated with a 10 mM EDTA solution (+0.01% v/v Tween) for 2-4 hours prior to the washes. Disks reacted with azide-PEG-biotin were incubated with 100 μg of Streptavidin-Alexa 647 or 40-100 μg Streptavidin-TRITC to label the biotin. The disks were washed again to remove unreacted material before imaging with CLSM. The buffer used was DI water with 1% v/v Tween 20 and all reactions were done at room temperature on a rotator.

For thiol-ene reaction with polymer **7**, disks were incubated overnight with 10 mg of thiol-PEG-FITC or 1 mM of thiol-iRGD-FITC in 1 ml of buffer. The disks were then washed numerous times to remove unreacted material. The buffer used was bicarbonate buffer (pH 10) with 1% v/v Tween 20 and all reactions were done at room temperature on a rotator.

2.2.6 Fabrication of Microparticles Responsive to an External Magnetic Field

To create anisotropic microparticles that respond to an external magnetic field, particles incorporating iron oxide in one compartment were fabricated. Similar to the

fabrication of the above-mentioned disks, fibers composed of PLGA and polymer **5** in one compartment were fabricated where the compartment containing polymer **5** also contained 3% w/w iron oxide nanoparticles. The resulting uniform fibers were micro-sectioned at 5 μm, washed, and purified in the same manner. The assembly of the microdisks using an external magnetic field was graciously done by Dr. Sangyeul Hwang.

2.3 Results and Discussion

Fabrication and Analysis of Chemically Orthogonal Three-Patch Microparticles:

As depicted in **Figure 2-1**, the preparation of multi-patch microparticles was achieved by electrohydrodynamic (EHD) co-jetting of up to three parallel polymer solutions. The EHD co-jetting process yielded well-defined microfibers that were subsequently sectioned into well-defined multi-patch particles.[71] In this study, we employed disk-shaped microparticles with an average diameter of 10-15 μm and an average aspect ratio of 1:2 (height:diameter). Size and shape of the microparticles can be controlled within a broad range,[71] but were ultimately selected in this work to be in the 10-20 μm range for practical reasons, such as optimal imaging of the individual chemical surface reactions via fluorescence and Raman confocal microspectroscopy. The base polymer used throughout this study was a biodegradable poly(lactide-*co*-glycolide) (PLGA) polymer. To impart chemical orthogonality, several different chemically functionalized polylactide (PLA) polymers were synthesized. The chemically orthogonal

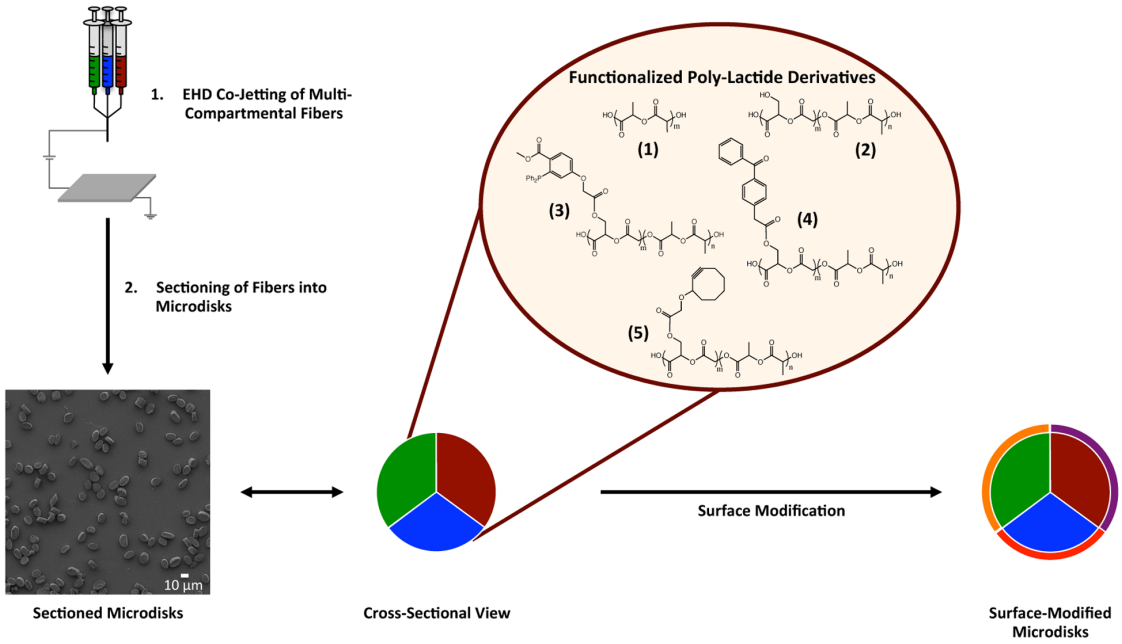

Figure 2-1: Fabrication of microparticles with orthogonally functionalized interfacial patches via EHD co-jetting. Functionalized PLA derivatives (**1**-**5**) are incorporated into different jetting solutions, leading to compartmentalized fibers, which can be sectioned into the corresponding microdisks. Each compartment surface establishes a unique surface patch that is then selectively modified via orthogonal reactions.

PLA derivatives can be added to the different PLGA compartments in order to provide chemical patches for directionally controlled surface modification. Here, a set of eight different PLA derivatives was selected for their ability to support orthogonal surface modification without cross-reactions (Figure 2-1).

The first step of the synthesis of the functionalized PLA derivatives **2**-**5** involved the ring-opening co-polymerization of monomer **1** and l-lactide in the melt, followed by the Pd-catalyzed hydrogenation of the benzyl ether bonds to yield the hydroxyl-modified PLA derivative **2** (Appendix A). Polymer **2** was then used as the starting point for broad diversification of the functionalities using a number of post-polymerization modifications: (i) Reaction with 3-(diphenylphosphino)-4-(methoxycarbonyl) benzoic acid with *N,N'*-Dicyclohexylcarbodiimide (DCC)/4-Dimethylaminopyridine (DMAP)

yielded the PLA derivative **3** for subsequent Staudinger Reaction. (ii) Alternatively, polymer **2** was converted with 2-(4-benzoylphenyl) acetic acid and DCC/DMAP under dry conditions to yield the photoreactive PLA derivative **4**. (iii) Polymer **5**, a cyclooctyne-modified polylactide, was derived from polymer **2** by straightforward conversion with 2-(cyclooct-2-yn-l-yloxy) acetic acid and DCC/DMAP.

In general, we found a satisfying compatibility of the PLA derivatives with the PLGA base polymer: For concentrations of up to 50% of the PLA additives, no adverse effect on the electrohydrodynamic co-jetting process was observed - independent of the chemical nature of the PLA derivative that was added to the jetting solutions. On the other hand, preliminary immobilization experiments demonstrated that PLA concentrations above 20% were adequate to ensure effective surface coupling of model ligands.

Next, we created a group of bicompartmental microparticles, which presented a single hemispheric patch of one of the functional anchor groups. In this case, the second hemisphere was comprised of the PLGA base polymer only and served as an internal reference for the surface reactions. **Figure 2-2** depicts three different particle architectures. These architectures allowed for spatially controlled modification of one hemisphere only. The reference patch showed only very low levels of non-specific ligand adsorption. In Figure 2-2A, PLGA particles with one hemispheric surface patch containing polymer **3** (with green dye) was reacted with azide-PEG-Biotin (PEG: polyethylene glycol) via Staudinger ligation. The biotin was then labeled with TRITC-Streptavidin^{TM} (red dye) for imaging purposes. Co-existence of the red and green fluorescence in the CLSM images (Figure 2-2A3) confirms the spatially controlled

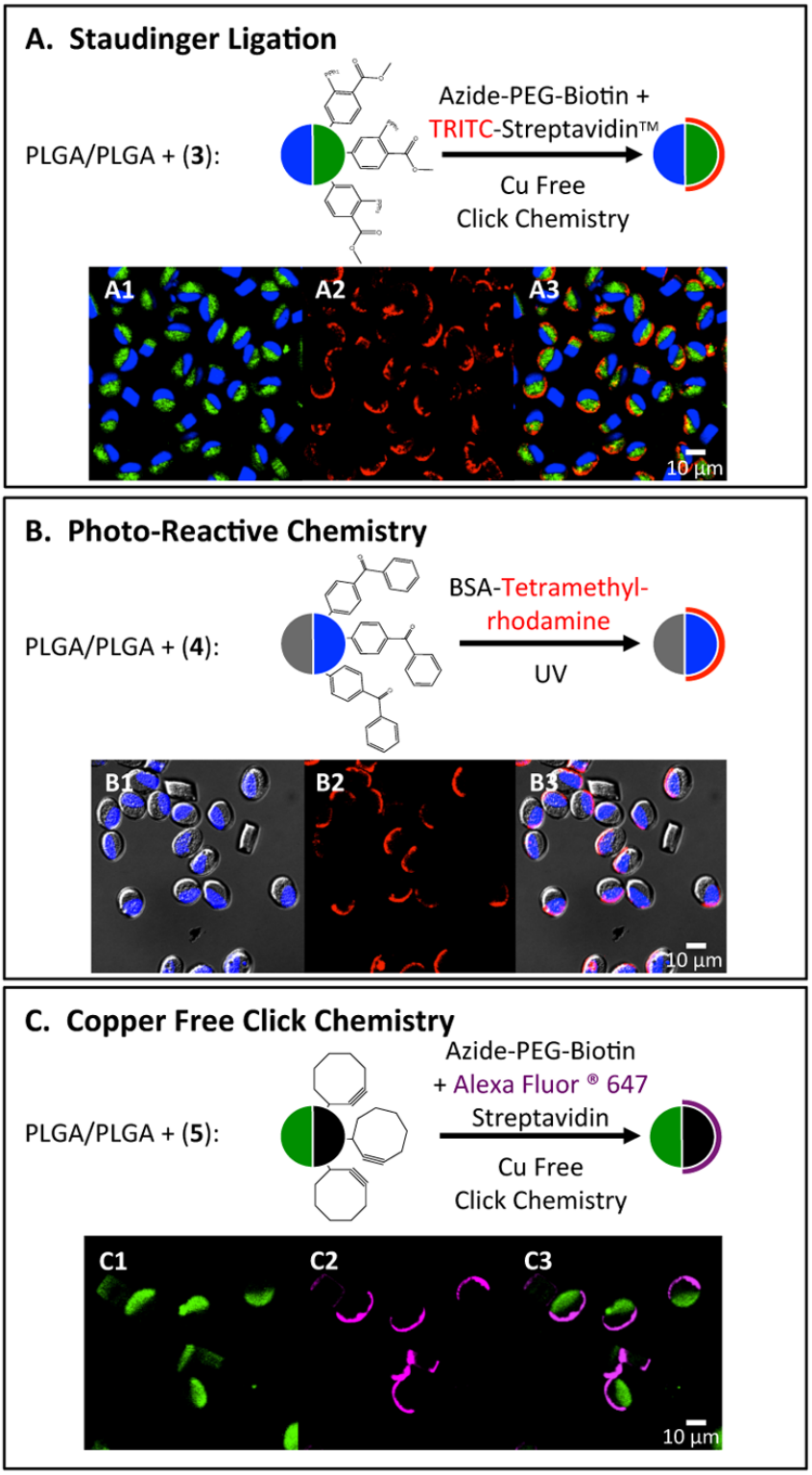

Figure 2-2: Selective surface modification of microparticles containing three different orthogonally functionalized PLA derivatives exclusively present in one hemisphere. In **2.A-C**, microparticles displaying polymers **3** to **5** in one hemisphere only are selectively surface functionalized through Staudinger ligation (A), photo-immobilization (B), and alkyne/azide click chemistry (C). CLSM images show the spatioselective nature of the surface modifications.

surface modification of the microparticles. Similarly, Figure 2-2B displays particles with polymer 4 in the blue hemisphere only. As found for all PLA derivatives, the functional polymer is restricted to only one hemisphere of the microparticles (Figure 2-2B1) underpinning the high degree of patchiness obtained by the EHD co-jetting process. The microparticles were subsequently incubated with a protein, Bovine Serum Albumin (BSA)-Tetramethylrhodamine (red dye), and exposed to UV light at 365 nm to initiate the photo-immobilization of the BSA to the reactive surface patch (Figure 2-2B2). The high degree of selectivity of the photo-immobilization reaction is confirmed by the spatially controlled surface binding of the protein, as depicted in the overlay images of Figure 2-2B3. Similarly, the copper-free click chemistry of bicompartmental microparticles using polymer **5** was successfully carried out, as verified by CLSM analysis (Figure 2-2C). Here, the unreactive PLGA hemisphere was labeled with a green fluorescence dye loaded in the bulk of the compartment, whereas the azide-reactive compartment that contained polymer **5** was non-fluorescent (Figure 2-2C1). The spatially controlled surface modification of these patchy microparticles with azide-PEG-biotin and Alexa Fluor ® 647 Streptavidin^{TM} (magenta dye) was confirmed by the selective surface binding shown in the overlay images of Figure 2-2C3. We further conducted selective surface modification of two-patch particles with one functionalized patch using both polymers **1** and **2** with analogue results (**Figure 2-3)**. In summary, this initial immobilization studies indicated two important findings: (i) The addition of functionalized PLA derivatives into one jetting stream resulted in well-defined patchy microparticles and (ii) the selected surface chemistries are fully orthogonal to the base

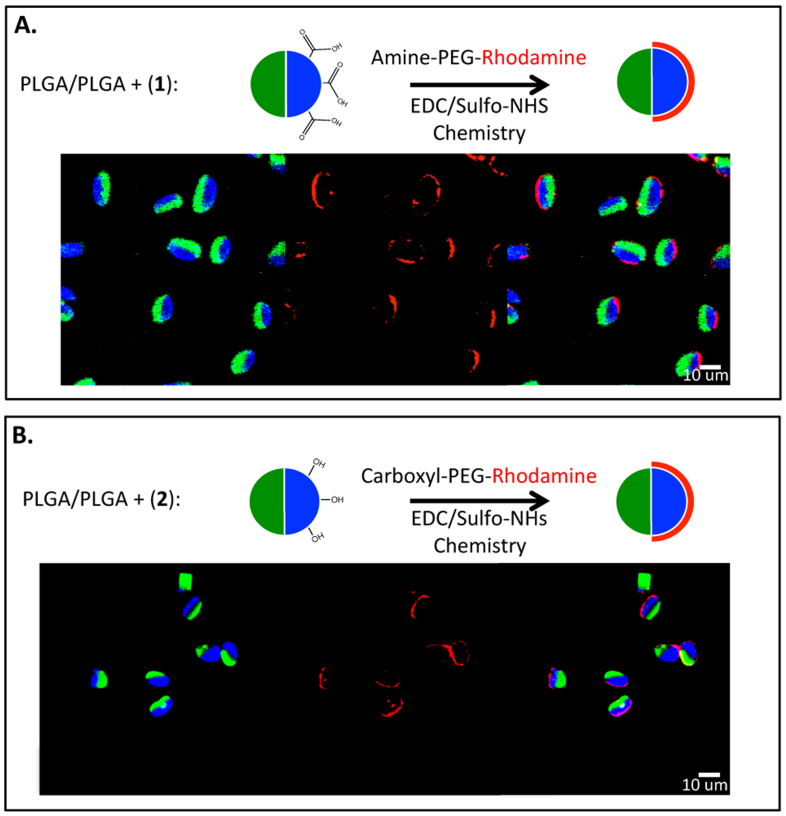

Figure 2-3: The selective surface modification of bicompartmental microparticles containing polymer **1** or **2** in one hemisphere. In **S.1A**, the microparticles contain polymer **1** in the blue patch and PLGA in the green patch. The carboxyl groups in polymer **2** are used to conjugate amine-PEG-Rhodamine (red) to the surface of one hemisphere using EDC/Sulfo-NHS chemistry. In **S.1B**, the microparticles contained polymer **2** in the blue hemisphere and PLGA in the green hemisphere. The hydroxyl groups in polymer **2** were used to attach carboxyl-PEG-Rhodamine using EDC/Sulfo-NHS chemistry.

polymer (PLGA), as evidenced by the fact that only negligibly low levels of non-specific binding were observed on the reference hemisphere.

Encouraged by these initial data, we conducted a second immobilization study that included two different functionalized PLA derivatives in two separate hemispheres of the same particle. For example, **Figure 2-4** displays the CLSM, Raman characterization, and surface functionalization of these two-patch particles containing the two functional polymers **1** and **4** in separate compartments. To confirm that polymers **1** and **4** were indeed localized in different hemispheres, rather than mixed throughout the

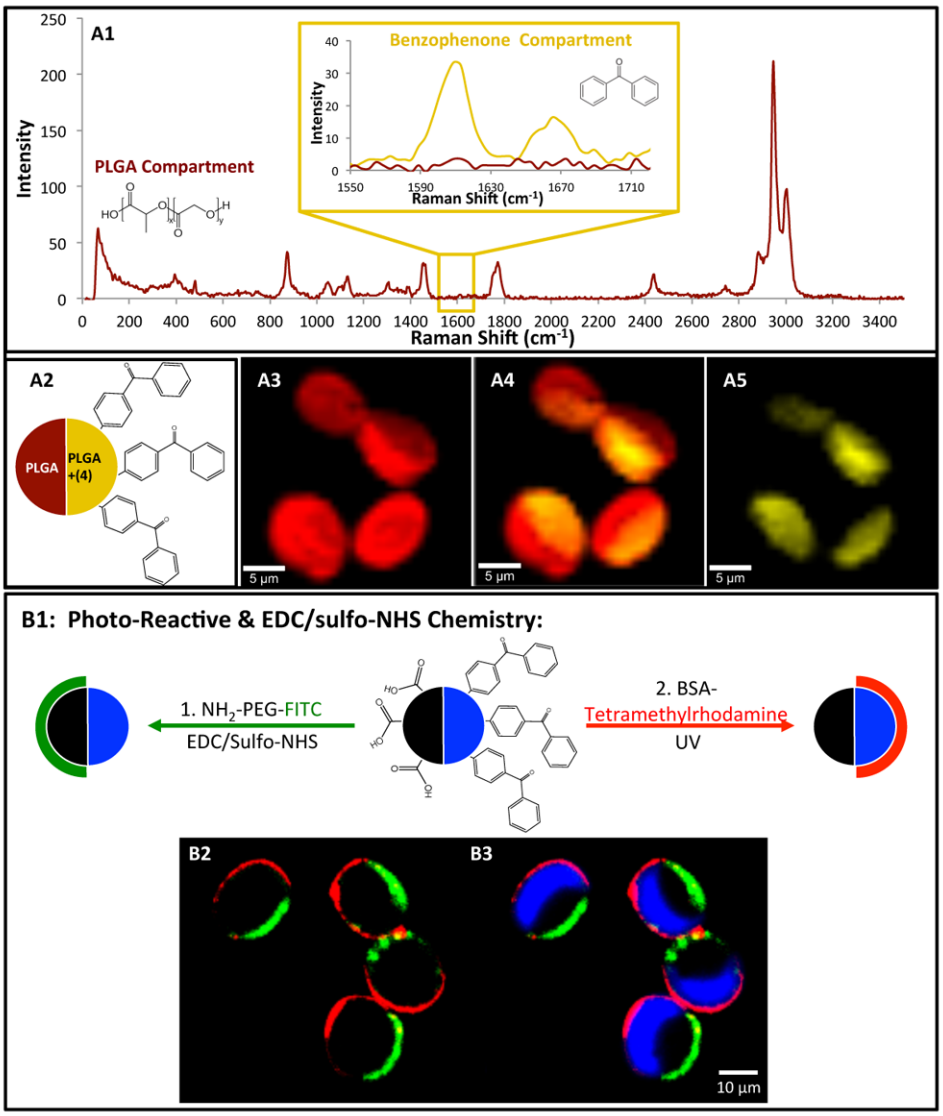

Figure 2-4: Selective surface modification of two-patch microparticles. Microparticles with chemically orthogonal polymers **1** and **4** in different hemispheres were characterized through Raman microspectroscopy (**Figure 2-4.A**), selectively surface-modified, and characterized using CLSM imaging (**Figure 2-4B**)

entire particle, Raman confocal microspectroscopy was employed. This method can be used to gain chemical information of two and three-dimensional substrates and has been previously used to characterize Janus particles.[72] Here, microparticles containing a low-molecular weight PLGA polymer with a higher number of free carboxylic acid end

groups in one hemisphere and a mixture of PLGA and polymer **4** in the second hemisphere were imaged via Raman microspectroscopy (Figure 2-4A). In Figure 2-4A1, the two Raman spectra that were obtained from the two different hemispheres are compared. The spectrum obtained on the PLGA hemisphere is shown in red, while the spectrum obtained on the hemisphere displaying polymer **4** is indicated by a yellow color. The yellow spectrum further revealed characteristic bands indicative of polymer **4**. Specifically, two additional bands at 1610 and 1660 cm^{-1} signify the presence of benzophenone groups (**Appendix B-1**). Therefore, the Raman maps shown in Figure 2-4A3-5 unambiguously confirm that the PLGA base polymer is present in both hemispheres (red), whereas the PLA derivative **4** is restricted to one side only (yellow). Next, the two hemispheres were allowed to react with BSA-Tetramethylrhodamine (red dye) in the presence of UV light (first step) and amine-PEG-FITC (green dye) and EDC/Sulfo-NHS (second step). Here, the hemisphere containing polymer **4** autofluoresces in the blue channel (Figure 2-4B3) to further distinguish the two compartments. Subsequent analysis with confocal laser scanning microscopy (CLSM) confirmed successful, yet highly selective surface modification of both surface patches (Figure 2-4B2-3). Taken together, the Raman microspectroscopic analysis and CLSM support the successful orthogonal surface reactions on these two-patch microparticles.

Beyond this particular combination of functionalized PLA derivatives, a number of different orthogonally substituted microparticles were prepared and selectively surface-modified, further elevating the potential scope of this novel approach. As depicted in **Figure 2-5**, two-patch microparticles containing polymer **2** (with blue dye)

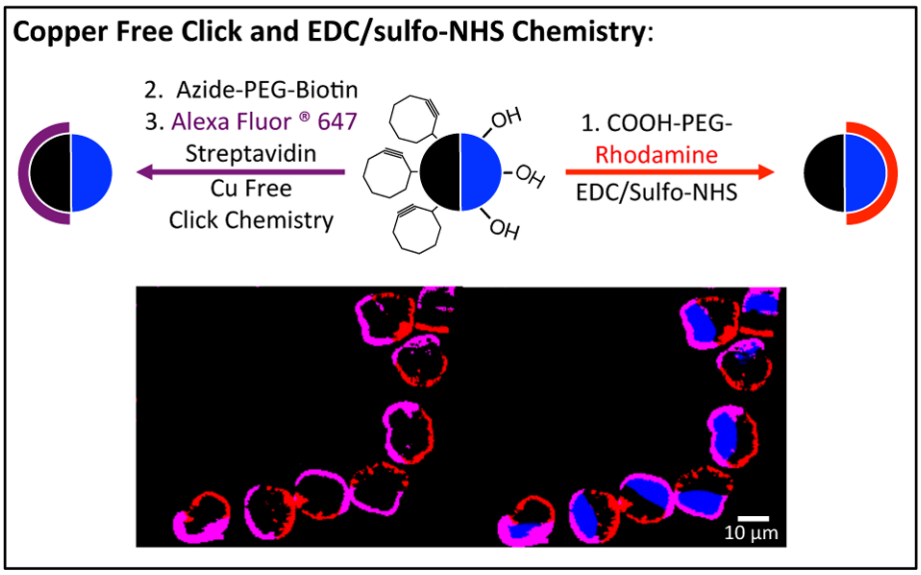

Figure 2-5: The selective surface modification of bicompartmental microparticles containing polymer **2** and **5** in separate hemispheres. Here, the blue compartment contains polymer **2** and the black compartment (no dyes) contains polymer **5**. The surface of the blue patch was first reacted with cooh-PEG-Rhodamine through EDC/Sulfo-NHS chemistry, followed by the click reaction on the other hemisphere using the azide-PEG-biotin and the cyclooctynes present on the surface. The biotins were then labeled with Alexa Fluor ® 647 Streptavidin for imaging purposes.

and **5** (black, no dyes) in different hemispheres were prepared and the selective surface functionalization was demonstrated as well.

Further expanding on the complexity of possible multifunctional particles, we adapted our EHD co-jetting strategy to create three-patch microparticles. These particles, shown in **Figure 2-6**, contained patches displaying three different functionalized PLA derivatives, i.e., polymers **1**, **4**, and **5**, respectively. As described above, it is important to ensure that the functionalized polymers are indeed localized in specific surface patches prior to conducting orthogonal surface modification. In fact, the defined localization of the reactive polymer species is an essential prerequisite for the spatially controlled surface modification. Figure 2-6A displays the results of the Raman microspectroscopic analysis of three-patch particles. The Raman spectra obtained from the three patches displayed characteristic bands of the PLGA base polymer (blue). In addition,

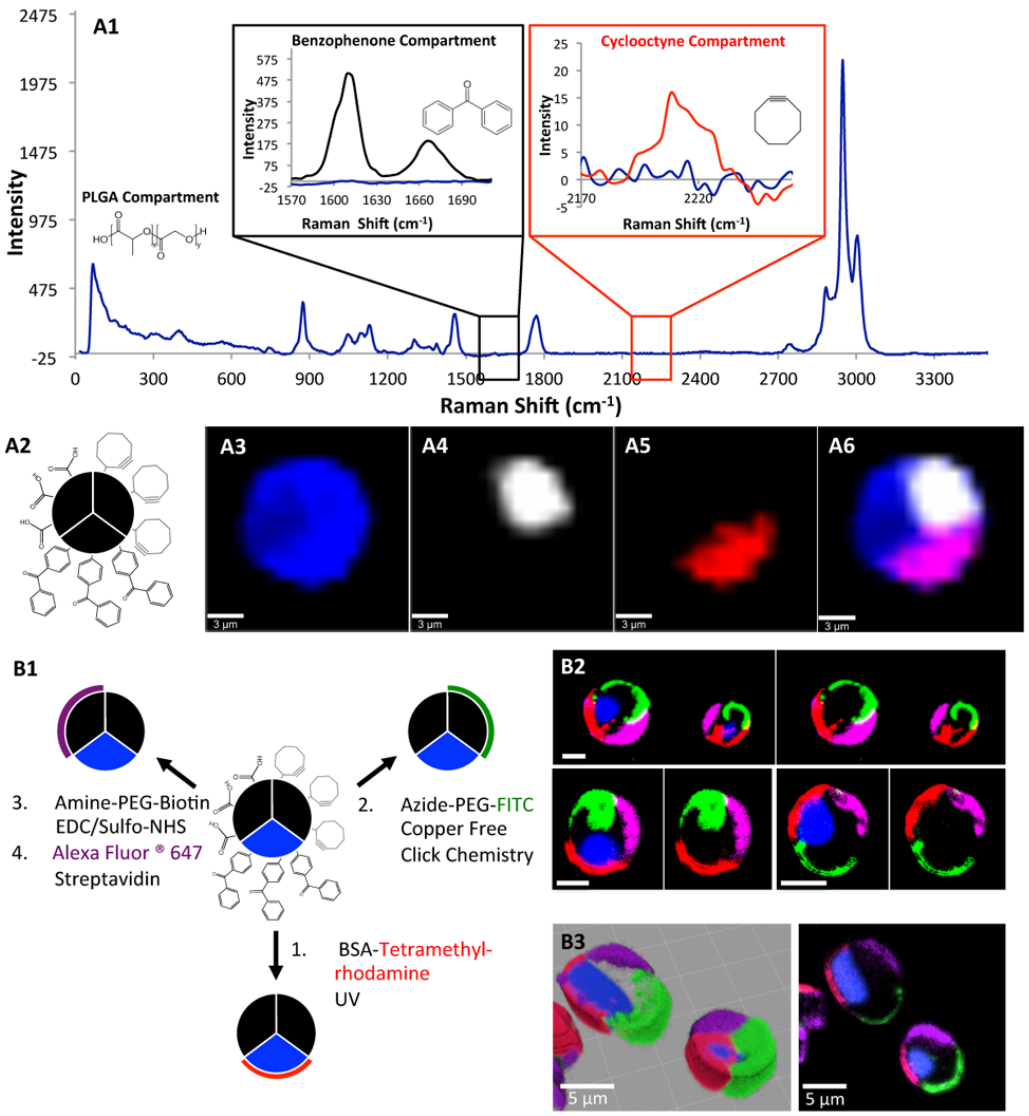

Figure 2-6: Characterization and selective surface functionalization of three-patch microparticles. Particles containing polymers **1**, **4**, and **5** in separate surface patches were characterized using Raman microspectroscopy (**4.A**). The surface of each patch was then selectively modified using orthogonal chemistries and analyzed through CLSM imaging (**4.B**). Unless noted, all scale bars are 5 µm.

characteristic bands of polymer **4** at 1610 and 1660 cm^{-1} for benzophenone (black), and at 2200 cm^{-1} for the cyclooctyne in polymer **5** (red) were selectively found in different surface regions, as shown in Figure 2-6A1 (Appendix B-2.) The two-dimensional reconstruction of the Raman spectra displays three distinct patches on these microparticles. The PLGA polymer is detected in the entire particle (blue, Figure 2-6A3),

while polymer **4** (white, Figure 2-6A4) and polymer **5** (red, Figure 2-6A5) are each restricted to two different surface patches. We further conducted a series of orthogonal surface reactions on these microparticles and analyzed them by fluorescence confocal microscopy. The schematic for the sequential chemistries and the results obtained by CLSM imaging are shown in Figure 2-6B1 and **2**, respectively. Here, the blue patch, containing polymer **4,** was functionalized by photochemical attachment of BSA-Tetramethylrhodamine(red dye), while the selective conjugation of azide-PEG-FITC (green dye) was restricted to the second surface patch that contained polymer **5.** Efficient binding was achieved through click chemistry with the cyclooctyne groups of polymer **5.** The third compartment, containing polymer **1,** was reacted with amine-PEG-Biotin through EDC/Sulfo-NHS chemistry and labeled with Alexa Fluor ® 647 Streptavidin™ (magenta dye) for CLSM imaging.

Figure 2-6B3 shows the three-dimensional reconstruction of the microparticles on the basis of the fluorescence images collected in the z-direction. The particles were imaged in the xy-plane with a step size of 250 nm and were then reconstructed to display the three-dimensional structure and characteristics of the patchy microparticles. We note that these results correspond well with the cross-sectional view (Figure 2-6B3 right image).

Applications of Established Techniques: Incorporation of Stealth & Targeting Moieties into Surface Patches of Particles

The ability to selectively surface modify various patches on the surface of particles is especially important in drug delivery applications, where the incorporation of

stealth and targeting moieties can determine the length of time the particles circulate in the blood stream and their specificity towards their selected target.[2, 9] Polyethylene glycol (PEG) is a well-established 'stealth' group in this field. PEG can enhance the circulation duration of particles in the body by creating a hydrophilic layer on the surface of the particles that repel the attachment of plasma proteins (opsonization) and delay the clearance of particles via the MPS (Mononuclear phagocyte system).[1] As a result, here we have explored the incorporation of PEG on the surface of multifunctional particles in select patches. In addition to long circulation, the targeting molecules used play a crucial aspect on the fate of the particles in the body and the attachment of two targeting molecules, folic acid and iRGD, are demonstrated. Folic acid receptors are overexpressed in cells in a number of tumors and decorating the surface of particles with folic acid will potentially enhance the uptake of particles by tumor tissue.[135] In addition to targeting to the tumor, in most cases (especially in solid tumors), the particles also need to penetrate through the different layers of the tumor to successfully eradicate it entirely. To this end, Professor Ruoslahti's group have discovered a tumor homing and penetrating peptide (iRGD) that is capable of not only targeting to the tumor site, but also penetrating through the different layers of solid tumors.[136]

Initially, we used particles with two distinct compartments, each with a different functional polymer, to attach stealth (PEG) and targeting (folic acid) groups on separate patches of the particles. Here, folic acid was chosen as a model targeting moiety in a proof of concept study. The particles contained polymer **6**[66] in one compartment and polymer **2** in the second compartment (**Figure 2-7**). The schematic explains the steps taken to functionalize each surface separately: the alkyne groups in polymer **6** were first

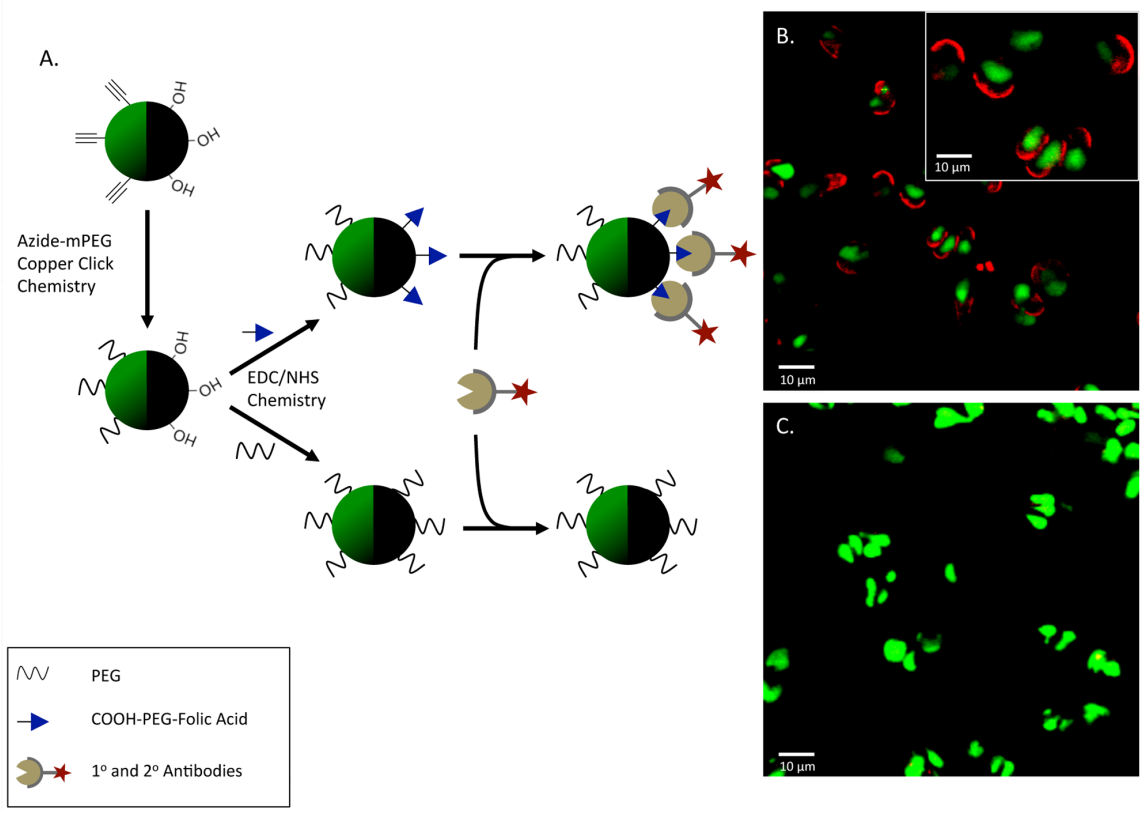

Figure 2-7: Attachment of PEG and folic acid to separate patches of particles. (A) Schematic of steps taken for the attachments. (B) CLSM image of particles containing folic acid and labeled with antibodies (red). (C) CLSM image of particles without folic acid and incubated with the same antibodies.

used to attach azide-mPEG via click chemistry to one patch, followed by the attachment of carboxyl-PEG-Folic Acid or carboxyl-PEGm via EDC/sulfo-NHS chemistry to the second patch. To demonstrate the attachment of the folic acid, primary and secondary antibodies specific to folic acid were used (Figure 2-7b). Here, the particles with PEG on both sides were used as a control to determine the specific attachment of the antibodies. As shown, the particles containing a patch of folic acid were labeled with the antibody (red on one surface, Figure 2-7b), while the control group did not have any antibody attachment (Figure 2-7c).

In addition to attaching a single functional moiety to a surface patch, we were interested in exploring the possibility of attaching multiple functionalities to the same patch. In multi-compartmental particles, this technique would enhance the functionalities per particle, where multiple targeting ligands and stealth groups at specific ratios could be evaluated for their targeting capabilities. Here a bi-functional polymer (**7**) containing both alkyne and acrylate groups at a 9:1 ratio was used (**Figure 2-8**). The polymer was incorporated into one compartment, while the second compartment was composed of neat PLGA and served as the control (Figure 2-8a). The particles were first reacted with azide-PEGm via copper catalyzed click chemistry to impart stealth functionalities, followed by

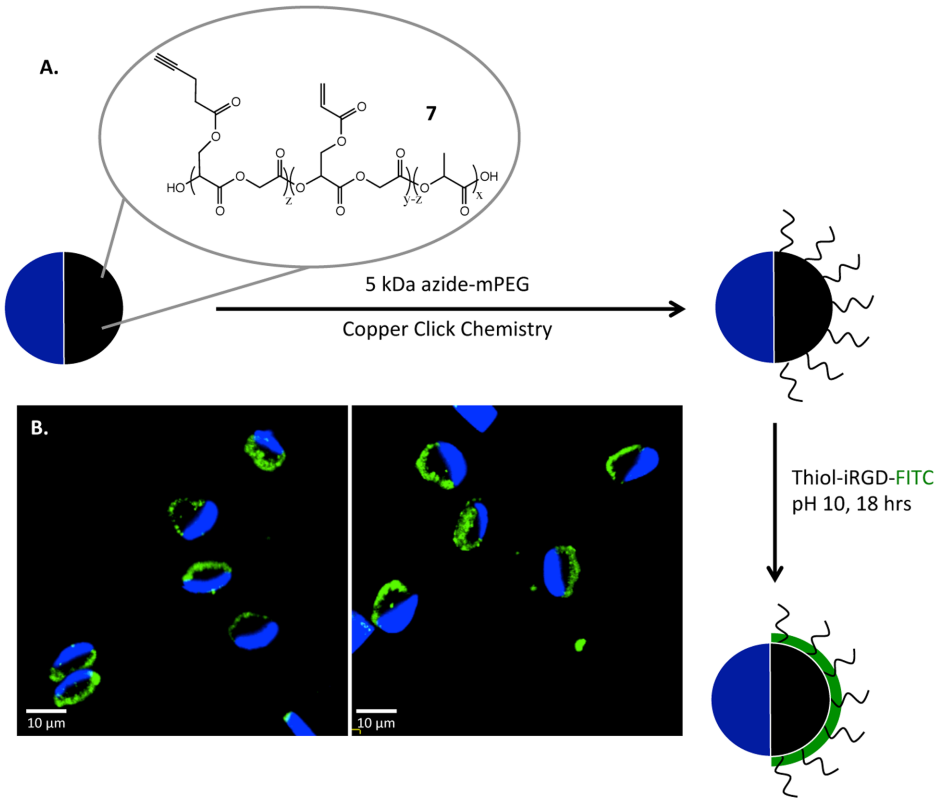

Figure 2-8: Dual orthogonal chemistries on a single particle patch. (A) Using polymer **7,** the attachment of azide-mPEG via copper catalyzed click chemistry and thiol-iRGD-FITC via thiolene click chemistry on the same patch are demonstrated. (B) CLSM images of particles showing the attachment of PEG and iRGD (green) to one side.

the thiolene click reaction of thiol-iRGD-FITC to attach a tumor homing and penetrating peptide to the particles. Using CLSM imaging, the incorporation of the FITC labeled iRGD can clearly be observed (Figure 2-8b).

This data, in addition to the previous figure showing the orthogonal attachment of targeting and stealth groups on distinct patches, demonstrate the capabilities of our system for the precise incorporation of a variety of targeting groups (small molecules, peptides, antibodies, etc.) and stealth moieties. Such systems can be used for the development of particles with multiple functionalities and can create a platform for the testing of the effect of multivalency and avidity on particle targeting.[137]

Applications of Established Techniques: Magnetic Self-Assembly of Anisotropic Disks

In addition to using multifunctional particles for drug delivery applications, anisotropic particles with distinct patches can also be used for various self-assembly applications. Here, we were interested in combining our well-established chemically orthogonal patchy particles with stimuli-responsive particles towards an external magnetic field to create self-assemblies of particles with unique architectures (**Figure 2-9**). Similar to the last section, fibers were fabricated using the EHD co-jetting system and were sectioned into microdisks. In this case, the microdisks contained iron oxide nanoparticles (Ocean Nanotech LLC, 30 nm) in select compartments that enabled the microdisks to be responsive to an external magnetic field. We were interested in exploring the alignment of such microdisks, expanding on the above mentioned surface patch work to include double click chemistries on distinct patches, and using a combination of these techniques to create unique self-assemblies of particles.

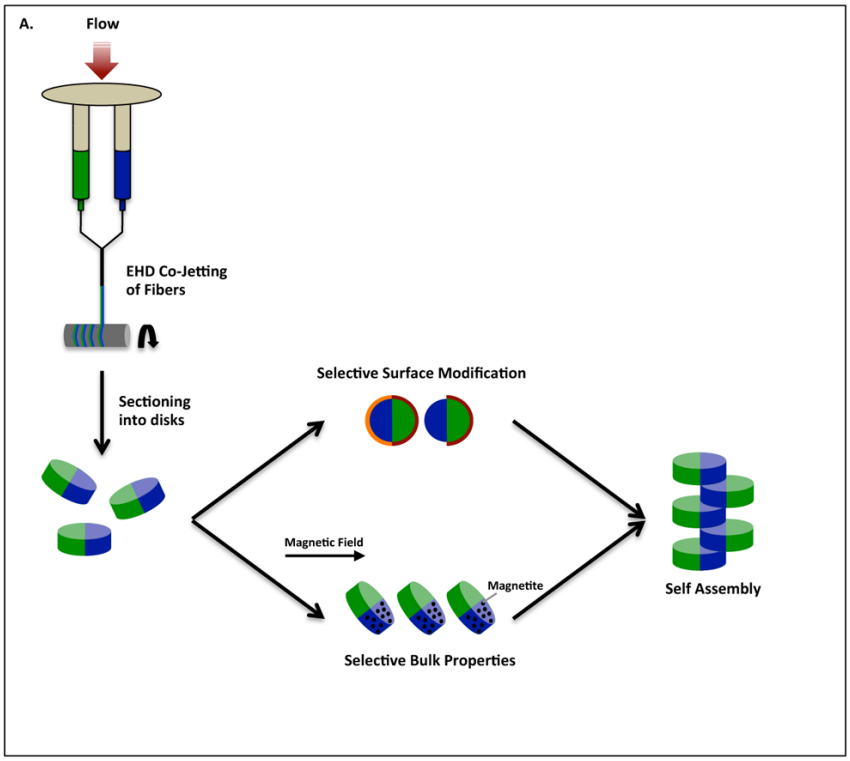

Figure 2-9: Schematic demonstrating the fabrication of the fibers via EHD co-jetting and subsequent sectioning into microdisks; the exploration of selective surface modifications and alignment of the particles to an external magnetic field; and the combination to yield self-assemblies of particles.

To begin, the responsiveness of microdisks with iron oxide nanoparticles in one compartment to an external magnetic source was explored (**Figure 2-10**). This work was done by Dr. Sangyeul Hwang, where it was observed that the particles aligned based on the applied magnetic field (Figure 2-10A, where B is the magnetic field and theta is the angle between the magnetic field and the normal to the loop of the area encapsulated in the field based on Farayday's law of electromagnetic induction). As the particles aligned in the direction of the magnetic field and moved toward the external magnet, they self-assembled into the structures seen in Figure 2-10B. At the removal of the magnetic field, the particle disassembled into individual, un-aligned particles.

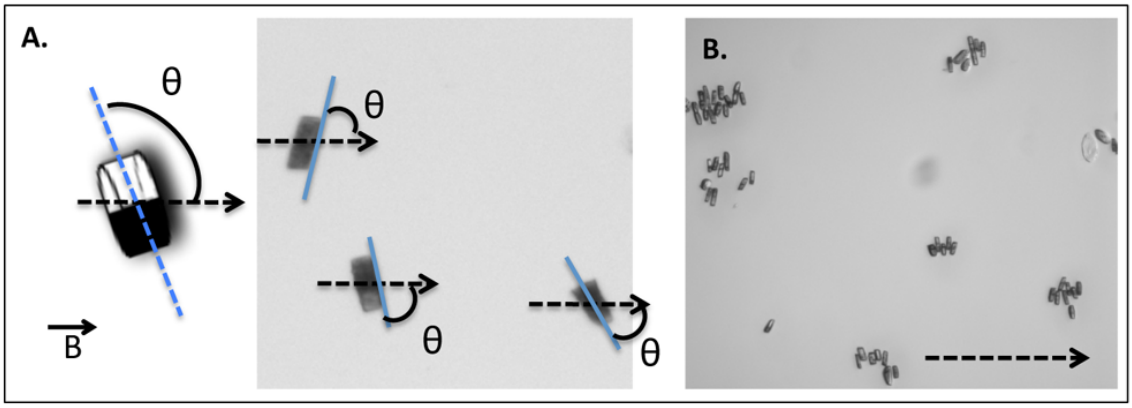

Figure 2-10: The responsiveness of microdisks to an external magnetic field. (A) The particles align according to the magnetic field and (B) move toward the external magnet. During this process, they assemble into structures of alternating compartments.

For this application, we were also interested in expanding our multipatch particles to include double click surface reactions. Such capabilities could be used to connect the particles in the structures seen in Figure 2-10 to make stable self-assembled entities, as well as potentially assemble them into hierarchical structures. To this end, particles containing polymer **5** and **6** were fabricated according to the above mentioned techniques. Both sides are reactive towards azide-containing molecules, however, while polymer **5** can react by simple incubation, polymer **6** requires the addition of a catalyst to complete the reaction. This was used to our advantage to create orthogonal double-click particles (**Figure 2-11**). The particles were first reacted with azide-PEG-FITC via copper free click chemistry with polymer 5, followed by incubation in excess azide-PEGm to ensure all functional cyclooctyne groups were reacted. After washing away all unreacted material, the particles were then incubated with azide-PEG-biotin and a catalyst (copper) to react with the alkyne groups in the second compartment. The particles were then incubated in Alexa Fluor ® 647 Streptavidin™ to label the biotin groups. As seen in

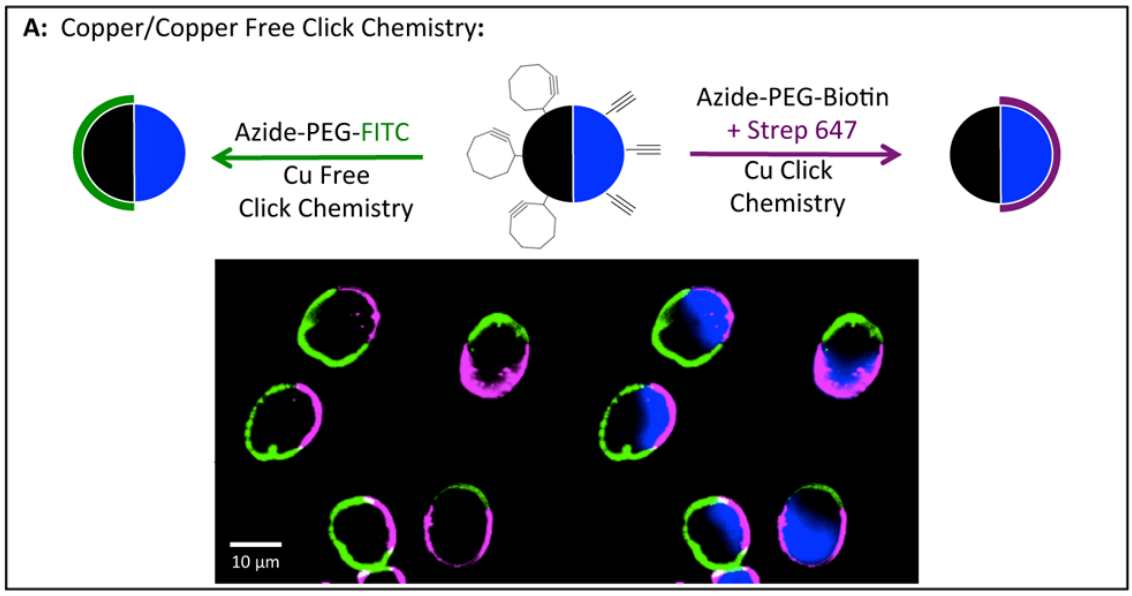

Figure 2-11: Orthogonal surface modifications using dual click chemistry on the same particle. The particles were first reacted with azide-PEG-FITC via copper free click chemistry with polymer **5**, followed by a reaction with azide-PEG-biotin and the respective labeling via copper catalyzed click chemistry with polymer **6**.

Figure 2-11, the surface modifications yielded orthogonal patches on two separate hemispheres of the particles.

Expanding on this technique, tricompartmental particles with polymers **1**, **5**, and **6** were fabricated and surface modified (**Figure 2-12**). Here, the same procedure as for bicompartmental particles in Figure 2-11 were followed, but in between the two click chemistry steps the particles were incubated with amine-PEG-Rhodamine to react with the carboxyl groups of polymer **1** via EDC/Sulfo-NHS chemistry. This resulted in microparticles with three distinct surface patches.

By combining these two techniques, self assembly of particles in a magnetic field and the creation of reactive patches on microparticles, one could fabricate permanent self-assemblies of microparticles in unique architectures using a bottom-up approach. For example, if the compartment containing the iron oxide nanoparticles also contains

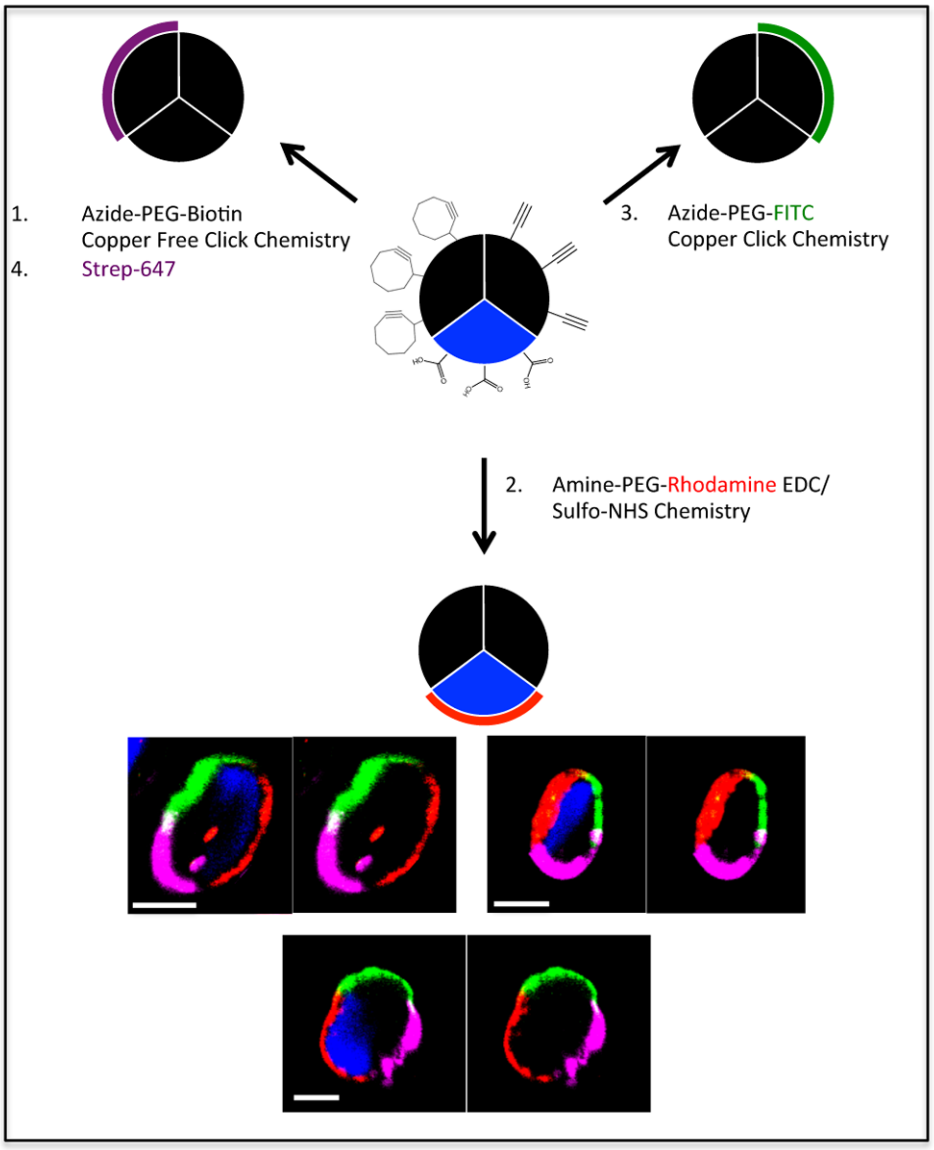

Figure 2-12: Particles with three distinct surface patches. Tri-compartmental particles with distinct functional polymers in each compartment were sequentially reacted to create particles with multiple patches.

polymer **5**, the self-assembled particles under the magnetic field can be cross-linked together using a bi-azide molecule via copper free click chemistry with the cyclooctynes in polymer **5** (during the assembly the compartments with iron oxide are typically next to each other as they are attracted to each other). Upon the removal of the magnetic field, these structures would retain their assembled geometries and can be used for further

designs. Higher ordered entities could potentially be created from these structures if the second compartment contains another functional polymer that can be used to further connect the structures together.

Here, we demonstrate the fabrication of permanent self-assembled structures from anisotropic building blocks as a first proof of concept study (**Figure 2-13**). Particles containing polymer **5** and iron oxide nanoparticles in one compartment were fabricated based on the previous mentioned techniques. The particles were aligned in an external magnetic field and incubated with azide-PEG-azide. As the particles move in the magnetic field and assemble, the compartments containing polymer **5** and iron oxide nanoparticles (blue) come together and are cross-linked via the azide-PEG-azide

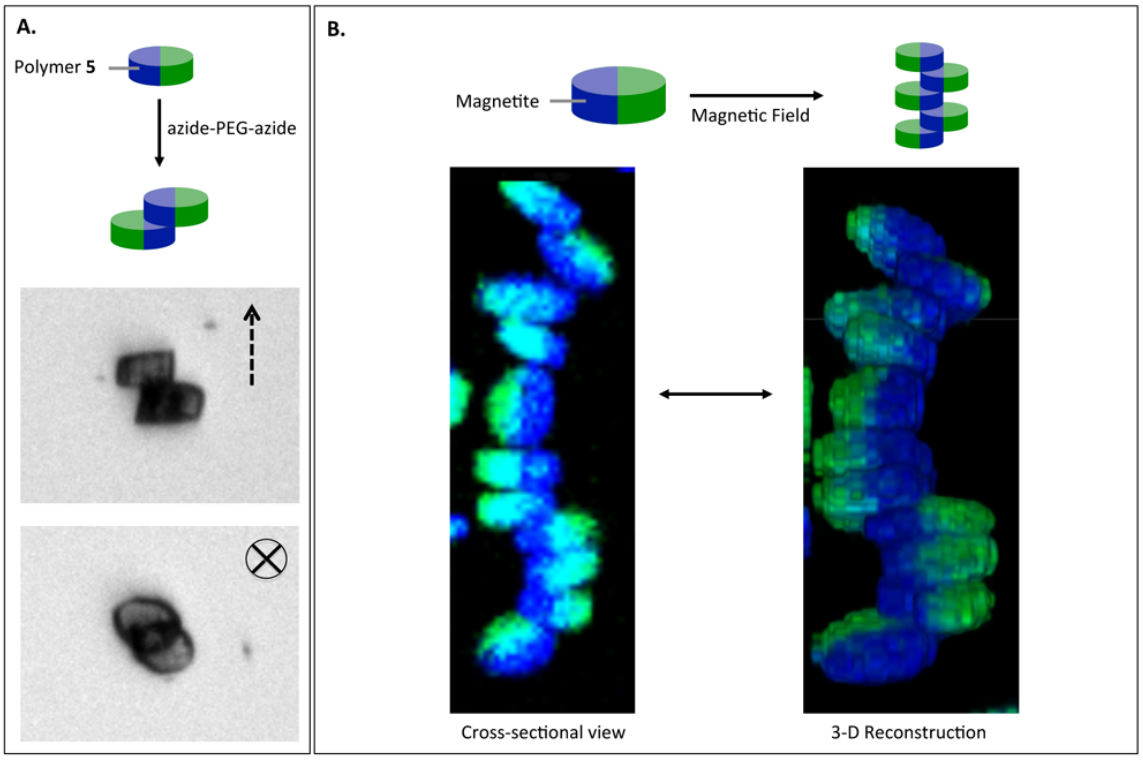

Figure 2-13: The self-assembly of anisotropic particles into permanent structures. (A) Particles containing polymer **5** and iron oxide nanoparticles are aligned in a magnetic field, cross linked using azide-PEG-azide, and their stability under varying magnetic field directions is shown. (B) Longer self-assembled permanent structures and their three-dimensional reconstruction.

molecules through copper free click chemistry with the cyclooctynes in polymer **5**. Figure 2-13A demonstrate the stability of these particles under varying directions of the external magnetic field (arrow pointing up signifies an upward magnetic field and the 'x' signifies a magnetic field pointed into the page). Looking at longer assemblies of these structures (Figure 2-13B), it can clearly be seen that the particles are assembled in a semi-chiral orientation around an axes, which in this case is the blue connecting compartment. This can also be seen in the three-dimensional reconstructions of these particles.

2.4 Summary

In conclusion, we have demonstrated a novel approach towards microparticles with fully orthogonal surface patches that takes advantage of a combination of novel chemically orthogonal polylactide-based polymers and their processing via electrohydrodynamic co-jetting to yield unprecedented multifunctional microparticles. These and other microstructured particles are highly sought after for their potential to present multiple distinct ligands in a directional manner. Applications may range from novel gels and particle self-assembly to use as carriers for cancer therapies with synergistic targeting effects from complementary ligands. For many of the above-mentioned applications, smaller particles are required. While designed as a proof-of-concept study to establish the feasibility of orthogonal reaction strategies on multivalent particles, future work will need to focus on refining critical particle characteristics, such as size or shape, while maintaining the same precision with respect to compartmentalization and spatially controlled surface modification. However, we have already shown that simpler versions of multi-patch particles can be made as small as 200 nm.[43] It is thus plausible that future work can access similar size ranges with the type of orthogonal multi-patch particles described in this study.

CHAPTER 3

Programming Physical Properties of Particles

The material in this chapter has been adapted with minor modifications from the following articles:

(1) S. Rahmani, T.-H. Park, A. F. Dishman, J. Lahann, "Multimodal Delivery of Irinotecan from Microparticles with Two Distinct Compartments", *J. Control. Release,* **2013**, 172, 239-245.

(2) S. Rahmani, A. F. Dishman, R. Hartmann, A. C Misra, W. Parak, J. Lahann, "Multicompartmental Nanoparticles and Their Characterizations", *In preparation*

3.1 Motivation and Background

In addition to surface properties, the physical properties of a carrier system can have profound influence over its fate in the body and the overall outcome of the treatment.[2] Extensive studies have demonstrated that physical properties, such as size, shape, texture, and charge can control carrier half-life, targeting, cell interactions, metabolism, and excretion from the body.[138] For example, the size of particles can affect drug loading, protein interactions that can increase/decrease the rate of opsonization, cell interactions with the MPS that could lead to lower/higher uptake and longer/shorter

circulation times, employ passive targeting using the enhanced permeation and retention (EPR) effect, or control the rate and extend of tumor penetration.[1, 9] On the other hand, the shape of particles can affect cellular uptake, flow dynamics in the blood, penetration into tumors, and excretion from the body.[139, 140] Due the importance of physical characteristics on the functional abilities of a carrier system, this chapter focuses on developing strategies for controlling such properties.

3.2 Experimental Methods

3.2.1 Materials

Dextran, chloroform, dimethylformamide (DMF), dimethyl sulfoxide (DMSO), pyridinium *p*-toluenesulfonate, 2-methoxypropane triethylamine, acetic acid, sodium acetate, phosphate buffered saline (PBS), poly[tris(2,5-bis(hexyloxy)-1,4-phenylenevinylene)-*alt*-(1,3-phenylenevinylene) (PTDPV), poly[(*m*-phenylenevinylene)-*alt*-(2,5-dihexyloxy-*p*-phenylenevinylene)] (MEHPV), ethyl amine, bromoacetyl bromide, dimethyl amino pyridine, benzyl alcohol, l-lactide, tin (II) ethyl hexanoate, anhydrous toluene, palladium 10% wt. on activated carbon, anhydrous tetrahydrofuran (THF), N-(3-Dimethylaminopropyl)-N'-ethylcarbodiimide hydrochloride (EDC), and tween 20 were used as purchased from Sigma Aldrich, USA. Polylactide-*co*-glycolides (PLGA) with ratios of 50:50 lactide to glycolide and a molecular weight of 17 or 44 kDa was purchased from Lactel Corporation. Irinotecan was purchased from Ontario Chemicals and O-benzyl-L-serine was purchased from Alfa Aesar. Sulfuric acid,

acetonitrile, sodium nitrite, dichloromethane, sodium carbonate, N-hydroxysulfosuccinimide (Sulfo-NHS), and acetone were purchased from Fisher Scientific. Diethyl ether was purchased from Acros Organics. Hydrogen was provided by Cryogenic Gases.

3.2.2 Fabrication of Particles with Various Shapes.

Particles with various shapes (rods, RBC shaped, & flat disks) were fabricated through the EHD co-jetting technique by changing different parameters such as concentration, flow rate, and molecular weight of the jetting solutions. Specifically, RBC shaped particles were jetted using a PLGA 85:15 (50-75 kDa) at a concentration of 7% w/v and a flow rate of 1 ml/hr. Flat disks were jetted using the same polymer but at a lower concentration of 4% w/v and a flow rate of 0.6 ml/hr. Rods were fabricated using a lower molecular weight PLGA (50:50, 17 kDa) at a concentration of 5% w/v and a flow rate of 0.1 ml/hr.

3.2.3 Fabrication of Particles with Controlled Texture.

Fabrication of Particles with Different Degrees of Roughness

Particles with the same jetting formulation (for RBC shaped particles) were jetted in different environments with increasing levels of humidity.

Fabrication of Porous Particles

Acetal-modified dextran (polymer **8**) was synthesized as previously described by Fréchet, *et al*. The synthesis and analysis of the polymer was graciously done by Dr. Tae-Hong Park. The polymer was analyzed via IR and NMR spectroscopy to confirm the presence of the appropriate functional groups and polymer purity. The analysis for the degree of protection and cyclic vs. noncyclic protection was done through NMR analysis. Jetting solutions used were a 97:03 ratio of chloroform to DMF and a polymer concentration of 15% w/v. For compartments that contained polymer **8**, 75% w/w of the total polymer was polymer **8** while the rest was PLGA. Microparticles containing polymer **8** in one compartment were tested for dextran deprotection and release in acidic and neutral conditions at physiological temperatures.

The neutral buffer (pH 7.4) used was PBS and the acidic buffer (pH 5) is a mixture of acetic acid and sodium acetate.[141] Both buffers contained 1% Tween 20 (v/v). Different aliquots were tested via the Bicinchoninic Acid (BCA, ThermoScientific) test to determine the amount of dextran released.

To impart porosity, fabricated anisotropic microparticles were suspended in neutral or acidic buffers, filtered through a 10 μm filter mesh, and placed in a 37^{o}C incubator. Samples were taken every five hours, washed 3-5 times with DI water, and imaged via SEM. Microparticle diameter measurements were done using Image-J software. More than 150 microparticles were measured per sample.

3.2.4 Fabrication of Particles with Controlled External Charge

Particles containing polymer **8** (acetal dextran) were fabricated according to 3.2.3. Particles containing polymer **2** (3-Hydroxyl PLGA), were jetted with a 10% w/v solution at 0.4 ml/hr, where the percentage of polymer **2** in one compartment was increased from zero to 100%. To determine the surface charge of these particles, each set was dispersed in DI water with 0.01% Tween 20 (v/v) and their zeta potential was measured with a Malvern Zetasizer in triplicates.

3.2.5 Fabrication of Nanoparticles and Their Separation via Centrifugation

Nanoparticles were fabricated using a 17 kDa PLGA (50:50) at 10% w/v with different solvent ratios of chloroform and DMF. The addition of cetyl trimethylammonium bromide (CTAB) at 5% w/v was used in some cases to reduce the size of the particles. The flow rate used was 0.1 ml/hr. To separate the particles into uniform size ranges, serial centrifugation at 9400 RCF and at various durations (1, 10, 20, and 30 minutes) was used to isolate specific size ranges.

3.2.6 Determining Ligand Density on the Surface of Nanoparticles

Nanoparticles containing polymer **6** at 25% w/w, PLGA at 75% w/w, and CTAB at 5% w/v with a solvent ratio of 97:3 Chloroform:DMF were fabricated and separated into monodispersed 100 nm nanoparticles. The nanoparticles were analyzed with Nanosight to determine their size distribution and concentrations, and thereby their effective surface area. The particles were then incubated with 0.01, 0.1, or 1 mg of azide-PEG-FITC to react with the alkyne groups on the particles via copper catalyzed click reaction. The unreacted material was removed from the sample after centrifugation to pellet the particles, and was measured using a UV visible Spectroscopy. The concentration of the unreacted material was determined using a calibration curve with the azide-PEG-FITC.

3.2.7 Nanoparticle for Biodistribution Studies

Nanoparticles were fabricated using a phenol-containing polymer (poly (4-vinylphenol-*co*-methyl methacrylate) (25% w/w), PLGA 40 kDa (50% w/w), and polymer **6** (25% w/w) to make particles that had dual functionalities. The flow rate used was 0.1 ml/hr. After fabrication, the nanoparticles were collected in PBS and 1% v/v Tween 20, separated via centrifugation (10 min samples were used), and PEG-ylated using an azide-PEG eight arm star (40 kDa, 10 mM) via copper catalyzed click chemistry. The particles were analyzed via DLS & Nanosight to determine their size

distribution & concentration. The nanoparticles were radiolabeled with I^{125}, purified, and then injected intra-orbitally into mice by the Muzykantov group at the University of Pennsylvania. Animals were sacrificed at 1, 4, and 24 hours and the biodistribution of the nanoparticles in the specific organs were measured using a TCA assay and a Wallac 1470 Wizard gamma-counter, as previously published by Muzykantov, et. al.[142]

3.2.8 Fabrication of Hydrogel Nanoparticles

Hydrogel nanoparticles composed of human albumin and PEG were fabricated using the EHD co-jetting technique. The solutions used were a human albumin concentration of 2.5% w/v; 10-30% w/w NHS-PEG-NHS as the crosslinker; and DI water and ethylene glycol as the solvents at a ratio of 4:1. After jetting, the particles were incubated in a 37^{o}C incubator for a week to ensure complete crosslinking of the albumin and NHS-PEG-NHS, before collecting them in DI water or PBS for further analysis. The size distribution of the dry particles was analyzed based on SEM images (ImageJ), and their size distribution in various solvents (DI water, PBS, and pH 5 buffers) were done using DLS and Nanosight analysis.

3.2.9 Fabrication of Nanoparticles for Potential Self-Assembly Applications

Nanoparticles with PMMA (poly (methyl methacrylate), 15 kDa), PtBMA (poly (tert-butyl methacrylate), 20 kDa), and biphasic particles with each polymer in a separate compartment were fabricated via EHD co-jetting. The concentrations and solvents used for each are as follows: i) PMMA nanoparticles with 5% w/v polymer, 2.5% w/v CTAB, 7:3 ratio of chloroform: DMF, and a flow rate of 0.1 ml/hr; ii) PtBMA nanoparticles with 5% w/v polymer, 2.5% w/v CTAB, 8.5:1.5 ratio of chloroform: DMF, and a flow rate of 0.1 ml/hr; iii) PMMA/PtBMA Janus particles by using each formulation separately in a distinct compartment. The nanoparticles were collected in DI water, separated via centrifugation (4000 RPM for 6 hours), and their size distribution and concentration were analyzed with DLS and Nanosight.

3.3 Results and Discussion

Fabrication of Particles with Various Shapes

The fabrication of particles with programmable physical properties were done by changing the various EHD co-jetting parameters, such as polymer molecular weight & concentration, flow rate, dielectric constant, viscosity, surface tension, external humidity, and the incorporation of charged species. To begin, we were interested in the fabrication of particles with a diverse set of shapes as this property has been well-established as a major factor in cellular uptake and clearance from the body.[139, 140] As demonstrated in

Figure 3-1, particles geometries including flat disks, red blood cell (RBC) shaped particles, and rods were fabricated by changing the concentration, flow rate, and molecular weight of the polymers use. To fabricate flat disks, PLGA 85:15 with a molecular weight of 50-75 kDa was used at a concentration of 4% w/v with a rapid flow rate of 0.6 ml/hr. As a comparison, using the same polymer at a 6.5% w/v concentration and 0.2 ml/hr has previously been shown to result in microspheres.[68] The change from microparticles to flat disks occurs due to the lower concentration of the polymer used (less chain entanglement) and the high flow rate, which results in the droplet's non-uniform drying procedure. Here, an outer solid layer of polymers on the surface of the

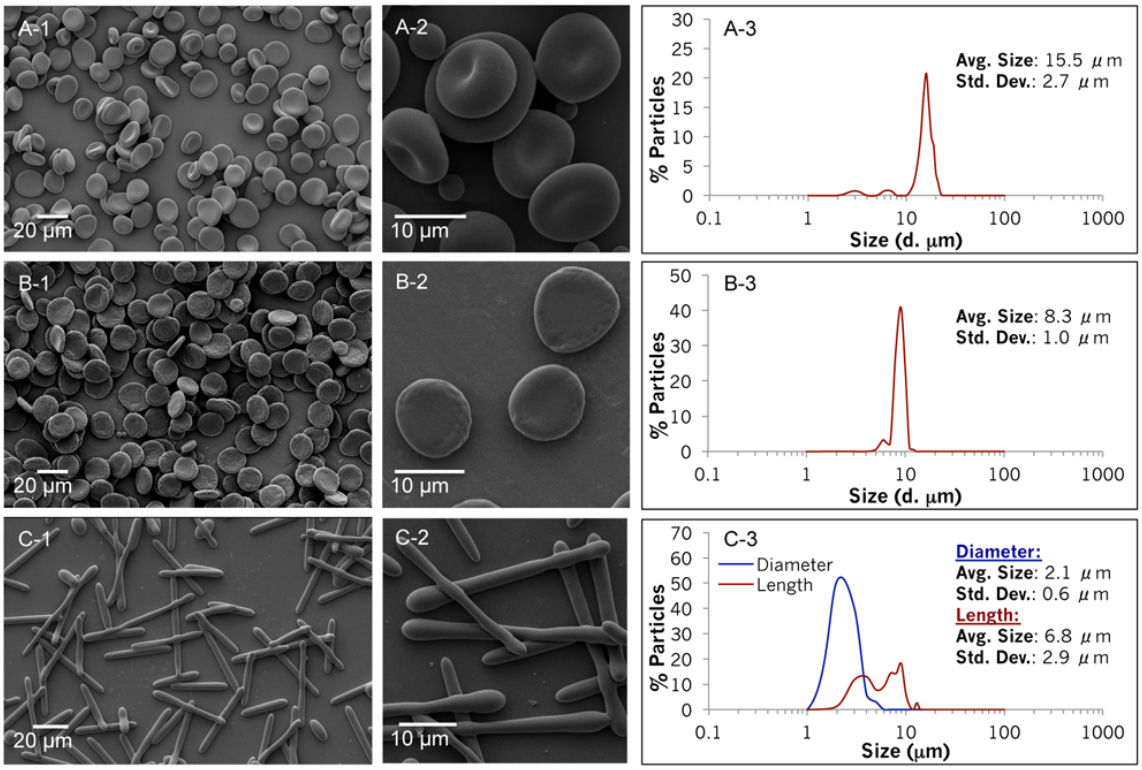

Figure 3-1: Particles with various shapes were fabricated. (A) SEM images of RBC particles (A-1 & 2) and their corresponding size distributions (A-3). (B) SEM images of flat disks (B-1 & 2) and their corresponding size distributions (B-3). (C) SEM images of rods and their corresponding size distribution where the blue represents the diameter measurements of the rods and red their corresponding length (C-3). The average size and standard deviation for each sample is also listed. All size measurements were done based on SEM images using ImageJ analysis.

particles is first formed before the solvents in the center have evaporated, thereby creating a void in the center. This together with the high flow rate means that the droplets contact the substrate before they are uniformly dried, which results in their collapse into a disk at the point of contact.[68] For RBC shaped disks, a higher concentration of the same polymer (7% w/v) at a higher flow rate (1 ml/hr) were employed. Here, due to the higher concentrations, the particles have the chance to partially form into a sphere, but again, due to the high flow rate they undergo non-uniform evaporation throughout the particles and form into RBC shaped particles upon contact with the substrate. For fabrication of rods, a low molecular weight PLGA polymer (17 kDa) at a concentration of 5% w/v with a low flow rate of 0.1 ml/hr was used. The low molecular weight and concentration of the polymer together yielded a solution with low chain entanglement between the polymer chains, which would then not have enough time to form into individual droplets from the ejected stream connecting the droplets before the rapid evaporation of the solvents, thus forming rods instead. The shapes of each set of particles were observed with SEM imaging (Figure 3-1 A-C1&2) and their size distribution and average size and standard deviation were determined using ImageJ analysis. For the rods, the diameter and the length of the particles were both quantified.

Fabrication of Particles with Different Textures

In addition to controlling the shape of the particles, we were also intrigued by the possibility of controlling the texture of such particles due to its influence in carrier-cell interactions. Here, we have explored establishing control over the texture of the particles in terms of the surface roughness and the degree of porosity in the particles. An aspect to

consider in fabricating such particles is the effect of the external environment, especially humidity, on the composition of the particles (**Figure 3-2**). When keeping other parameters such as solutions used, flow rates, applied voltage, and environmental temperature constant, an increase in the humidity resulted in particles with a 'rough' surface (Figure 3-2B). The same solution jetted at a lower humidity resulted in smooth particles (Figure 3-2A). Having a higher percentage of humidity in the air reduces the rate of evaporation of the solvents used in the jetting solutions and the non-uniform evaporation results in the non-energetically favorable rough surfaces.

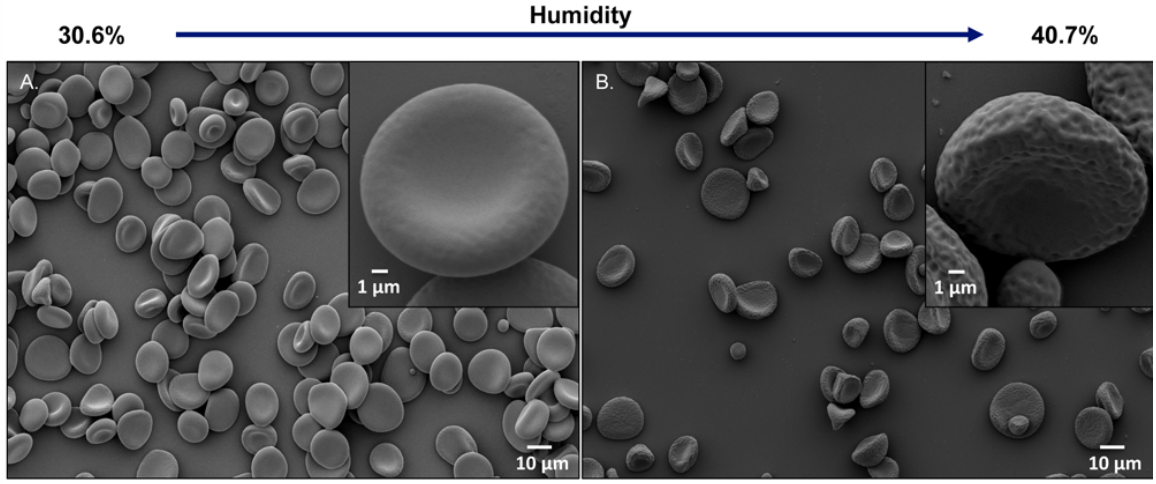

Figure 3-2: Fabricating particles with rough surface properties. The same jetting solution was used for both particle sets and the only variable used was an increase from 30.6% humidity (A) to 40.7% humidity (B) that resulted in particles with rough surfaces.

In addition to fabricating particles with rough surfaces, the fabrication of porous particles was also explored. Unmodified dextran polymers are water-soluble polysaccharides that have been used extensively in many biomaterial applications.[143] It is this water-solubility, however, that limits the broader use of dextran for drug delivery and tissue engineering, because drug carriers, implants, or scaffolds fabricated from dextran will dissolve in water within a matter of minutes.[144] Masking of the hydroxyl groups on

the backbone of the dextran polymer can render this polymer water-insoluble and thereby increase its applicability in this field. Depending on the type of chemistry used, this protection can be pH-responsive and, in so doing, a polymer that can be water soluble or insoluble upon demand can be synthesized.[141, 145, 146] In addition to PLGA, we have employed polymer **8**, as a pH responsive polymer that is water-insoluble at physiological pH, but water-soluble in acidic environments.[141] This change in solubility is caused by the hydrogen-catalyzed cleavage of the acetal groups that chemically protect the hydroxyl groups of the unmodified dextran (**Figure 3-3**). Here polymer **8** can potentially be used in the fabrication of pH sensitive carriers that can respond selectively to specific physiological or pathophysiological cues such as the extracellular matrix surrounding tumors or inflamed tissue.[147, 148] Such possible applications of this polymer are further

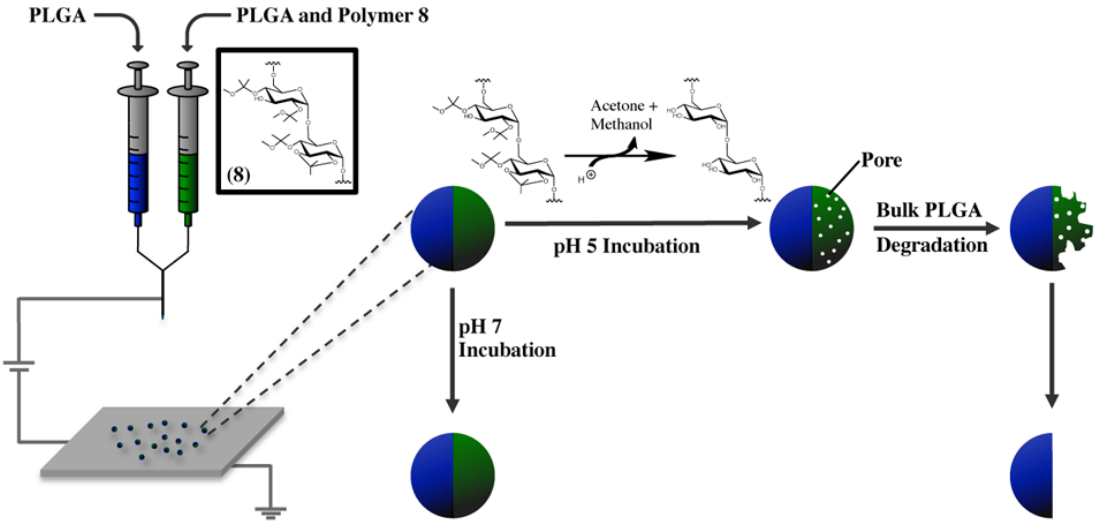

Initial Polymer Molecular Weight	Degree of Protection	Cyclic vs. Non-Cyclic Protection
Low MW P. Dextran	75%	1.1:1

Figure 3-3: Particle fabrication procedure and hypothesized structure of particles depending on pH of environment. The table contains the polymer characterization information of polymer **8**.

explored in Chapter 4 of this dissertation.

Polymer **8** was synthesized according to previously published procedures[141] and characterized by NMR analysis. Based on this analysis, approximately 75% of the hydroxyl moieties of the polysaccharide were protected with acetal groups. Among the protected moieties, the ratio of cyclic to non-cyclic units was approximately 1.1:1. This degree of protection resulted in a polymer that was water-insoluble in physiological pH, while retaining some of its polar characteristics due to the small amount of free hydroxyl groups present.

Upon confirmation of the polymer structure and characterization, we focused on the preparation of anisotropic microparticles from these polymer systems using the EHD co-jetting technique as described in Chapter 1 of this dissertation. To demonstrate this, we first fabricated bicompartmental microparticles containing a mixture of polymer **8** and PLGA in the same compartment. The bicompartmental microparticles containing polymer **8** were characterized by Confocal Laser Scanning Microscopy (CLSM) and Scanning Electron Microscopy (SEM), as demonstrated in **Figure 3-4**. The CLSM images indeed confirmed the bicompartmental geometry of the microparticles, which contained a "green" fluorescent dye (PTDPV) in the first compartment (Figure 3-4A) and a "blue" fluorescent dye (MEHPV) in the second (3-4B) compartment. Figure 3-4C is an overlay image of the two channels confirming that the dyes do not mix and that the microparticles are, therefore, composed of distinct compartments. The three-dimensional shape and size distribution of the microparticles was assessed by SEM (Figure 3-4D). Using the Image-J analysis software [149-151], it was found that the as-jetted microparticles

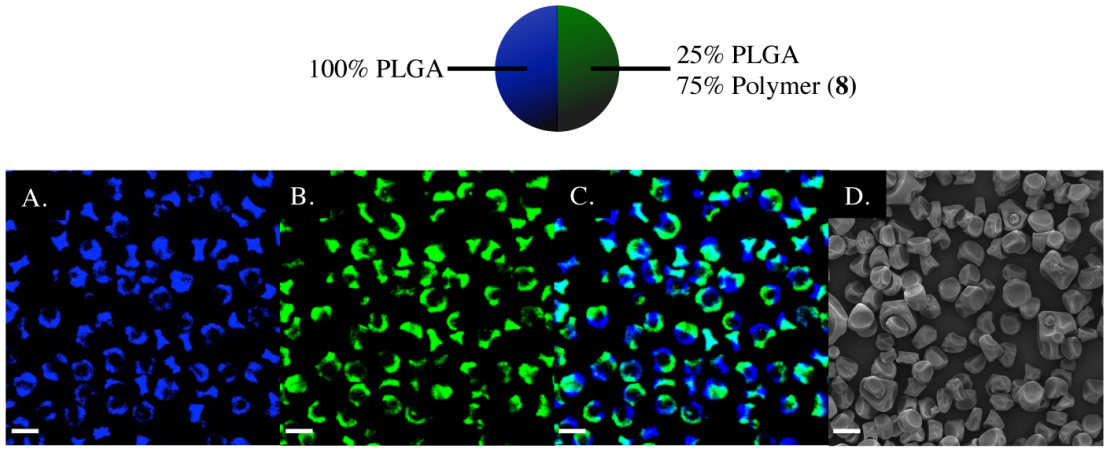

Figure 3-4: Characterization of microparticles containing polymer **8** + PLGA in one compartment and PLGA in the other compartment. A.-C.) Confocal images of the particles, where A.) is the blue channel (PLGA compartment), B.) is the green channel (PLGA + polymer **8** compartment), and D.) is the overlay of the two images. E.) SEM image of the particles showing their three-dimensional shape and size.

are approximately 8.4 ± 0.07 μm in diameter on average, with few, larger microparticles at 10-15 μm that were easily removed via filtration.

To verify the anisotropic nature of these microparticles and their ability to selectively respond to environmental changes, microparticles were incubated in two different pH environments, pH 5 and pH 7.4, at physiological temperatures and the release of free dextran and its effect on the structure of the microparticles was quantified. As illustrated in **Figure 3-5**, release of dextran was observed at acidic pH, while no dextran was released at pH 7.4, indicating that soluble dextran is released only in the acidic environment. The small burst release observed in the pH 7.4 sample is most likely due to a small fraction of polymer **8** with a lower level of protection that can make this polymer water soluble. Overall, these results confirm that a differential release of water-soluble dextran from our microparticles can be achieved.

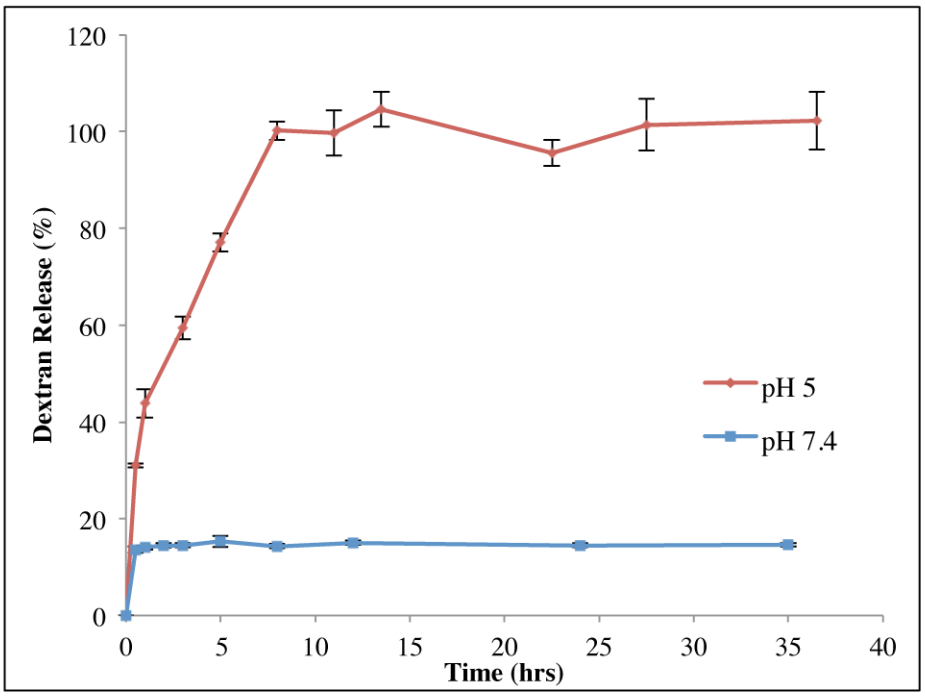

Figure 3-5: Release of dextran from bicompartmental microparticles. The release at two pH values, pH 5 and 7.4, are displayed.

To quantify the effect of dextran release on the structure of the microparticles, filtered microparticles (to remove a small fraction of larger microparticles) were incubated in two different pH environments (pH 5 and pH 7.4) at physiological temperatures and their degradation kinetics were monitored via SEM imaging (**Figure 3-6**). The initial dextran release studies (Figure 3-5) confirmed that the release of dextran was completed within 10 hours of incubation. Hence, the appearance of pores due to this release should be observed within that period, followed by rapid bulk degradation of the rest of the compartment (now composed of PLGA) due to the porous remaining network. Pores were observed within the first 10 hours of incubation: within 5 hours (Figure 3-6B) small pores covered one half of the microparticles in comparison to the control at pH 7.4 (Figure 3-6F). After 10 hours, larger pores were observed (Figure 3-6C), as all of the dextran was released. By this time, the size of the microparticles had also decreased and

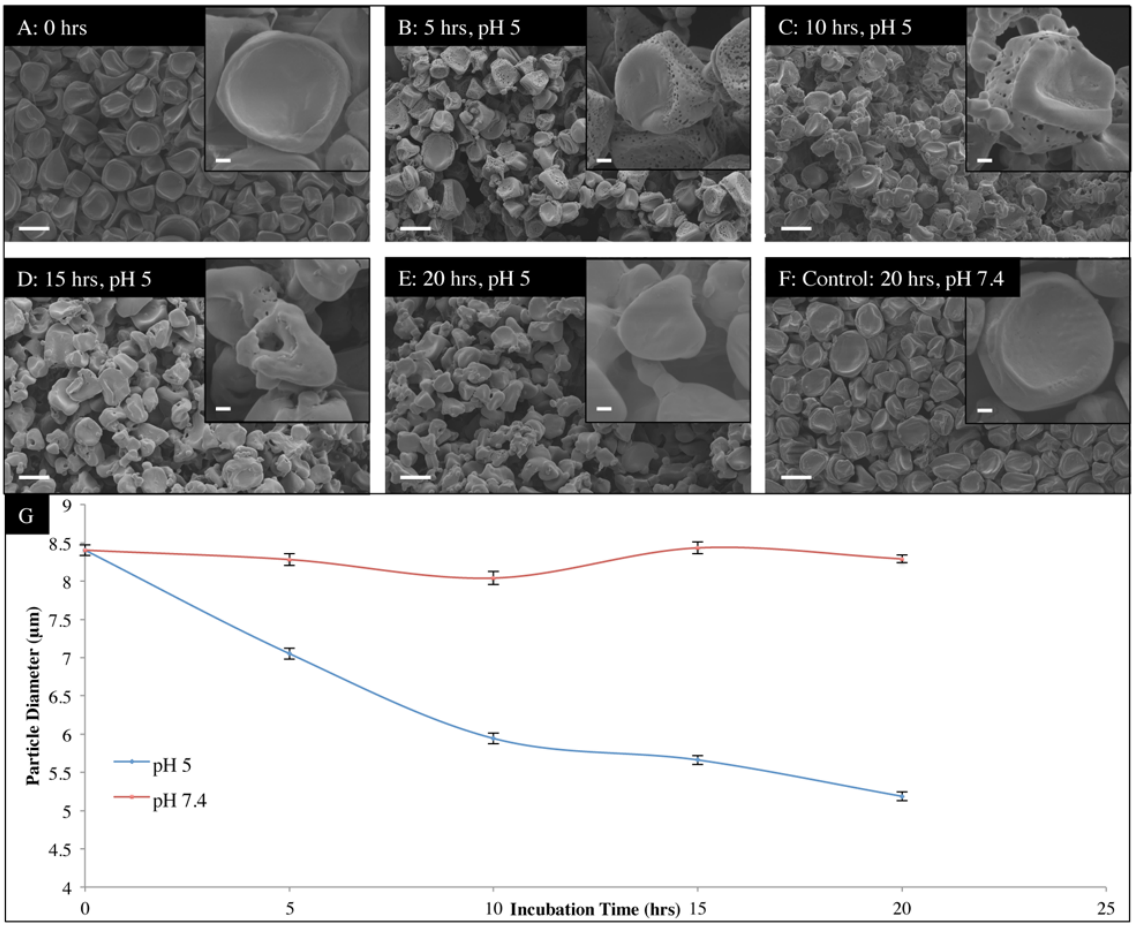

Figure 3-6: Characterization of polymer **8** containing microparticles in two different pH environments. A.-F.) SEM images of the microparticles over time in pH 5 and 7.4. G.) Change in the microparticle diameter over time based on ImageJ analysis.

bulk erosion of the PLGA material had begun. After 15 hours (Figure 3-6D) very few pores could be seen as most of the porous compartment had eroded away. Complete degradation of one side was observed within 20 hours (Figure 3-6E). In comparison, the same microparticles incubated at pH 7.4 for 20 hours (Figure 3-6F) remained intact and were approximately twice the size of those incubated for the same period in the acidic environment.

In order to quantify the results and confirm the complete and exclusive degradation of one compartment, the size of the microparticles as a function of time was

quantified using Image-J software [149-151]. The measurements were done based on SEM images taken of the microparticles at zero, 5, 10, 15, and 20 hours for both pH 5 and 7.4 incubations. As seen in Figure 3-6G, the pH 7.4 samples were consistent in size 8.29 ± 0.07 µm, while the pH 5 samples decreased to approximately 60% of their original size 5.18 ± 0.06 µm. Based on this analysis, as well as the SEM images, we have demonstrated the fabrication of anisotropic microparticles and control on the selective porosity of one compartment through stimuli responsive chemical degradation.

Fabrication of Particles with Controlled External Charge

To fabricate particles with an external charge hydrophilic polymers **2** and **8** were incorporated into the particles and their zeta potential measurements were measured. The hydrophilicity of polymer **8** can be attributed to the residual hydroxyl groups; while most hydroxyl groups are protected (75%), the polymer still retains enough free hydroxyl

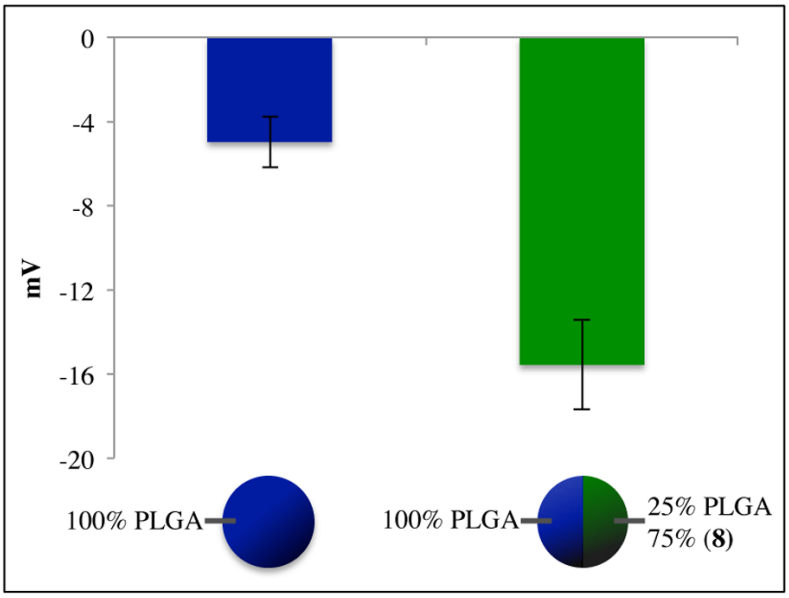

Figure 3-7: Zeta potential measurements of PLGA and PLGA + Polymer **8** containing microparticles.

groups to make the surface of the microparticles hydrophilic. This assumption was further supported by zeta potential measurements, which allowed for approximating the surface charge of the bicompartmental microparticles. The graph in **Figure 3-7** displays the differences in surface charge between pure PLGA microparticles and polymer **8** containing microparticles. PLGA microparticles have a zeta potential of -4.5 ± 1.2 mV, while polymer **8** containing microparticles have a more negative zeta potential measurement of -15.6 ± 2.1 mV. These results confirm that the polymer **8** containing microparticles are more hydrophilic and polar than PLGA microparticles due to the free hydroxyl groups present on their surface.

Similarly, particles containing polymer **2** with free hydroxyl groups were fabricated using the EHD co-jetting system. Three sets of particles with 0, 50, and 100% w/w of polymer **2** in one compartment and PLGA in the other compartment were jetted and their zeta potentials were measured. A decreasing level of zeta potential was observed for particles sets with increasing amounts of polymer **2** incorporation, as

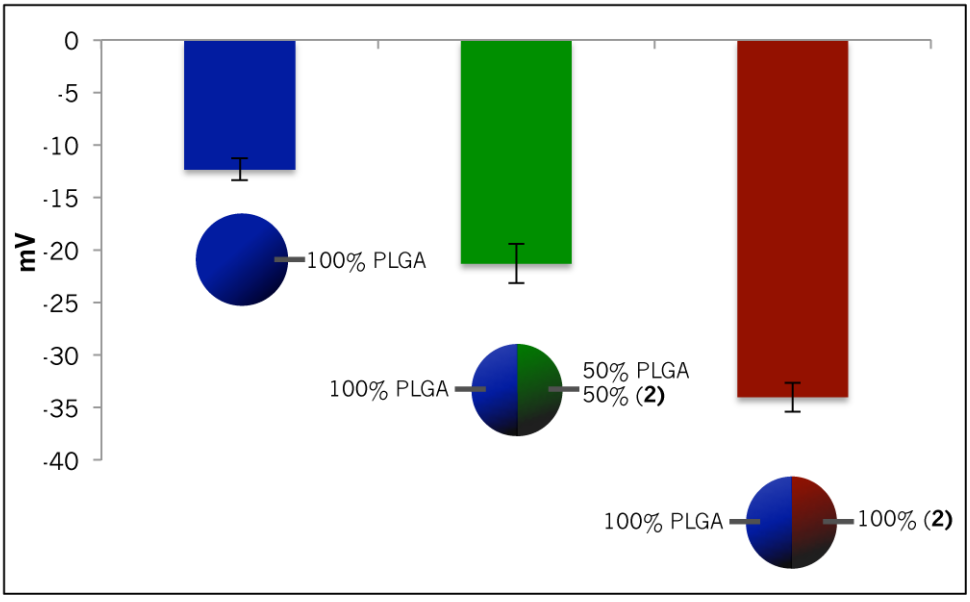

Figure 3-8: Zeta potential measurements of PLGA and PLGA + Polymer **2** containing microparticles.

expected (**Figure 3-8**). As a result, the control over the external charge of the particles depending on the polymers used was established using two types of functional polymers.

Fabrication and Analysis of Nanoparticles

Size is an important physical parameter for particles used in drug delivery applications due to their influence over circulation times, rates of opsonization, cellular uptake, passive targeting to tumors via the EPR effect, tumor penetration, and excretion from the body.[138] In the EHD co-jetting system several parameters, such as polymer molecular weight & concentration, solvent viscosity & dielectric constant, and applied voltage control the size and uniformity of particles ranging from micro- to nano-meters in diameter. One of the most common routes of fabricating nano-particles and -fibers through electro-spraying and -spinning, respectively, is the use of dilute polymer concentrations.[152] Accordingly, to fabricate nanosized particles using the EHD co-jetting technique, various solutions with dilute concentrations of a low molecular weight PLGA (4.1 kDa) were jetted (**Figure 3-9**). Based on these studies nanoparticles as small as 100-200 nm could be fabricated. However, due to the dilute concentration used, the yield of the nanoparticles were extremely low (as a reference, the images shown in Figure 3-9 were taken after 4-10 hours of jetting on the same substrate, where typically the entire sheet is covered with particles after approximately 30 minutes). As a result, other routes of fabricating nanoparticles were explored.

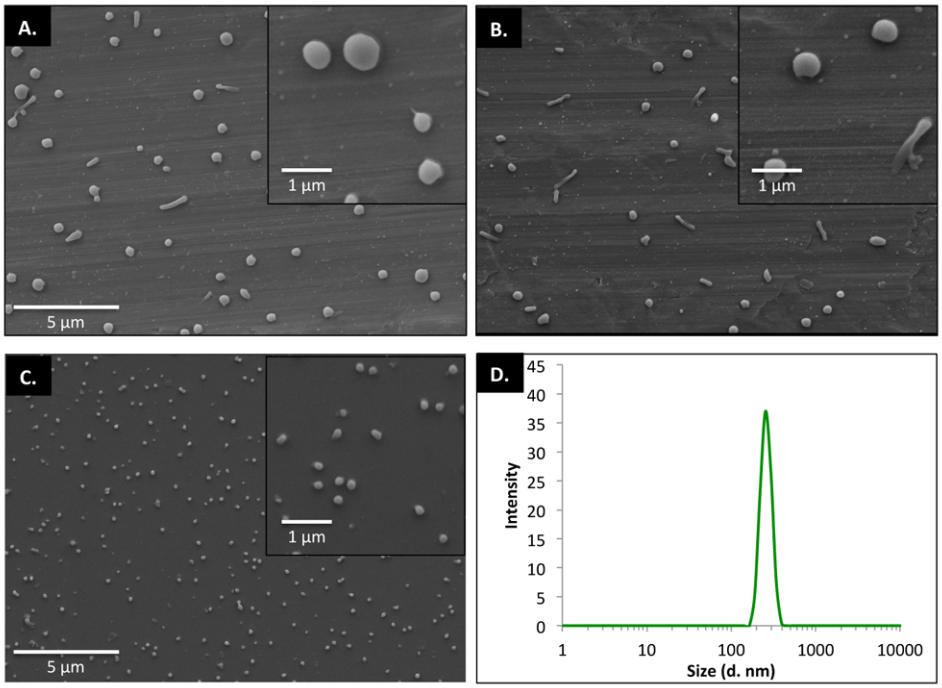

Figure 3-9: PLGA nanoparticles fabricated through the EHD co-jetting technique. PLGA concentrations of 1, 0.5, and 0.03% w/v in DMF (A-C respectively) were sequentially tested to determine the lower particle size range. (D) The DLS measurement of the nanoparticles in (C) were taken, which show an average diameter size of approximately 250 nm. This is larger than the observed size in the SEM images and is most likely due to aggregation of the nanoparticles.

The other parameters investigated for the fabrication of nanoparticles include the use of solvents with higher dielectric constants and surface tensions and the incorporation of charged species, which affected the dielectric constant and overall charge of the jetting solutions. The effect of each of these parameters, using the same polymer (PLGA 50:50, 17 kDa) and at the same concentration of 10% w/v, on particle size and their combined effect were subsequently studied. It was observed that a solvent ratio of 97:3 chloroform: DMF yielded polydispersed microparticles (**Figure 3-10A**), while the same solution with a solvent ratio of 1:1 chloroform: DMF yielded bimodal, yet uniform particles with one set of particles at approximately 50-150 nm and a second set at approximately 1 µm (Figure 3-10B). Alternatively, keeping the same ratio of solvents (97:3) but adding a

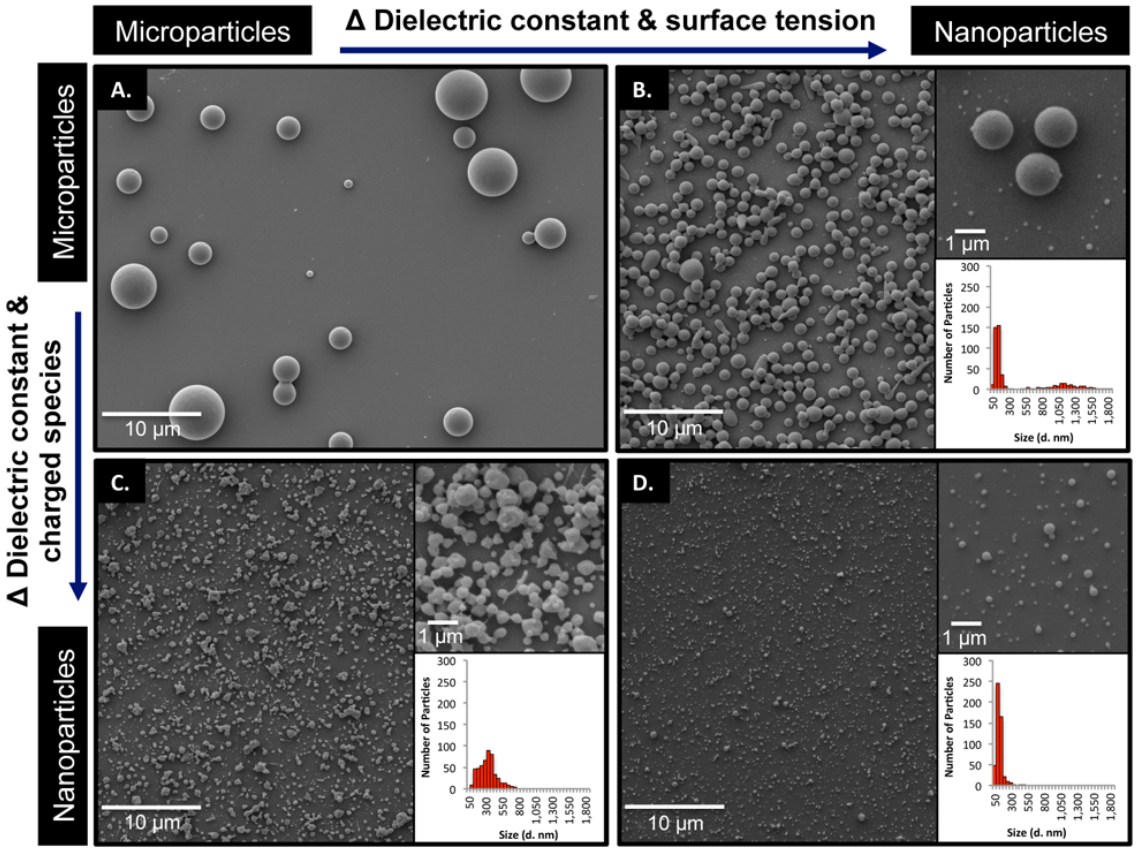

Figure 3-10: Using the same polymer (PLGA 50:50, 17 kDa) and concentration (10% w/v) particles ranging in size from the micrometers (A) to nanometers (D) were fabricated. By increasing the amount of DMF (higher dielectric constant and surface tension) instead of chloroform, polydispersed microparticles (A) could be downsized to bimodal particles where one set was at approximately 1 µm and one at 100 nm (B). Alternatively, by adding a charged surfactant (higher dielectric constant and charge) polydispersed microparticles (A) could be downsized to polydispersed nanoparticles ranging in size from 50-800 nm. Combining both higher DMF content and charged species resulted in monodispersed nanoparticles in the 50-150 nm range. The insets in each image represent the zoomed in image of the particles (top) and the size distribution of the particles based on Image J analysis of SEM images (bottom).

charged surfactant (CTAB) at 5% w/v resulted in a polydispersed population of nanoparticles ranging from 50-800 nm (Figure 3-10C). Combining these two parameters (particles with 5% CTAB addition and a ratio of 1:1 chloroform:DMF) resulted in monodispersed nanoparticles ranging from 50-150 nm in diameter (Figure 3-10D). The size distribution of the nanoparticles based on ImageJ analysis of SEMs are included as insets for each set of particles

Once the fabrication of nanoparticles using EHD co-jetting was established, we were interested in determining whether the particles were still compartmentalized. Due to the small size of the nanoparticles, super resolution Structured Illumination Microscopy (SIM) was used to determine the bicompartmental nature of the particles. Nanoparticles containing red and green dyes in separate compartments were jetted using 5% w/v CTAB and a 97:3 ratio of chloroform: DMF. The particles were then imaged (**Figure 3-11**) via SIM imaging, which clearly confirms the compartmentalized nature of the nanoparticles.

In addition to fabricating monodispersed nanoparticles, the separation of a single polydispersed sample into uniformly sized fractions can be of interest, especially since it

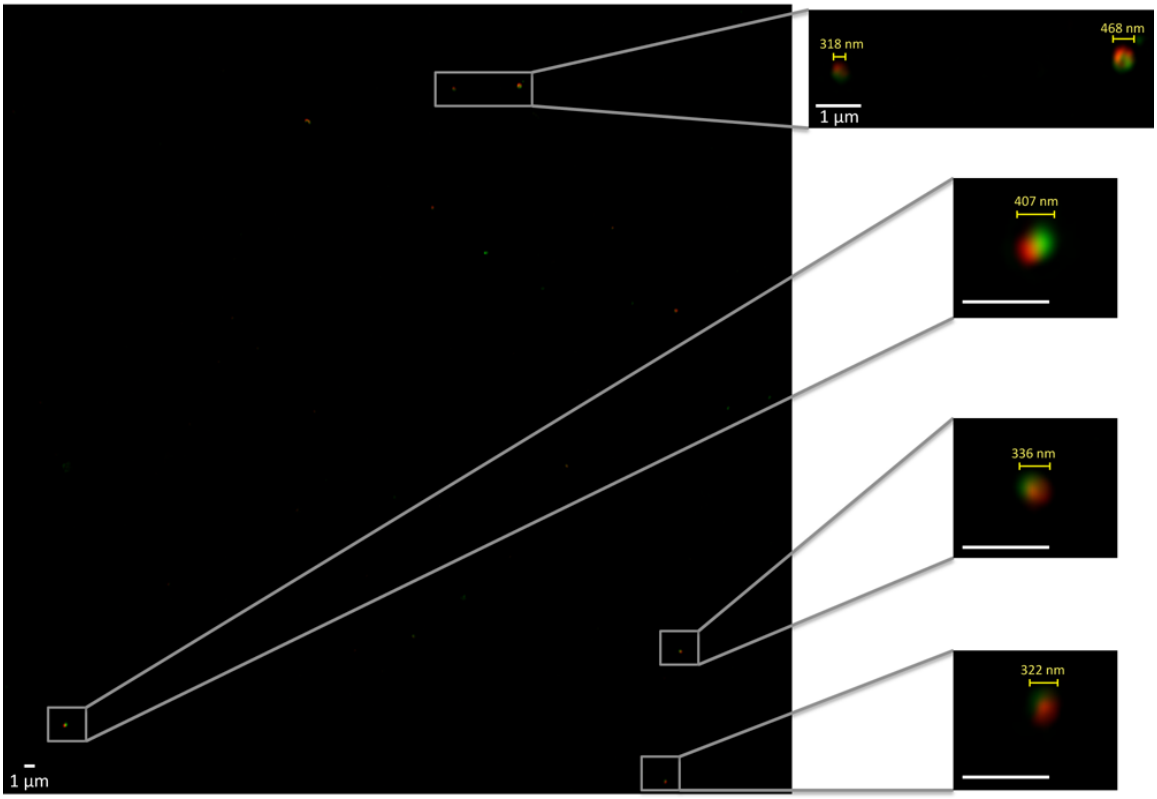

Figure 3-11: Super resolution Structured Illumination Microscopy (SIM) analysis of nanoparticles. Particles with a green dye in one compartment and a red dye in the second compartment were jetted using a 5% incorporation of CTAB and a 97:3 ratio of solvents chloroform:DMF. The insets on the right are individual particles zoomed out image on the left.

allows for the side-by-side testing of nanoparticles from the same batch (same material and physical characteristics) but with different size ranges. This fractionation can be achieved by using serial centrifugation (**Figure 3-12A**), where a polydispersed sample of particles (here the sample in 3-10C) is centrifuged at 9400 RCF (relative centrifugal force) for increasing times to pellet increasingly smaller particles. The size distribution of several fractions (1, 10, 20, and 30 minutes) are shown in Figure 3-12B and a SEM image of the 30 minute sample is shown in Figure 3-12C.

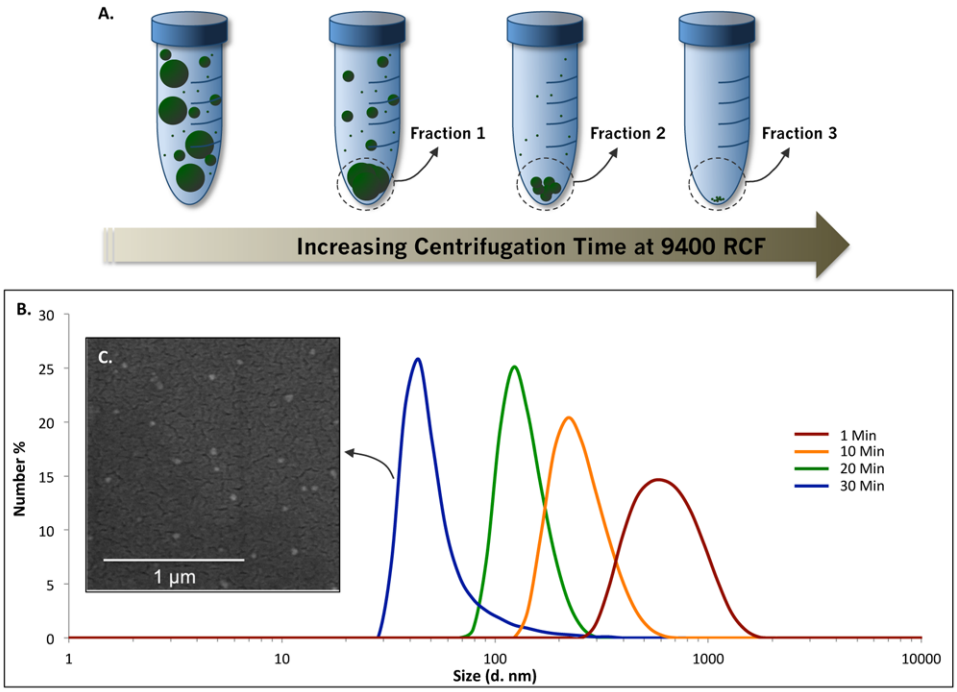

Figure 3-12: Separation of a polydispersed group of nanoparticles into monodispersed fractions using serial centrifugation. (A) Schematic displaying serial centrifugation. (B) Size distribution of different fractions (1, 10, 20, and 30 minutes) based on DLS measurements and (C) a representative image of uniform 50 nm particles from the 30 minute sample.

Towards Multifunctional Nanoparticles

With the establishment of the fabrication and purification of nanoparticles into uniform size ranges, the use of these techniques in addition to those outlined in Chapter 2

were explored for the fabrication of multifunctional nanoparticles. To begin with, the ability to functionalize the surface of nanoparticles with ligands and the density of such ligands on the surface was determined (**Figure 3-13**). This information can be of interest in determining the density of stealth and targeting molecules on the surface of nanoparticles, especially when multi-valency experiments with respect to the effect of the number of ligands on circulation or targeting is of interest. Nanoparticles with polymer **6** were fabricated and purified into an approximately 100 nm fraction (Figure 3-13C). These alkyne-functionalized nanoparticles were then incubated with 0.01, 0.1, 1 mg of azide-PEG-FITC and the surface of these particles was functionalized with this molecule through copper catalyzed click chemistry (Figure 3-13A). The nanoparticles were then pelleted via centrifugation and the unreacted azide-PEG-FITC was removed and

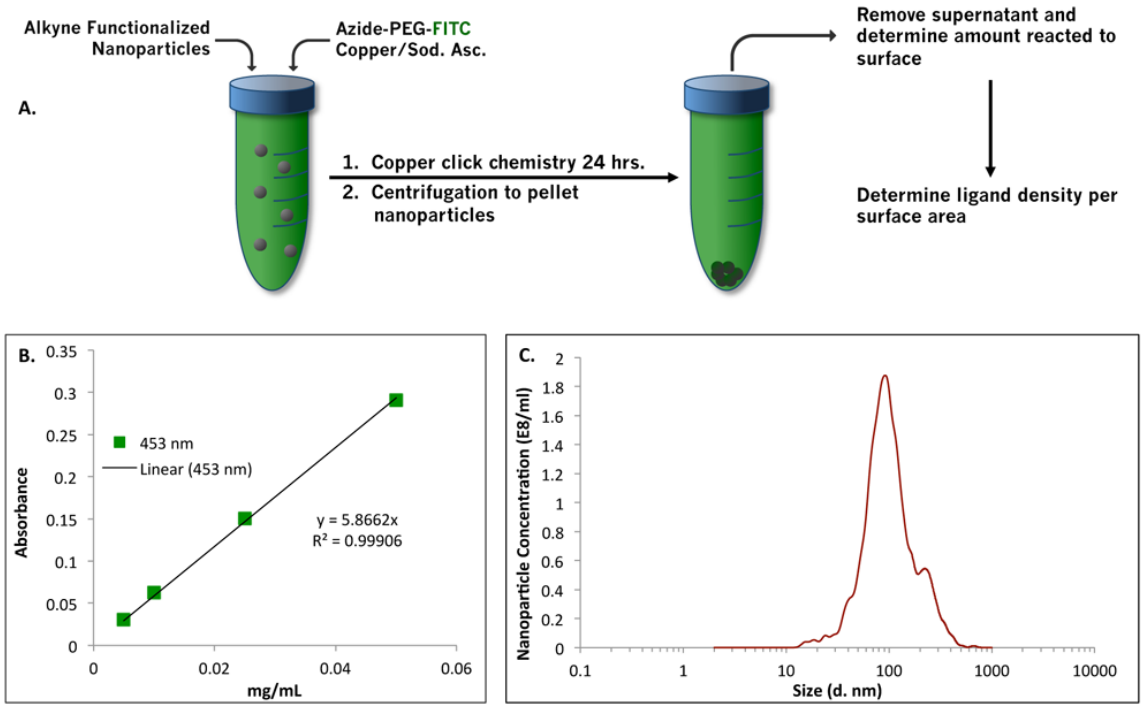

Figure 3-13: Functionalizing the surface of nanoparticles with azide-PEG-FITC to determine the ligand density per surface area. (A) Schematic displaying methods used. (B) Calibration curve of azide-PEG-FITC at different concentrations using UV visible spectroscopy and (C) the size distribution of the nanoparticles as a function of concentration.

measured via UV visible spectroscopy based on a previously established calibration curve (Figure 3-13B).

Based on this information, the total amount attached to the nanoparticles and the total surface area of the nanoparticles could be calculated, where the amount of azide-PEG-FITC attached is the total amount incubated subtracted by the amount removed at the end of the experiment and the total surface area of the nanoparticles can be calculated based on the known diameter and the concentration of nanoparticles at each given diameter. Together, this data was used to plot the ligand number per nm^2 of the nanoparticles (**Figure 3-14**). As expected, the ligand number per surface area increases with increasing concentration used for the surface modification from 0.02-6.04 ligands per nm^2. This data corresponds well with other reported data in the literature that range from 4.2-28.5 ligands per nm^2 depending on the particles, chemistries, and techniques used.[153, 154] Repeating the same experiments with particles with only one compartment

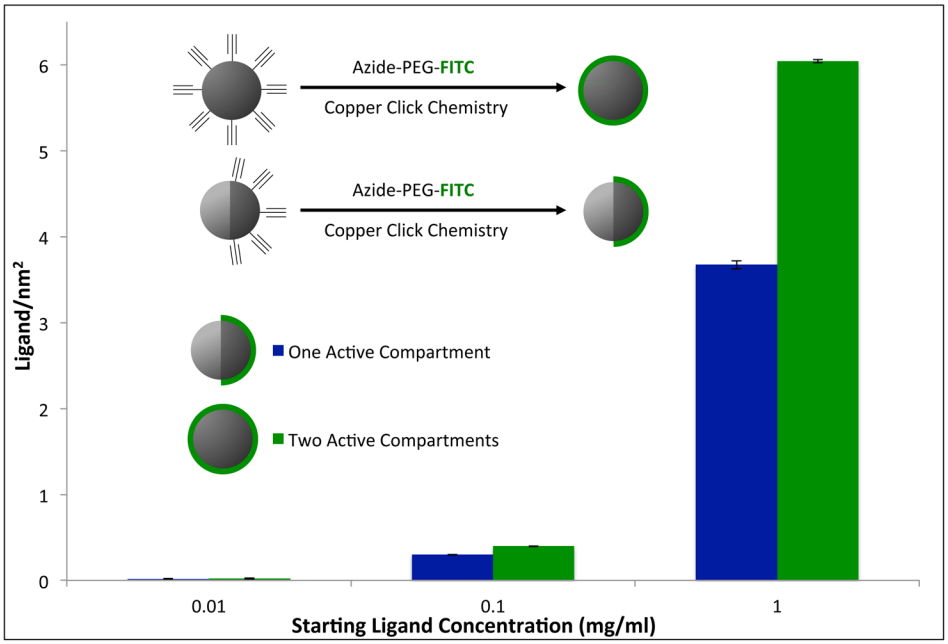

Figure 3-14: Ligand density determination on the surface of nanoparticles. The ligand density per nm^2 is graphed based on the nanoparticle used (one or two active compartments) and the starting concentration of ligands incubated for the reaction.

containing the active ligand (alkyne), a distinct difference at the higher concentrations closer to the saturation point of the functional groups on the surface can be observed. This data further confirms the compartmentalization of the functional polymers and their surface ligands on the multicompartmental nanoparticles.

With the establishment of surface modifications on nanoparticles and an estimate of the PEG ligands on their surface, we were interested in using this information to functionalize the surface of nanoparticles for biodistribution studies in animals. Nanoparticles containing polymer **6** for surface functionalization with an eight-armed PEG and a phenol-containing polymer for radioactive labeling with I^{125} were fabricated. The base polymer used (50% w/w) was PLGA and each of the functional polymers were present at a 25% w/w in the nanoparticles. The route used for the functionalization of the nanoparticles, SEM images directly after fabrication, and their size distribution before and after PEG-ylation with an eight-arm azide-PEG molecule is shown in **Figure 3-15**. The size distribution of the particles after separation was at approximately 140 nm, and this size was increased to approximately 200 nm with the addition of the PEG molecules (40 kDa) to the surface.

Further functionalization of the nanoparticles with I^{125} and their biodistribution in mice were done in collaboration with Prof. Muzykantov's group at the University of Pennsylvania based on previously published results.[142] Briefly, the nanoparticles were incubated with I^{125} and iodobeads to attach the I^{125} to the phenol groups of the nanoparticles through the electrophilic aromatic substitution where the iodione is inserted in the ortho position to the hydroxyl group of the phenol molecule.[142] The I^{125} substitution allows for the detection in animal models via gamma counters and I^{124} incorporation can

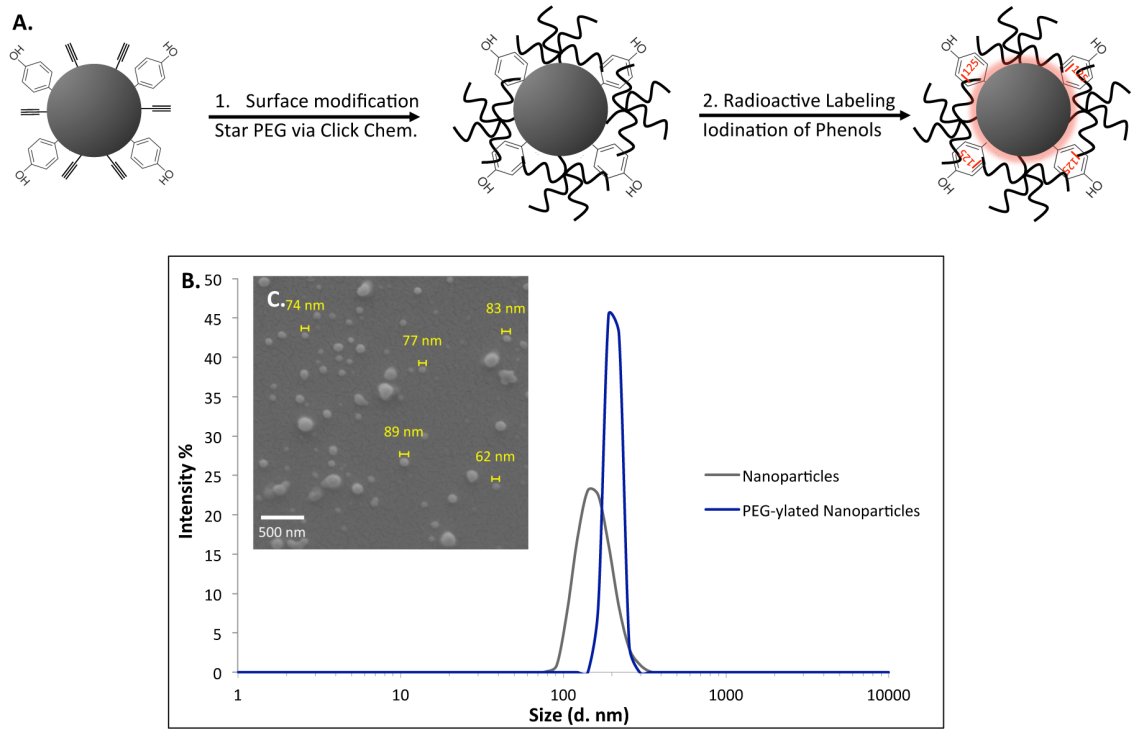

Figure 3-15: Functionalization of nanoparticles with star PEG and I^{125} for use in biodistribution studies. (A) Schematic outlining the steps taken to first surface functionalized the nanoparticles with star-PEG-azide via copper catalyzed click chemistry and the subsequent radioactive labeling of the phenol groups. (B) DLS measurements of nanoparticles before and after PEG-ylation and (C) the as-fabricated nanoparticles with a size range of 60-150 nm.

be used for the detection of beta emitters using PET (positron emission tomography) or SPECT (single photon emission computer tomography) imaging. After attachment, the nanoparticles are purified from unreacted material through multiple washes and centrifugations before inserting them into animals intra-orbitally. The animals (3 groups of 5 animals each) were sacrified at 1, 4, and 24 hour periods and their various organs were analyzed to determine the distribution of the nanoparticles within them as a function of the injected dose (ID) per mass of organ (g) (**Figure 3-16**). As a note, the animals were not perfused with a buffer before taking the measurements and each organ contained its respective blood supply. Not surprisingly, the majority of nanoparticles accumulate in the

liver and spleen, especially since these nanoparticles were not targeted to a specific site in the body. However, a not insignificant portion of the nanoparticles (approximately 4% ID/g) continued to circulate after one hour, which droped to 1.2% ID/g even after 24 hours. This distribution compares well with published results of similar nanoparticles fabricated through the double emulsion technique where less than 1% ID/g of PEG-ylated nanoparticles were seen after 12 hours.[155]

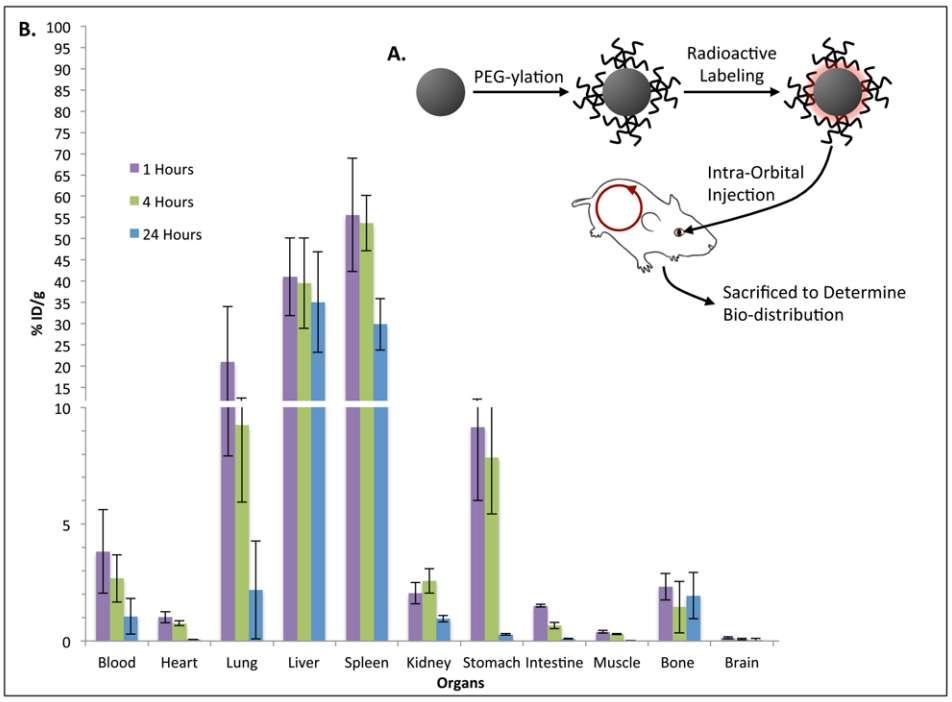

Figure 3-16: Biodistribution of the nanoparticles in mice. (A) Schematic of the particle fabrication method and intra-orbital injection into mice and (B) the biodistribution of the nanoparticles (% Injected Dose (ID) per gram of tissue) for individual organs.

Fabrication of Hydrogel Nanoparticles

In addition to fabricating biodegradable nanoparticles using PLGA derived polymers, the possibility of producing biocompatible hydrogel nanoparticles was explored. Hydrogel nanoparticles have the benefit of being hydrophilic, pH responsive, flexible, and biocompatible given the materials used to synthesize them.[156] Here,

nanoparticles composed of human serum albumin and NHS-PEG-NHS were fabricated. The NHS-PEG-NHS molecules acted as the cross-linker in the nanoparticles where the various albumin molecules were connected via their free amine-groups to each other. Albumin and PEG were chosen due to their biocompatibility and their low opsonization rates in the body.[1] It was observed that uniform nanoparticles with an average diameter of 125 nm could be fabricated in high yields through this process (**Figure 3-17**). This size increased to 300-400 nm in a buffered solution at pH 7.4 and an increased swelling in size to 600-700 nm could be achieved by reducing the pH of the solution to 5 (Figure 3-17C). This could be of interest when fabricating nanoparticles for endosomal escape (pH of 4-6) or targeted release of therapeutics near tumor tissue or inflamed sites where the pH is significantly lower than the physiological range.[147, 148]

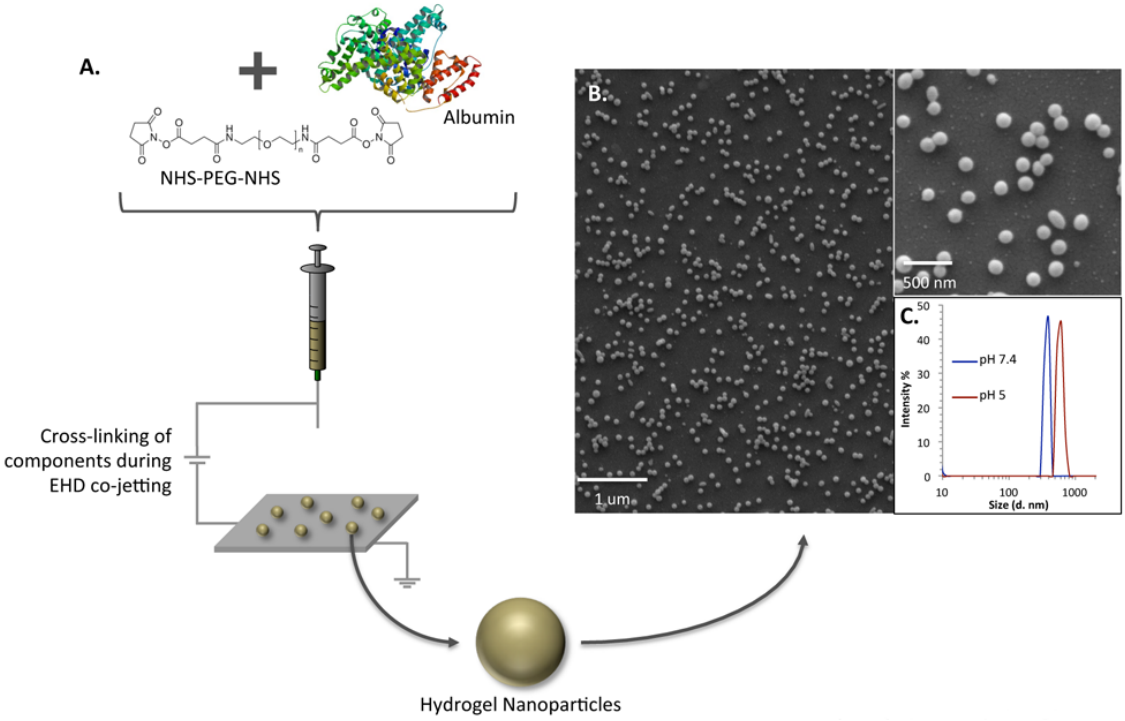

Figure 3-17: Fabrication of hydrogel nanoparticles. (A) Schematic of nanoparticle fabrication from albumin and NHS-PEG-NHS via EHD jetting. (B) SEM images of uniform nanoparticles and (C) their size distribution in various pH buffers.

One of the unique aspects of hydrogel nanoparticles is their tunability with respect to their size, swelling properties, and loading. Here their swelling properties as a function of increasing cross-linker concentration was explored. As displayed in **Figure 3-18** an increase in the cross-linker density does not significantly affect the dry-state size of the nanoparticles (Figure 3-18 A-C SEMs and D size distributions), but has a significant affect on their size distribution in a buffered solution (Figure 3-18E). The size of the nanoparticles can be controlled by increasing their cross-linker density from approximately 400 nm to 180 nm. This can have important implications in terms of the release of payloads as well as their functionality within the body depending on their flexibility and mechanical properties.[156]

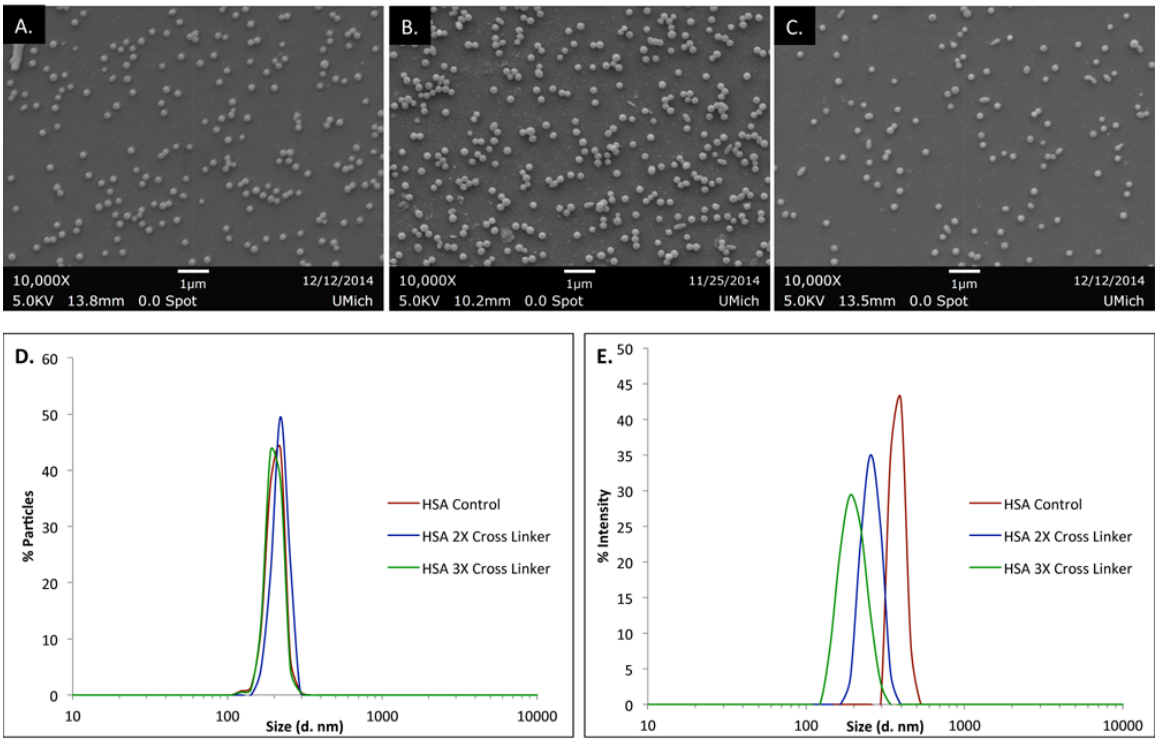

Figure 3-18: Controlling the swelling properties of hydrogel nanoparticles. (A-C) SEM images of nanoparticles with increasing amounts of cross-linker density from 1-3X respectively. (D) The size distribution of the nanoparticles in their dry state based on SEM images and (E) their size distribution in pH 7.4 depending on their cross-linker density.

Fabrication of Janus Nanoparticles for Possible Self-Assembly Applications.

Thus far, while the fabrication of multicompartmental nanoparticles composed of a variety of different polymers has been established, the incorporation of dissimilar materials in each compartment has not extensively been explored. To this end, the fabrication of nanoparticles with two different polymers was attempted. The polymers used were polymethyl methacrylate (PMMA) and poly-tert-butyl methacrylate (PtBMA) where one is more hydrophilic than the other, respectively. Nanoparticles composed of such polymers in distinct compartments have the potential of being used as functional surfactants due to their self-assembly capabilities at water-oil or water-air interfaces. To begin nanoparticles with each polymer separately were fabricated to determine the conditions needed for each (**Figure 3-19**). It was discovered that a different solvent ratios

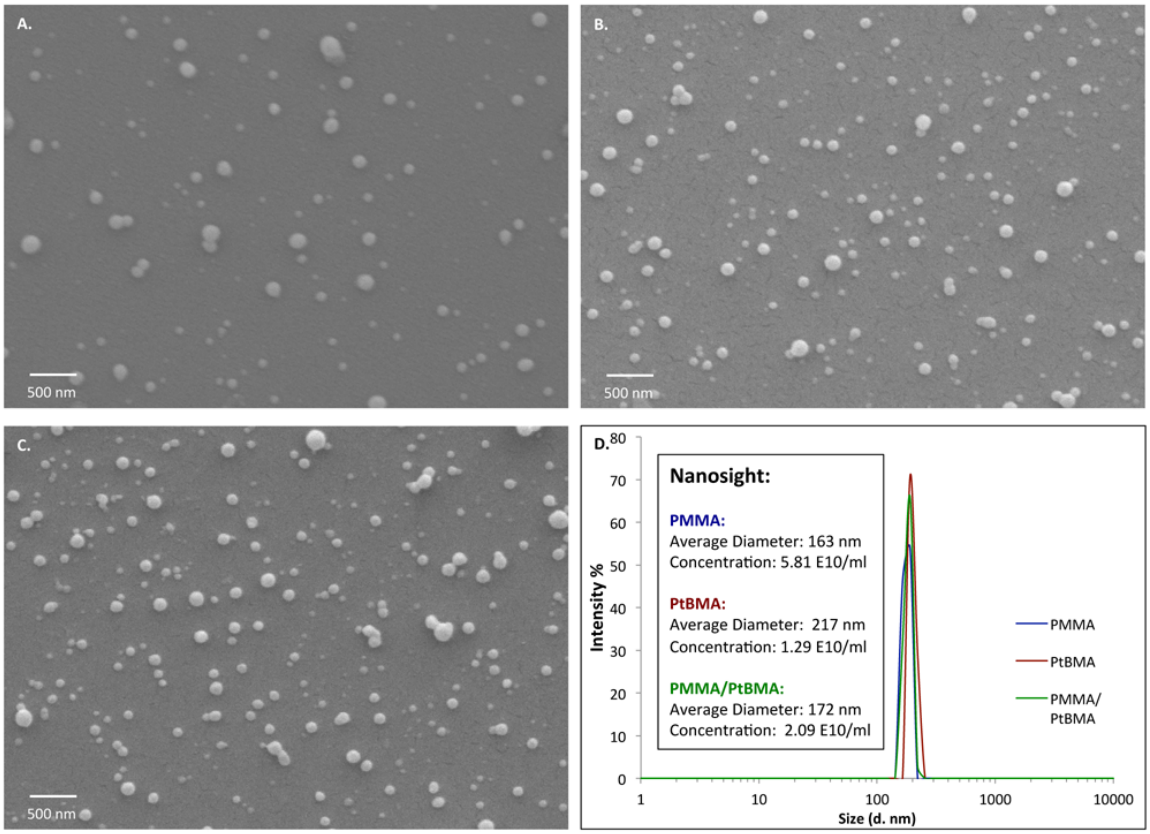

Figure 3-19: Fabrication of Janus nanoparticles. (A-C) SEM images of as-fabricated nanoparticles of PMMA, PtBMA, and both polymers, respectively. (D) The size distribution, average diameter, and concentration of the fabricated nanoparticles.

of chloroform to DMF (7:3 vs. 8.5:1.5) was needed for the fabrication of PMMA versus PtBMA nanoparticles, respectively. The combination of these two separate formulations in a side-by-side jetting orientation resulted in the fabrication of Janus nanoparticles. The nanoparticles as fabricated can be seen in Figure 3-19 A-C with PMMA, PtBMA, and both polymers, respectively. The size distribution of the nanoparticles after centrifugation for 6 hours at 4000 RPM as well their concentration in high yields are noted. Additionally, the compartmentalization of the nanoparticles was determined using SIM imaging. Here, the Janus particles contained either a green or red dye in separate compartments and their bicompartmental nature can be seen in **Figure 3-20**.

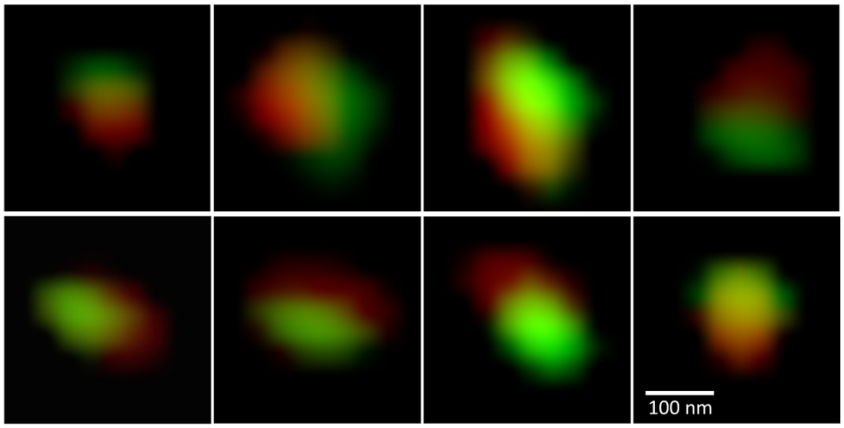

Figure 3-20: SIM imaging of Janus nanoparticles composed of PMMA and PtBMA polymers in separate compartments.

3.4 Summary

Throughout this chapter, control over various physical properties of a particle have been explored. Such properties as shape, roughness, porosity, charge, and size were imparted to the particles by controlling different variable in the EHD co-jetting fabrication process such as polymers used, solution characteristics, and external environmental conditions. A focus was placed on the fabrication and testing of nanoparticles with respect to controlling their as-fabricated size range, separation into specific size fractions for polydispersed samples, displaying their bicompartmental nature, determining their surface functionalization and ligand density, and their biodistribution in animal models. Additionally, the fabrication of uniform hydrogel nanoparticles and Janus nanoparticles with two different polymers in separate compartments were investigated. Together, this chapter establishes a set of methodologies that can be used to program the different physical properties of a particle system for a given application.

CHAPTER 4

Fabrication of Particles with Complex Release of Therapeutics

The material in this chapter has been adapted with minor modifications from the following published article:

(1) S. Rahmani, T.-H. Park, A. F. Dishman, J. Lahann, "Multimodal Delivery of Irinotecan from Microparticles with Two Distinct Compartments", *J. Control. Release,* **2013**, 172, 239-245.

(2) S. Rahmani, S. Saha, A. Donini, J. Lahann, "Controlled Degradation and Release from Anisotropic Particles", *In preparation*.

(3) E. Sokolovskaya, S. Rahmani, A. C Misra, S. Bräse, J. Lahann, "Dual Stimuli Responsive Microparticles", *Submitted*, **2014**.

4.1 Motivation and Background

One of the many challenges in designing a multifunctional carrier for the delivery of therapeutics is their ability to encapsulate therapeutics and deliver them with the desired pharmacokinetics. The challenge here is not necessarily the simple release of the therapeutic, but the release at constant and pre-determined rates that can reach therapeutic levels. Another concern is that as delivery carriers become more efficient in increasing

local therapeutic concentrations, the risks associated with the unsolved issue of cellular drug resistance can arguably be elevated.[157, 158] A promising approach to avoid drug resistance may be the combined use of multiple therapeutics. This delivery will require complex release profiles to accommodate the differences in the pharmacological windows of the respective drugs.[159] Thus, a new generation of drug carriers is needed that can release (i) two or more drugs; (ii) with fully decoupled release profiles. If chosen carefully, such carrier systems would also benefit from possible synergistic effects of the drugs that can further enhance the therapeutic efficacy of the combined delivery.[160, 161] Several researchers have proposed possible strategies for the incorporation of complex release profiles in carrier systems, some of which include the use of stimuli responsive material for on-demand and complex release kinetics.[19, 148, 162-164] Responsive material can be highly sensitive to external stimuli such as pH, temperature, light, and oxidative stress.[164] The structure and degradation of particles composed of stimuli responsive material can then be controlled, and on-demand pharmacokinetics of the encapsulated therapeutics can be achieved.[148, 164, 165] Beyond simple prolongation of the release,[17] these drug carrier systems can be tailored to the therapeutic window associated with a specific disease.[162, 163]

4.2 Experimental Methods

4.2.1 Materials

Dextran, chloroform, dimethylformamide (DMF), dimethyl sulfoxide (DMSO), pyridinium *p*-toluenesulfonate, 2-methoxypropane triethylamine, acetic acid, sodium acetate, poly[tris(2,5-bis(hexyloxy)-1,4-phenylenevinylene)-*alt*-(1,3-phenylenevinylene) (PTDPV), poly[(*m*-phenylenevinylene)-*alt*-(2,5-dihexyloxy-*p*-phenylenevinylene)] (MEHPV), Triethyl amine, bromoacetyl bromide, dimethyl amino pyridine, Benzyl alcohol, l-lactide, tin (II) ethyl hexanoate, anhydrous toluene, Palladium 10% wt. on activated carbon, anhydrous tetrahydrofuran (THF), Allyl glycidyl ether (AGE), naphthalene, potassium, 2,2α-azobis(2-methylpropionitrile) (AIBN), poly(lactic-*co*-glycolic acid) (PLGA, 85:15, M_w= 50000 – 75000 g/mol), manganese chloride, tetramethylrhodamine-5-(and 6)-isothiocyanate (TRITC, red emission dye), phosphate buffered saline (PBS), bovine serum albumin (BSA), tris-buffered saline (TBS), and tween 20 were used as purchased from Sigma Aldrich, USA. Thioglycolic acid, *o*-nitrobenzyl alcohol, hydrogen peroxide solution (30%), calcium hydride, sodium, anhydrous sodium sulfate, concentrated sulfuric acid, and acetic acid were purchased from Merck KGAA**.** Polylactide-*co*-glycolide (PLGA) with a ratio of 50:50 lactide to glycolide and a molecular weight of 44 kDa was purchased from Lactel Corporation. Irinotecan was purchased from Ontario Chemicals. 2-Methoxyethanol and O-benzyl-L-serine was purchased from Alfa Aesar. Sodium bicarbonate, dichloromethane, methanol, toluene, acetonitrile, *N,N*-dimethylacetamide (DMAc) were purchased from BDH Prolabo.Sulfuric acid, acetonitrile, sodium nitrite, dichloromethane, sodium carbonate,

Tissue-Tek O.C.T, and acetone was purchased from Fisher Scientific. Diethyl ether was purchased from Acros Organics. Hydrogen was provided by Cryogenic Gases. Prolong Gold Antifade Reagent was purchased from Life Technologies.

4.2.2 Fabrication & Testing of Drug Loaded Particles with a Rapidly Degrading Polymer

The synthesis of polymer **2** (3-Hydroxyl PLGA) was done Dr. Sampa Saha and the details are outlined in Appendix A. The solutions used for jetting particles were made with a 97:03 ratio of chloroform: DMF and a polymer concentration of 10% w/v. Depending on the particle set, a certain percentage (10, 50, and 100%) of the polymer used in the jetting solution on one side was polymer **2**, while the rest was PLGA. In all cases, the other compartment was composed of neat PLGA. The flow rate used was 0.4 mL/hr. For degradation studies, particles were incubated in PBS at 37 ^{o}C and at predetermined intervals samples were taken, washed, and imaged via SEM to determine their degree of degradation.

For release studies, particles with 2% drug loading per compartment were fabricated using the same procedure as described above. The 2% loading was determined based on conventional methods:

$$\text{Drug \%} = \frac{\text{Drug}}{\text{Drug + Polymer}} \times 100$$

The pre-determined amount of drug was mixed into the jetting solutions along with the polymers prior to the jetting. To determine the particles' release kinetics, the jetted particles were collected into four 20 mg samples, suspended in five mL of PBS and 1% v/v Tween 20 buffer, and placed in a 100-kDa dialysis membrane. The membrane was inserted into a Falcon tube containing 35 mL of the same buffer and gently shaken at 37 ^{o}C. At predetermined intervals, the tubes were removed from the incubator, the membranes were inserted in new tubes with 35 mL of fresh buffer, and replaced back in the incubator. The drug containing buffers in the Falcon tubes were then measured via a UV Visual spectroscopy machine at 367 nm to determine the amount of drug released based on a calibration curve done at the same wavelength previously. The amount of the drug released at each point was added to the previous ones to determine the total amount released at each stage, while taking into account released drug remaining in the membranes. The one-hundred encapsulation percentage was determined by dissolving a known amount of particles in DMF and measuring the final encapsulation based on a corresponding calibration curve done in DMF. The release was plotted as a function of the total cumulative release versus time.

4.2.3 Fabrication & Testing of Drug Loaded Particles with a pH Responsive Polymer

The details regarding the fabrication of pH responsive particles using polymer **8** and their degradation study are outlined in section 3.2.3. Drug loaded microparticles were

fabricated using the same procedure. Here, the drug (irinotecan) was mixed in the jetting solution containing polymer **8** prior to the jetting. The encapsulation was done as a drug-to-polymer ratio (5:100, 10:100, 25:100, and 50:100). These ratios correspond to 2.4, 4.8, 11.1, and 20% drug loading of the particles, respectively, taking into account both compartments. The drug loading was calculated as the drug mass divided by the combined mass of the polymer and drug, as shown in section 4.2.3.

For release studies, 20 mg of the microparticles were dispersed in 5 ml at pH 7.4. The solutions were then placed in dialysis membrane tubing before inserting them into containers filled with 35 ml of the same buffer. The dialysis membrane separated the internal solution and limited the diffusion of material at a cut-off range of 100 kDa, thereby allowing the diffusion of the drug, but not the microparticles, out of the membrane. The samples were incubated at 37 ^{o}C. Eight samples were prepared for each of the drug-to-polymer ratios. At predetermined intervals, the membranes were switched to a new container with fresh buffer, and the buffer containing the released drugs was measured using a UV spectrometer to determine the amount of drug released according to a calibration curve. The amount released at each stage was added to the previous amounts to determine the total amount of drug released at each fixed point. At 24 hours, four out of eight samples for each ratio were centrifuged down and the buffer was fully replaced with a pH 5 buffer. The samples were placed back in the incubator and the release was continued with 4 samples at pH 5 and 4 samples at pH 7.4.

4.2.4 Fabrication of Particles with a Dual Responsive Polymer

The synthesis of the dual responsive polymer was graciously done by Dr. Ekaterina Sokolovskaya and are fully described in **Appendix C**. Particles were fabricated by the EHD co-jetting process. Two different polymer solutions were prepared: one solution contained 15 w/v% PLGA (50:50, 40 kDa), another 15 w/v% 1:1 w/w mixture of PLGA and polymer **10** or polymer **11**. A mixture of chloroform and DMF (97:3 v/v) was used as the solvent. For confocal Raman microscopy analysis of PLGA/polymer **11** microspheres, the ratio of PLGA and polymer **11** in the second solution was changed to 3:1 w/w correspondingly.

Microfibers were generated using a setup similar to that used for the generation of microspheres except the concentration of polymers in both solutions was changed to the following: one solution contained 30 w/v% PLGA, another solution was prepared by mixing 30 w/v% of PLGA with 22.5 w/v% of polymer **10** or polymer **11** (75% by weight of PLGA). For both compartments PLGA (85:15, 55 – 75 kDa) was used. The flow rate was set to 0.05 mL/h and the microfibers were collected at a distance of 7 cm using a rotary collector and embedded in a freezing medium (OCT). For confocal Raman microscopy analysis of PLGA/polymer **9** microfibers the concentration of polymer **11** in the second solution was decreased to 15 w/v% (50% by weight of PLGA).

For photo-degradation, PLGA/polymer **10** and PLGA/polymer **11** microspheres or microfibers were exposed to 365 nm light on the collecting substrate for 30 min, followed by incubation in a buffer composed of TBS and 0.01% Tween 20 for 1 h while rotating. Next, the particles were washed 5 times with DI-water, analyzed by SEM. As a

control experiment, incubation of non-irradiated particles in the same conditions was performed.

The particles were collected from the metal substrate using a buffer composed of PBS, 0.01% Tween 20, and 10% BSA. Once collected, the particles were filtered through a 40 μm filter to remove large aggregates and then were counted using a cell counter to determine the final concentration in the solution. Raw264.7 cells were seeded in a 12-well plate with cover glass slides at a concentration of ~80000 cells/well. The following day, the cells were incubated with particles at different concentrations (in fresh media) for four hours. After the incubation, the cells were washed with PBS and fixed in 4% paraformaldehyde. Following fixation, the cells were washed with PBS once more and stained with far-red phalloidin, as per the protocol provided by Invitrogen. The coverslip samples were then mounted on glass slides using ProLong Gold Antifade Reagent with DAPI and imaged through CLSM. The scanned images were then analyzed to determine particle uptake per cell at the different particle concentrations.

Results and Discussion

Particles with Controlled Release of Therapeutics:

The precise control over the release rate of therapeutics from particles is responsible for determining whether a carrier system is capable of reaching therapeutic indices in the body. Here, we were interested in working with rapidly degrading polymers as a means for fabricating particles with controlled therapeutic release. One of the

synthesized polymers in Chapter 2, polymer **2**, contains free hydroxyl groups on its backbone. In the previous chapters, the use of this polymer for surface functionalizing particles via EDC/Sulfo-NHS chemistry and as a method of imparting surface charge to particles were investigated (Chapters 2 and 3 respectively). Due to these hydroxyl groups, the polymer is also expected to degrade at a faster rate than neat PLGA polymers with similar molecular weights. To validate this hypothesis, particles with different percentages of polymer **2** in one compartment (0, 10, 50, and 100% w/w) were fabricated. Upon incubation of the particles in physiological conditions and their imaging with SEM, the degradation of the microparticles dependent on the amount of polymer **2** incorporated was observed (**Figure 4-1**). The particles containing 100% polymer **2** in one compartment degraded rapidly and by day one only the hemisphere containing PLGA remained. Further degradation starting at the interface of the two compartments and

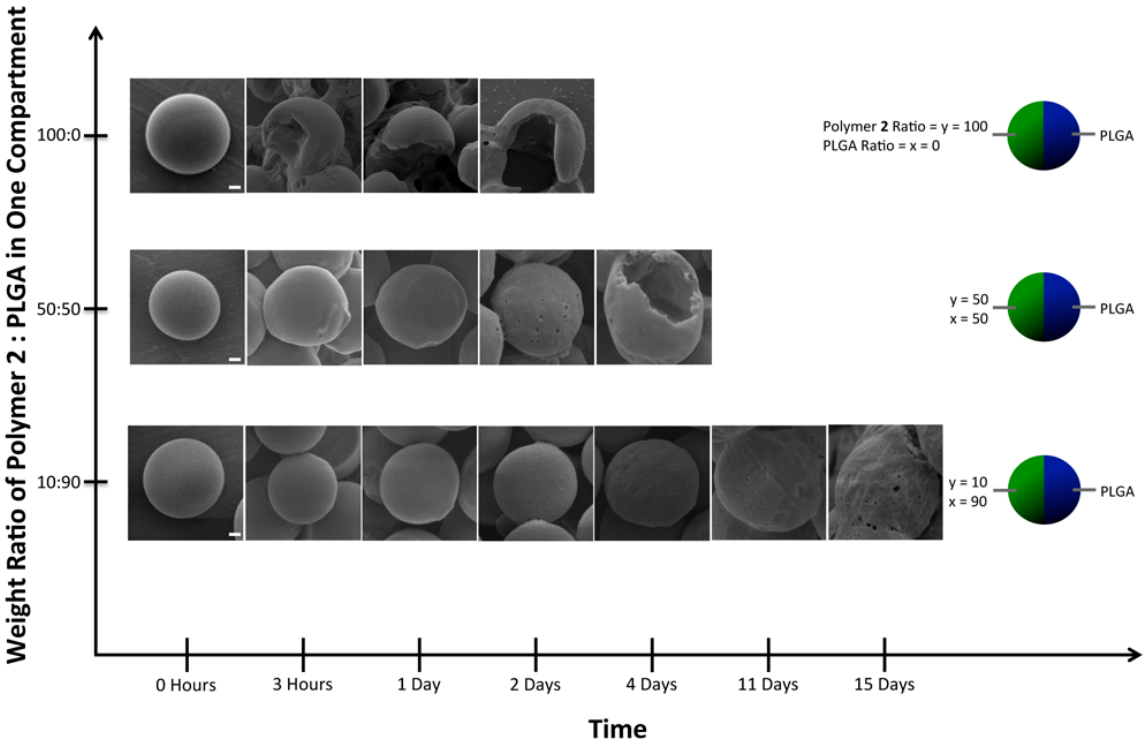

Figure 4-1: Degradation of microparticles with various percentages of polymer **2** in one compartment. Each row represents a different particle composition, while the x-axis represents the time points used.

through the bulk of the second compartment yielded hollow half spheres by the second day. This rapid degradation of the PLGA compartment is most likely due to the lower pH environment induced by the degradation of polymer **2**. The particles with 50% of this polymer degraded at a slower rate, with pores seen selectively in one compartment by day 2, followed by the degradation of one compartment by day 4. The particles containing only 10% of polymer **2** in one compartment degraded at a much slower rate with pores seen only after 11 days.

Based on these studies, the controlled degradation of a selective compartment was established. Next, we employed these particles to establish controlled release of a cancer therapeutic (Irinotecan). The same particles used in Figure 4-1 with a 2% w/w loading of irinotecan were used for the release studies (**Figure 4-2**). A control with only PLGA on both sides and loaded with irinotecan was used as a reference. A similar trend to the degradation can be observed here: the higher the ratio of polymer **2**, the faster the

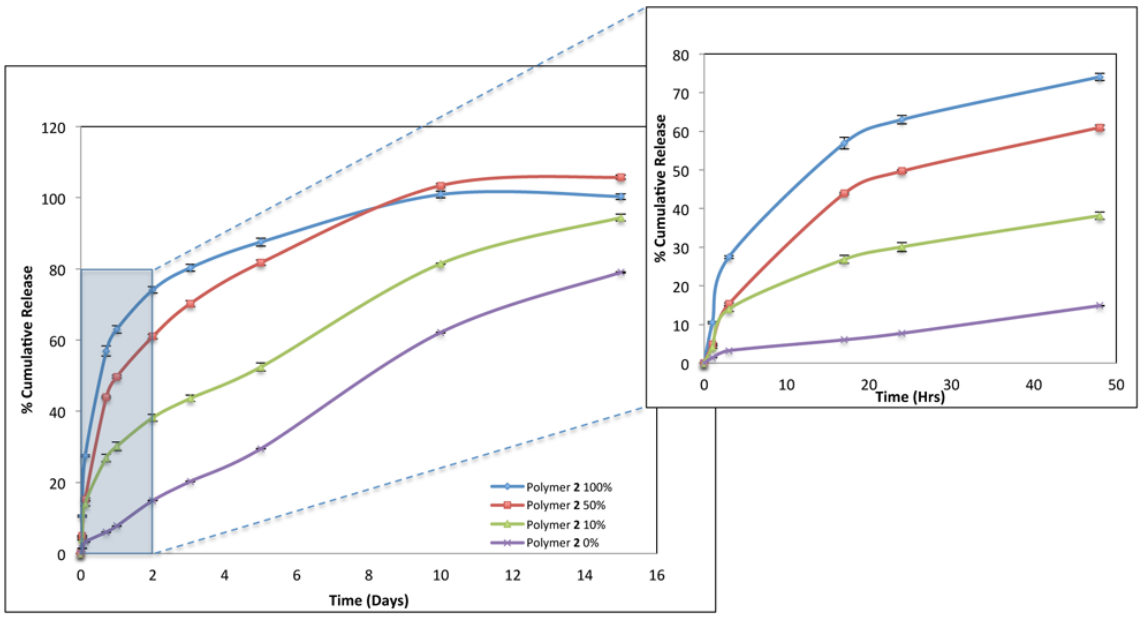

Figure 4-2: Release of irinotecan from microparticles containing various percentages (0, 10, 50, 100%) of polymer **2**. The inset shows the first 48 hours of the release in detail.

degradation of the particles and the release of their therapeutic loading. By 15 days, the control particles composed of PLGA had a constant release of irinotecan to ~75%. The incorporation of polymer **2** at 10% w/w increased this rate to 95% by 15 days. However, the incorporation of this polymer at 50 and 100% resulted in a rapid release of irinotecan where approximately 100% of the encapsulated therapeutic was released by 10 days. The inset in Figure 4-3 highlights the first 48 hours of the study, where the precise control over the release kinetics of the therapeutic is clearly demonstrated. Such formulations could potentially be used for the fabrication of particles with controlled release kinetics.

Particles with pH Responsive Release of Therapeutics:

The synthesis of polymer **8** (Acetal Dextran) was done by Dr. Tae-Hong Park and the details are outlined in detail in section 3.2.3. The porosity and degradation of the compartmentalized particles with polymer 8 in one compartment is also discussed in detail in section 3.3. Here, we were interested in exploring the pH responsive capabilities of this system to fabricate responsive release of therapeutics from the particles. To this end, microparticles encapsulating different amounts of irinotecan in the compartment containing polymer **8** were fabricated. Microparticles with a range of different drug-to-polymer ratios (5:100 to 50:100, drug: polymer ratio, wt./wt.) could be fabricated using the same polymer formulation and processing parameters. Even for extremely high loading ratios of up to 50:100, microparticles were obtained that maintained similar size and shapes to unloaded microparticles. Next, four different microparticle sets were fabricated with drug-to-polymer ratios of 5:100, 10:100, 25:100, and 50:100. We hypothesized that at physiological pH, there would be a relatively slow release of the

drug from our microparticles, while in acidic pH, there would be a rapid release of the majority of the drug. Finally, the rapid release at pH 5 was anticipated to follow a similar pattern (time and rate) as that of the dextran release (Figure 3-5).

To test this hypothesis, release studies were conducted with the bicompartmental microparticles. Two sets of samples were used for each drug-to-polymer ratio. For the first 24 hours both sets were incubated at pH 7.4 to determine if the release between the sets were consistent, then one set was switched to pH 5 while the other was kept at pH 7.4 as a control. As predicted, the two sets were consistent with a slow release of irinotecan during the initial 24-hour period, after which point the samples were switched to pH 5 and underwent rapid release. Meanwhile, the reference samples, stored at pH 7.4, continued to display a very slow release of the therapeutic (**Figure 4-3B**). The detectable, albeit small, burst and the continuous release thereafter match those of the dextran release at the same pH (Figure 3-5). We note that the rapid release of irinotecan at pH 5 is consistent with our previous results. While the majority of the compartment was composed of polymer **8**, there is still a significant PLGA component in this compartment (25%), which, does not completely degrade within the 10-hour period and retains some of the irinotecan. Thus, irinotecan can be released in two stages: a rapid stage through the release of polymer **8** within a 10-hour period and a slower release phase as the PLGA component degrades.

In addition to establishing that pH-triggered, on-demand release of therapeutics can be achieved with bicompartmental microparticles, we were also able to demonstrate that the rate and amount of release can be tuned, depending on the amount of the therapeutic encapsulated in the microparticles. As demonstrated in Figure 4-3, as the

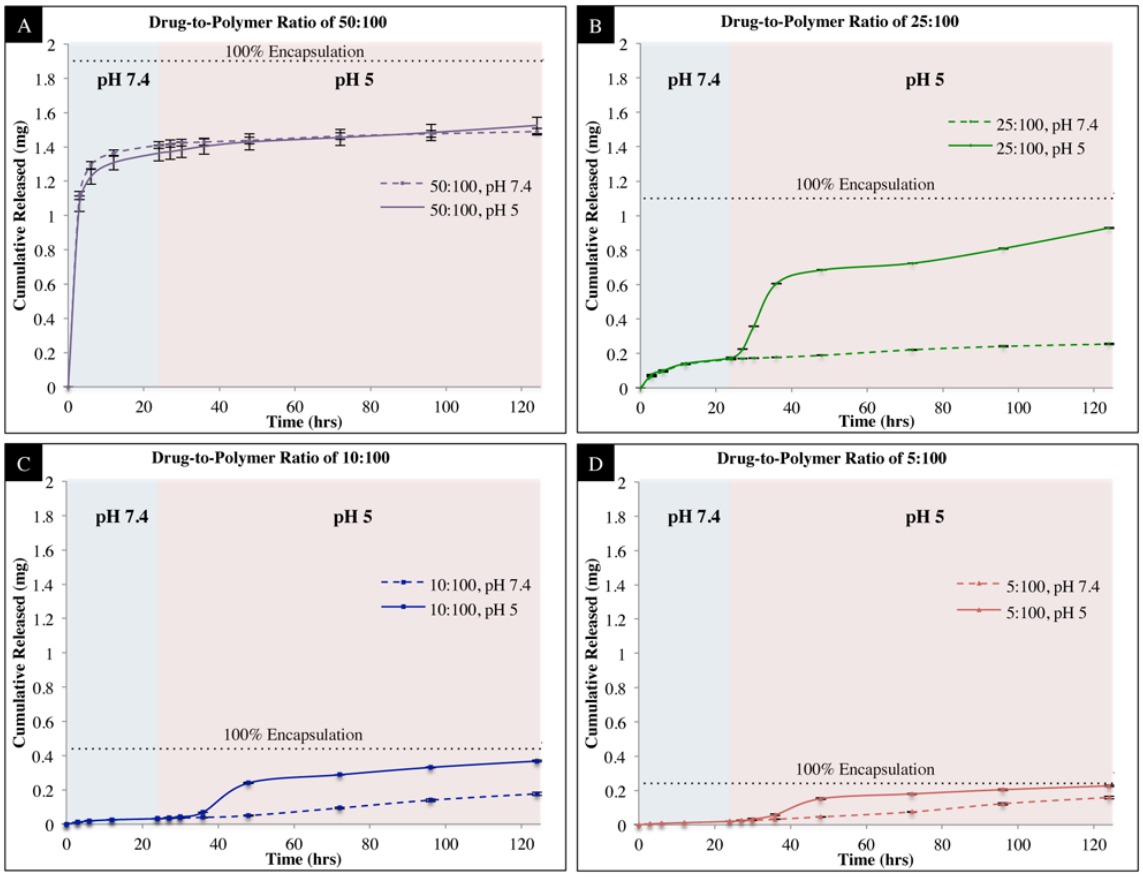

Figure 4-3: Release of irinotecan from bicompartmental microparticles. A.-D.) Release profiles from microparticles with drug-to-polymer ratios of 50:100 (A.), 25:100 (B.), 10:100 (C.), and 5:100 (D.). The solid lines are of the release in pH 5 and the dotted lines are the release in pH 7.4.

drug-to-polymer ratio was increased (Figure 4-3D to Figure 4-3A), the amount of drug and the rate of release were also increased. This is in agreement with previously published results[166] confirming that at higher drug concentrations, the release of the therapeutic is faster due to percolation effects.[167, 168] This is particularly evident in the case of the microparticles with a drug-to-polymer ratio of 50:100 (Figure 4-3A) where the release of the drug is very fast, irrespective of the pH of the release environment.

Another potentially useful characteristic of bicompartmental carriers containing polymer **8** is their ability to localize high drug content in one compartment without spill over into the second one. This is a feature that was not possible in microparticles containing PLGA. **Figure 4-4** displays the selective encapsulation of the drug, irinotecan, at high drug-to-polymer concentrations (25:100) in the same compartment containing polymer **8** (Figure 4-4A). For comparison, the same drug at the same concentrations was also loaded in bicompartmental microparticles comprised of PLGA in both compartments. For microparticles without polymer **8**, diffusion of the drug between the two PLGA compartments was observed (Figure 4-4B). In contrast to the microparticles

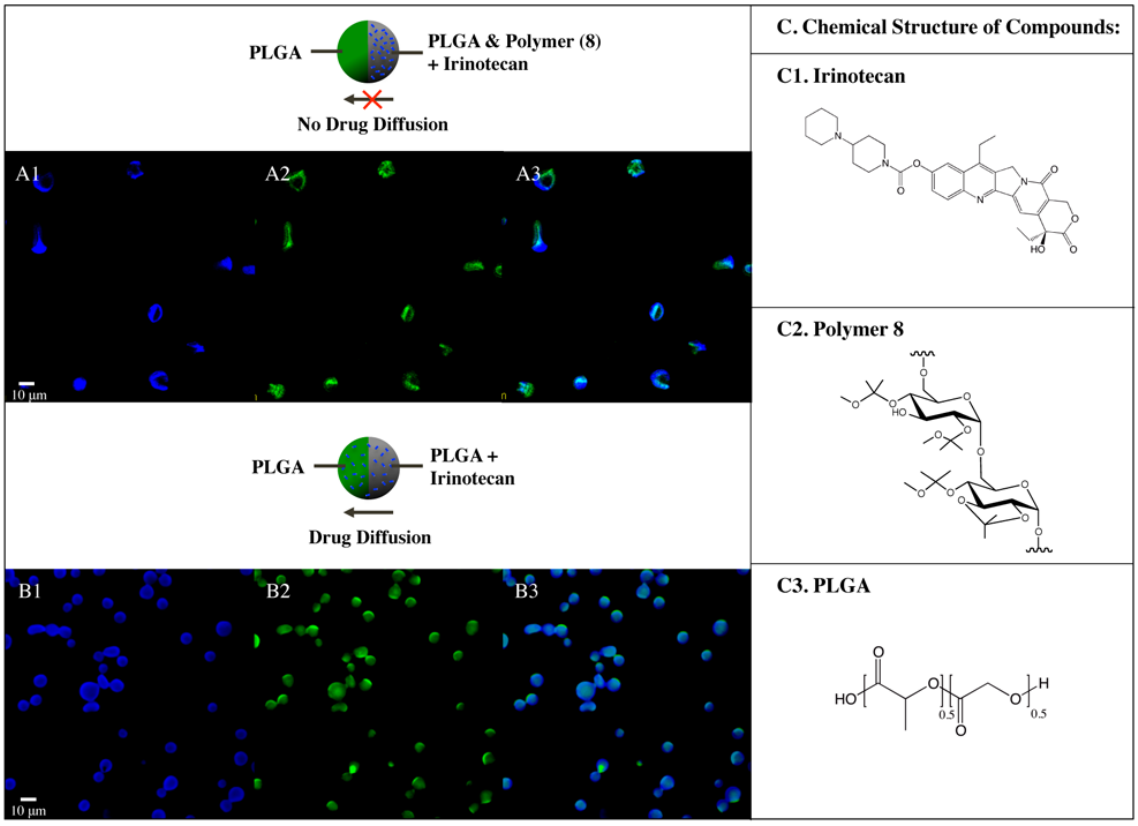

Figure 4-4: Selective encapsulation of irinotecan in microparticles. A.) In polymer **8** containing microparticles, irinotecan (autofluorescing in blue channel) is compartmentalized in one compartment, as the two dyes do not mix in the overlay image (A3.). B.) In the PLGA containing microparticles, the encapsulated irinotecan is not compartmentalized, as in the overlapped image, B3.), the blue dye is in both compartments. The structure of the drug, irinotecan, and the polymers, polymer **8** and PLGA, are displayed in C1-3.

containing polymer **8**, irinotecan is distributed throughout the entire microparticle as indicated by the overlay of the blue fluorescence from irinotecan (Figure 4-4A3 and 4-4B3) and green fluorescence used to label the irinotecan-free compartment (Figure 4-4A2 and 4-4B2).

Selective Degradation of Particles Using a Dual Responsive Polymer:

Materials capable of changing their properties in a controlled and reversible manner in response to changes in their environment or a specific trigger, such as light, are defined as "smart" materials.[169] Stimuli-responsive materials have been designed in various forms including switchable surfaces,[169-172] responsive hydrogels,[173] or anisotropic particles.[73, 169, 174] Compared to many known triggers, light switching can be performed in milder conditions and in a more specific manner due to control over light intensity and wavelength.[175] A wide range of photoresponsive systems has been developed thus far.[173, 176, 177] For example, azobenzene derivatives and spiropyrans were successfully used for the fabrication of photoresponsive surfaces.[172] In the field of drug delivery, photocleavable protecting groups are commonly used to switch the solubility of carrier polymers. A variety of photolabile protecting groups are available for different functionalities.[178, 179] In particular, *o*-nitrobenzyl (NB) groups have found a range of different applications.[180] Originally designed for use in organic synthesis,[181] these groups were successfully applied to biochemistry.[42] When incorporated into a copolymer, the photocleavage of the NB groups takes place readily upon illumination with UV light, releasing alcohol or acid and a nitroso derivative.[180]

Besides light, potential triggers for stimuli responsive material include changes in temperature, pH, salt content, presence of specific molecules, and electrical or magnetic fields.[162, 176, 177] To date, there exist only a very few examples of stimuli-responsive materials triggered by changes in the oxidative environment of a tissue, as it is commonly observed in inflammatory tissues.[162] A change in the redox environment of a cell due to oxidative stress is an important indicator of many diseases including cancer,[182] atherosclerosis,[183] neurodegenerative diseases such as Parkinson's disease and Alzheimer's disease,[184] or heart failure.[185]

Oxidative stress may originate from the overproduction of reactive oxygen and nitrogen species. The latter are generated as byproducts of aerobic metabolic cell processes involving reduction of oxygen to superoxide anions followed by formation of hydrogen peroxide, hydroxyl radicals, hypochlorite, peroxynitrite, and other molecules.[186, 187] At high dosages, oxidants can cause significant damage to proteins, lipids, and DNA, and finally lead to cell death. Therefore, the presence of oxidants can be used as a marker for inflamed tissues and can activate a specific action of a biomaterial, such as drug release.[188] Here, we were interested in the synthesis of a new multifunctional poly(ethylene glycol) (PEG)-based polymer particle that contains both redox-responsive thioether moieties and light-sensitive NB groups. Specifically, this design takes advantage of the co-operative effects of hydrogen peroxide reactive moieties (endogenous stimulus) and photoresponsive groups (exogenous stimulus).

We used electrohydrodynamic co-jetting to formulate anisotropic microparticles containing a dual-stimuli responsive polymer in one compartment. Oxidation of the thioether into sulfoxide groups under conditions of oxidative stress (endogenous

stimulus) and photocleavage of NB groups (exogenous stimulus) can then act cooperatively to increase the polymer solubility in water and lead to the rapid resorption of one compartment in these microparticles. If the particles are placed in an oxidative environment in the absence of UV light, no resorption will occur. The same is true for a particle that is exposed to light in the absence of the oxidative trigger (**Figure 4-5**).

We chose PEG as the main chain polymer, because PEG is known to have outstanding properties such as biocompatibility, hydrophilicity, protein resistance, and non-toxicity, which are particularly important for biomedical applications and have

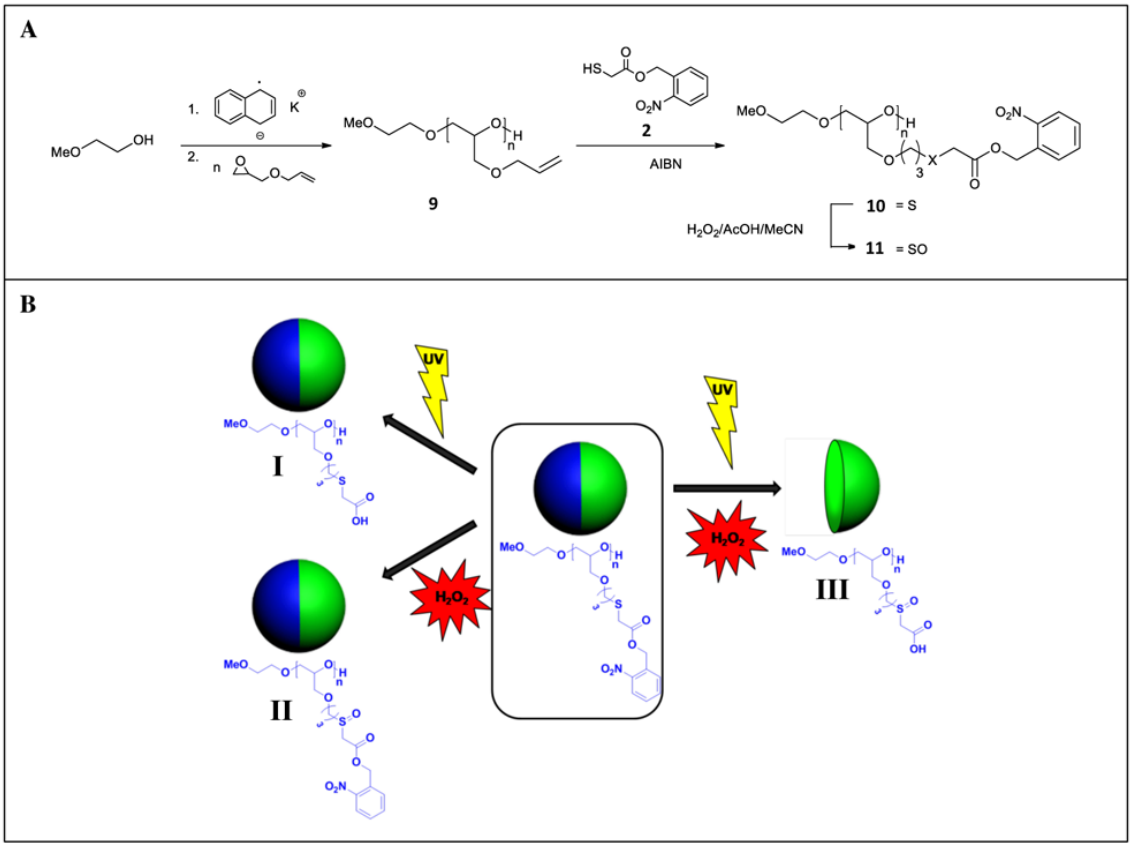

Figure 4-5: A) Polymerization of AGE and synthesis of multifunctional *o*-nitrobenzyl PEGs. B) Schematic representation of bicompartmental particles having the dual stimuli responsive polymer in one compartment (blue). The polymer contains NB groups, which are cleaved upon exposure to UV light releasing carboxylic acid groups (I) and thioether moieties, which undergo oxidation into sulfoxide groups upon hydrogen peroxide action (II). Only upon action of both light and oxidant does the polymer become completely water soluble due to the conversion into the corresponding polyacid with sulfoxide moieties leading to the degradation of the corresponding compartment of the particle (III).

already made PEG one of the most attractive polymers in biomaterial synthesis.[189-191] Moreover, the hydrophilicity of the PEG backbone contributes to the solubility of the polymer after combined exposure to endogenous and exogenous stimuli. Typically, PEG polymers are functionalized via their end groups, which limit the number of functional groups per PEG chain. This disadvantage can be overcome by the synthesis of multifunctional derivatives via anionic ring-opening polymerization of functional epoxides and subsequent post-polymerization modifications.[192, 193] Thus, we first prepared poly(allyl glycidyl ether) (PAGE) as a starting polymer for the synthesis of the stimuli responsive polymer. Subsequently, polymer-analogue modification via thiol-ene "click" reaction yielded the polyether **10**.

Polymer was synthesized by anionic ring-opening polymerization of allyl glycidyl ether using 2-methoxy ethanol and potassium naphthalenide as the initiating system. The crude polymer was purified chromatographically over silica gel (Figure 4-5). The synthesis of the target PEG-based polymer containing both thioether and NB moieties was performed by post-polymerization modification of poly(allyl glycidyl ether) via thiol-ene reaction with a thiol bearing NB protected acid groups (Figure 4-5A). This method allowed the introduction of both stimuli reactive moieties in a single modification step. The thiol **2** NB bearing protected carboxylic acid group was then synthesized by esterification of thioglycolic acid with *o*-nitrobenzyl alcohol. Reaction of polymer **9** with thiol **2** was performed in the presence of Azobisisobutyronitrile (AIBN) using an excess of thiol to avoid undesired crosslinking reactions. Complete conversion of allyl moieties was confirmed by ^{1}H NMR spectrometry (Appendix C). The resulting polymer **10** was further purified chromatographically over silica gel.

The final product, polymer **10,** has the potential to function as a sensory material: Under conditions of oxidative stress, conversion of the thioether groups into sulfoxide groups will take place generating a substantially more polar polymer with enhanced resorbability in aqueous media. To compare the hydrophilic properties of polymer **10** and its sulfoxide analogue, the oxidation of polymer **10** with hydrogen peroxide into the corresponding polymer **11** was performed (Figure 4-5). To ensure that oxidation of thioether moieties proceeded just until the formation of sulfoxide groups and to avoid generation of sulfone groups in the polymer product, the oxidation reaction was allowed to proceed at 0 °C. Oxidation to the sulfone is highly undesirable, not only because of the difference in solubility of sulfoxides and sulfones, but also because of the low stability of sulfones, which can undergo degradation upon irradiation.[187] However, detailed characterization of polymer **11** with ^{1}H NMR and IR spectroscopy revealed no presence of sulfone groups (Appendix C). Moreover, the complete oxidation of the thioether groups was confirmed by the disappearance of a signal at 3.28 ppm in the NMR spectrum corresponding to the sulfur neighboring methylene protons (d') and the appearance of a new signal at 3.81 ppm from the corresponding protons (d") in polymer **11** (Appendix C). This was also confirmed by IR spectroscopy, which revealed the appearance of a characteristic band at 1010 cm^{-1} corresponding to the (S=O) stretching bands in sulfoxides (Appendix C). GPC analysis indicated only a minor shift of the elution band of polymer **11** towards shorter elution times. We concluded that this shift is too small to be indicative of appreciable levels of degradation of polymer **10** during oxidation (Appendix C). Since the in vivo concentration of hydrogen peroxide under the conditions of

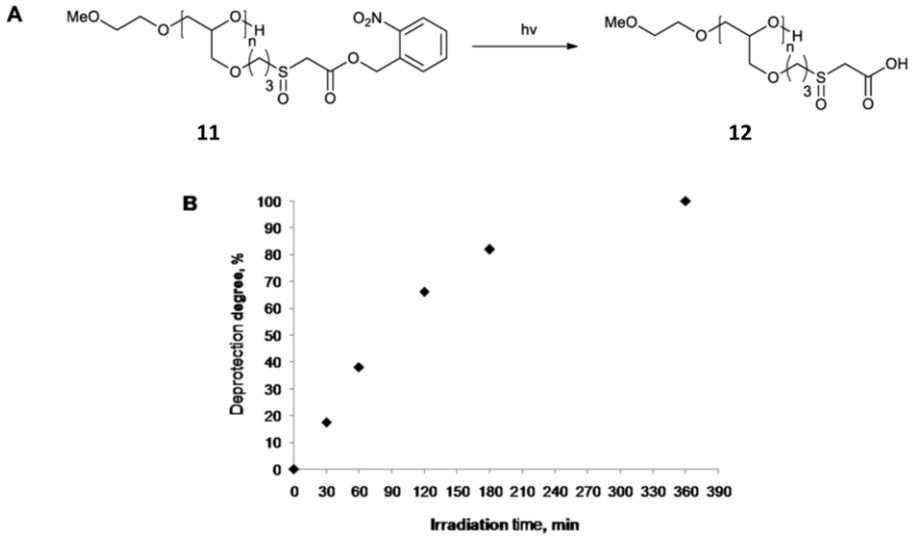

Figure 4-6: Photocleavage of NB protecting groups in polymer **11** resulting in the formation of the corresponding polyacid **12** (A). Dependence of polymer **11** deprotection degree on the time of irradiation with 312 nm light (B). Deprotection degree was calculated based on ^{1}H NMR spectra.

oxidative stress is relatively low,[189] we expect the in vivo oxidation of polysulfides to predominantly result in sulfoxides, not sulfones.

Due to the combined redox-responsiveness and photoreactivity of the polymer, cleavage of the NB protecting groups of polymer **11** will result in the formation of the more polar polymer **12** (**Figure 4-6**). To validate this aspect systematically, the deprotection of polymer **11** was monitored by ^{1}H NMR spectrometry in DMSO-d_6 solution through various exposures to UV light with a maximum wavelength of 312 nm. Disappearance of signals corresponding to aromatic (e–h) and benzylic (d) protons of the NB groups explicitly confirmed the cleavage of NB esters (**Figure 4-7**).

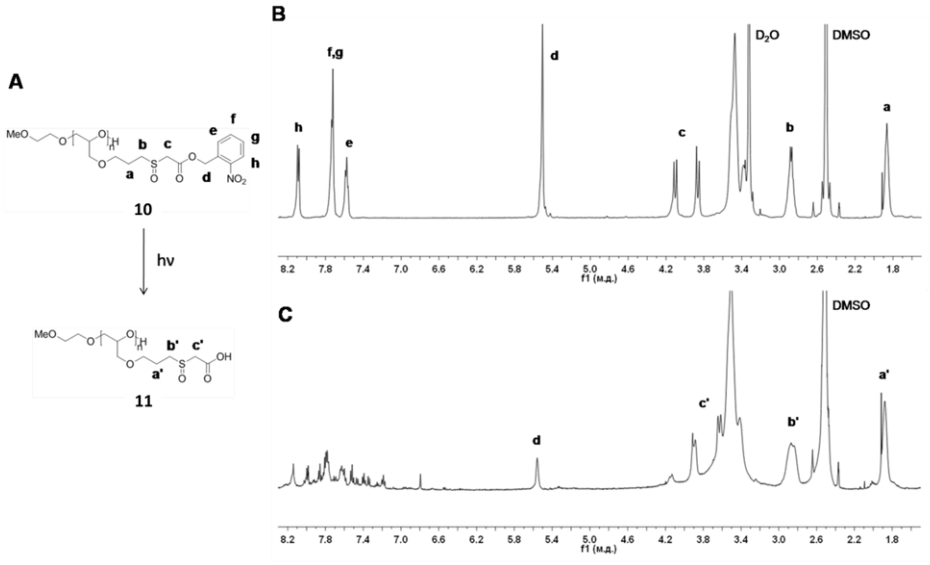

Figure 4-7: UV induced cleavage of NB protecting groups in polymer **11** (A) and comparative ^{1}H-NMR spectra of polymer **11** before (B) and after (C) 4 h of irradiation with 312 nm light. Solvent DMSO-d_6.

On the other hand, methylene protons (a–c) were still present in the NMR spectrum showing the expected shifts (a'–c') after light exposure of the polymer. This aspect provides further evidence that degradation of the polymer can be ruled out (Figure 4-7). Dependence of the deprotection degree of the polymer on UV exposure time is displayed in Figure 4-6. A somewhat longer than expected exposure period was needed for complete cleavage of NB groups, which was attributed to the used solvent (DMSO) and high concentration of the polymer (5 mg/ml). However, these conditions were necessary for proper detection and assignment of signals in the NMR spectra. To identify the optimum UV exposure time in bulk, polymer **11** was spin coated on gold wafers and exposed to light at a wavelength of 365 nm for different periods of time. Cleavage of the NB groups was then monitored by IR spectroscopy (**Figure 4-8**). The deprotection of NB groups was directly correlated to the disappearance of the characteristic nitro bands at

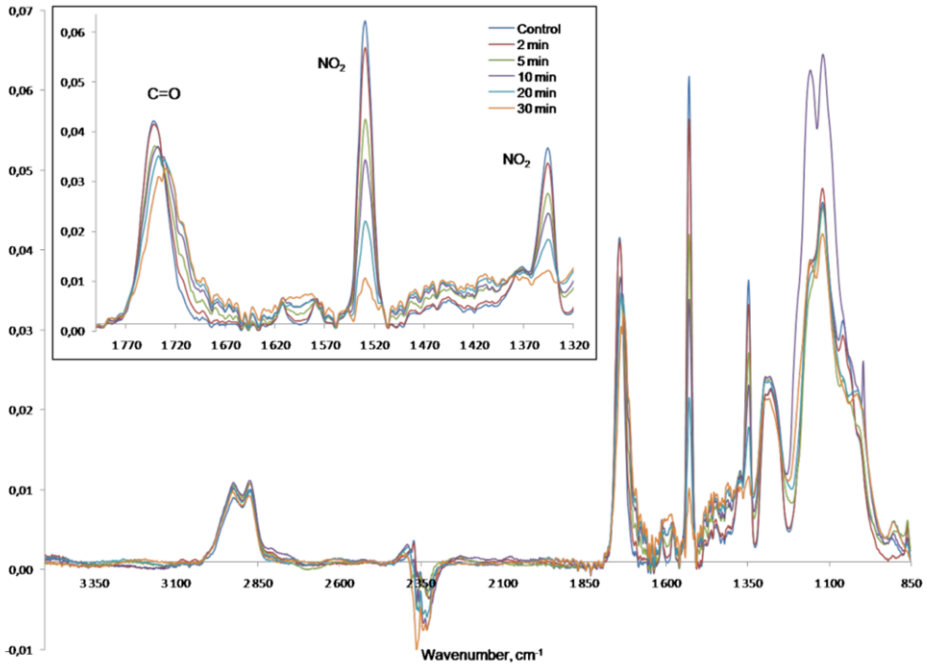

Figure 4-8: Comparative IR spectra of polymer **11** before (control) and after different times of irradiation with 365 nm light. Polymer was spin coated on the gold wafers.

1530 and 1346 cm^{-1}, as well as the shift of carbonyl band from 1742 to 1729 cm^{-1}. Complete cleavage of NB protection was finally detected after light exposure for 30 min.

Anisotropic bicompartmental microspheres made of poly(lactic-*co*-glycolic acid) (PLGA) and containing the stimuli-responsive polymer **11** in one compartment only were prepared by EHD co-jetting (**Figure 4-9**).[64] For bicompartmental particles, one jetting solution contained PLGA only, while the second solution contained PLGA/Polymer **11** mixtures at a ratio of 1:1 (w/w). Both jetting solutions were loaded with fluorescent dyes, which allowed for confirmation of the bicompartmental structure of the microspheres via confocal laser scanning microscopy (CLSM) (Figure 4-9B). The spherical shape of the particles was confirmed by SEM (Figure 4-8C).Furthermore, the selective localization of polymer **11** in one compartment only was verified by confocal Raman microscopy

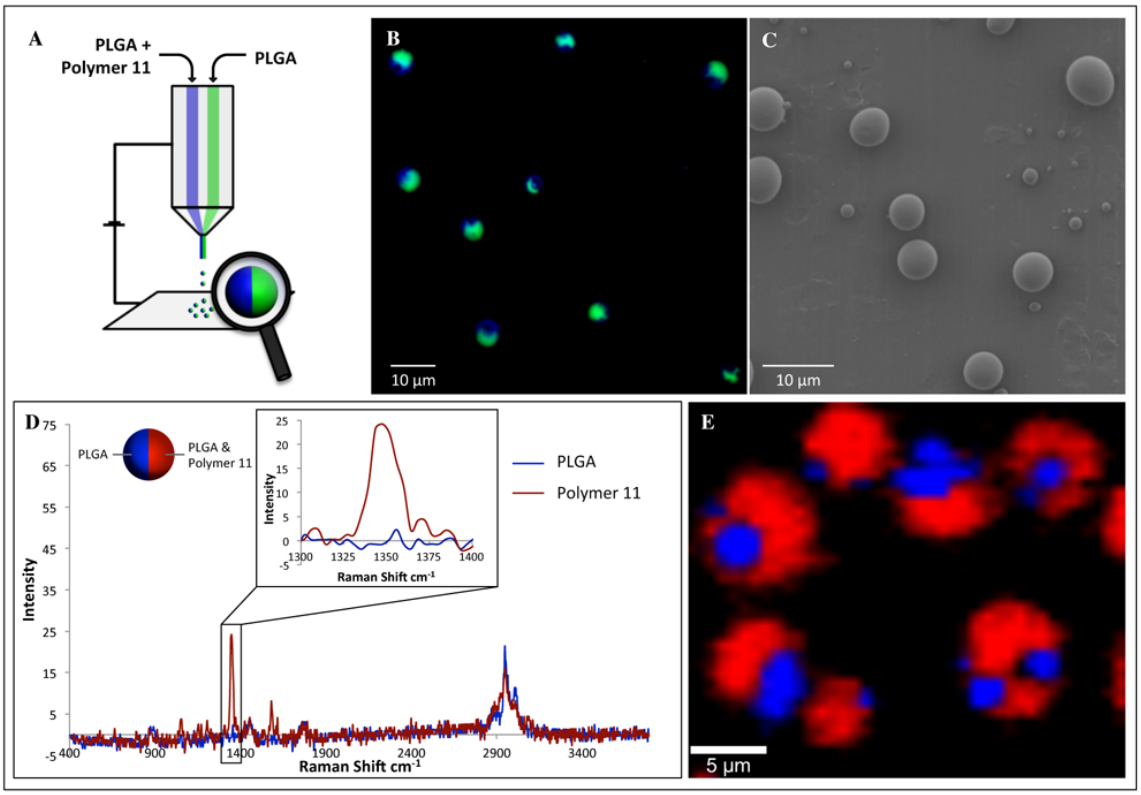

Figure 4-9: A) Schematic representation of the bicompartamental microparticles containing polymer **11** localized in one compartment; B) CLSM image of the particles, where green and blue dyes indicate PLGA and polymer **11**, respectively; C) SEM image of the particles, D) Confocal Raman microscopy spectra of the bicompartmental PLGA/polymer **11** microspheres; and E) 2D reconstruction of the Confocal Raman spectra, confirming the selective localization of polymer **11** (red) in one compartment (the ratio PLGA:polymer **11** in one compartment was 3:1).

(Figure 4-9D-E). The characteristic signal of the nitro group at 1348 cm^{-1} was used as the reference band for assessing the spatial distribution of polymer **11** within the particle. Confocal Raman microscopy revealed the selective location of polymer **11** in only one hemisphere of the microsphere as indicated by the red signal. For comparison, the PLGA polymer is indicated by the blue color.

For comparison, bicompartmental particles with PLGA and polymer **10** were also prepared by EHD co-jetting and were characterized by SEM and CLSM. Based on the combined analysis of these results, both microspheres were found to be bicompartmental

and structurally identical. Next, the resorbability of PLGA/polymer **10** and PLGA/polymer **11** particles upon UV-irradiation was evaluated. For this purpose, dry particles were exposed to 365 nm light and washed with a Tris Buffered Saline (TBS) for 30 minutes before imaging with a SEM. The SEM images of particles with and without UV exposure are shown in **Figure 4-10B-E**.

Without UV exposure, no resorption was detected for either PLGA/polymer **10** or PLGA/polymer **11** particles (Figure 4-10B and C). After exposure to markers of oxidative stress, the thioether moieties of polymer **10** underwent oxidation into sulfoxide groups, which make polymer **11** more hydrophilic than polymer **10**. However, due to the

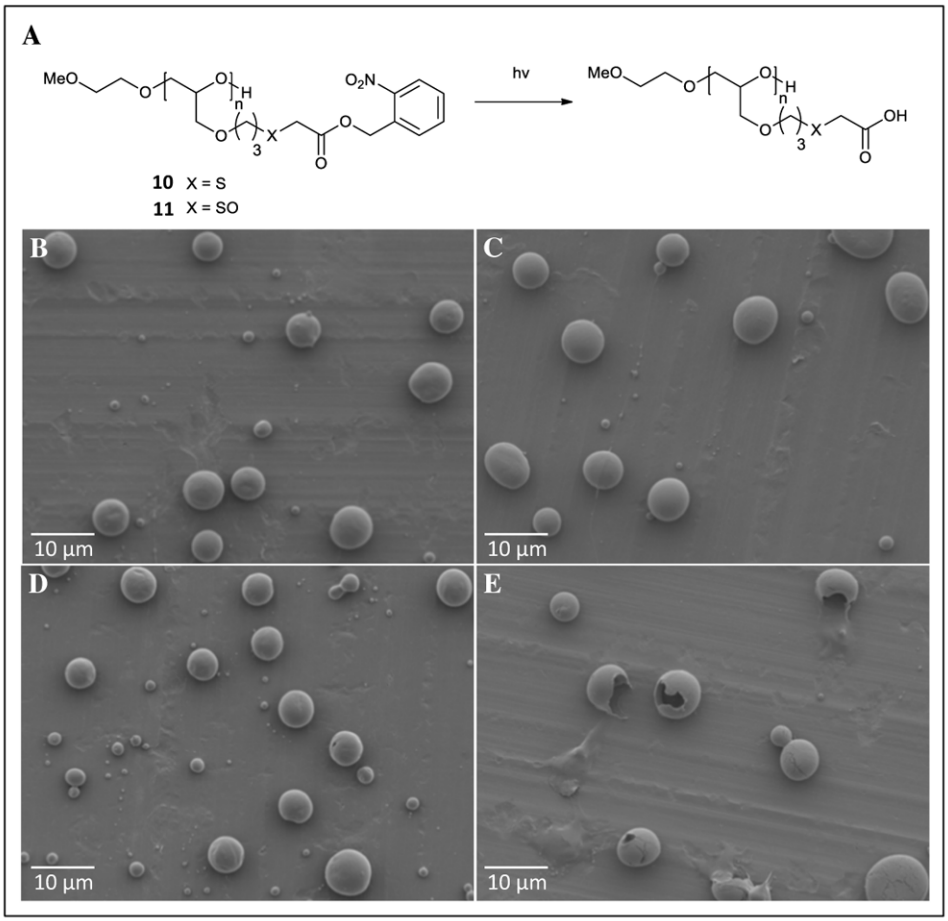

Figure 4-10: Deprotection of polymers **10** and **11**, respectively**,** into the corresponding polyacids upon exposure to light at 365 nm (A). SEM images of bicompartmental microparticles without light exposure (PLGA/polymer **10** (B)) and PLGA/polymer **11** (C)) and after 30 min light exposure (PLGA/polymer **10** (D) and PLGA/polymer **11** (E)).

presence of the hydrophobic NB groups in both polymers, the resorbability of both polymers was still negligible. Similarly, particles comprised of PLGA/polymer **10** showed no signs of resorption, even after exposure to UV light (Figure 4-10D). Even though photocleavage of NB protection in polymer **10** yielded the corresponding polyacid (Figure 4-10A), the absence of sulfoxide moieties was sufficient to prevent resorption of the deprotected polymer **10** (Figure 4-10D). In contrast, incubation of UV-treated PLGA/polymer **11** particles led to fast resorption of polymer **11** (Figure 4-10E). Taken together, the results confirmed that only simultaneous exposure to both stimuli, light and markers of oxidative stress, allowed for the rapid resorption of polymer **10**, whereas each stimulus on its own did not have sufficient effects to induce polymer resorption (Figure 4-10C-D). This suggests that PLGA/polymer 10 particles are a promising multi-stimuli responsive system by the dual actions of oxidants and UV exposure.

To further prove that the particles containing of polymer 3 and PLGA, and not just the polymer **11** containing particles that are pre-exposed to oxidative stress, are responsive to two stimuli, particles with polymer **10** were fabricated and their resorbability was examined by combined exposure to oxidative stress and UV light. As displayed in **Figure 4-11**, the particles were first exposed to hydrogen peroxide, which resulted in the more hydrophilic polymer **4**. The particles were then exposed to UV light at 365 nm for 30 minutes, then washed and analyzed with SEM. The results clearly demonstrate that degradation of one hemisphere was achieved.

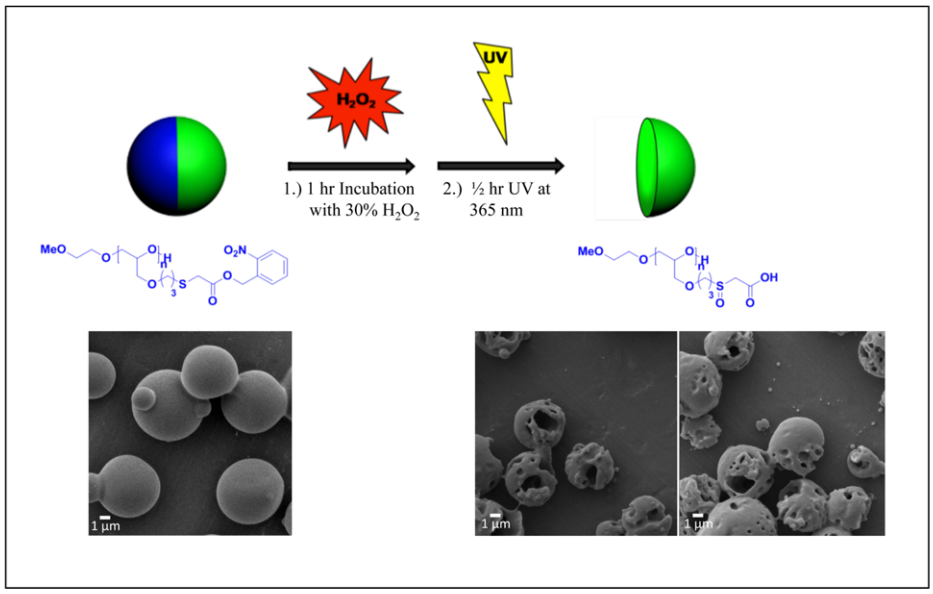

Figure 4-11: Degradation of one compartment through oxidation and UV-illumination of bicompartmental microparticles. Here, microparticles composed of PLGA in one compartment (blue) and polymer **10** and PLGA in the second compartment (green) were incubated in 30% v/v hydrogen peroxide for 1 hour, followed by UV illumination at 365 nm for 30 min. Similar to the treatment of the neat polymer, the hydrogen peroxide oxidizes the polymer **10** polymer to polymer **11**, which is then water soluble upon UV illumination and the cleavage of the nitrobenzyl group. Upon oxidative and UV treatment, the particles were washed with DI water several times before imaging with a SEM to visualize the degradation of the particles.

3.4 Summary

In this chapter the incorporation of functional polymers in microparticles for controlled and stimuli-responsive selective degradation of particles and the release of their payloads is investigated. Particles containing polymer **2**, a rapidly degrading polymer, were used to establish controlled release systems with release rates of therapeutics ranging from 2-3 days to over 15 days. We have also demonstrated the fabrication of environmentally responsive anisotropic microparticles containing polymer **8** and characterized their pH responsive release of therapeutics. Additionally, the use of a novel dual stimuli responsive PEG-based polymer (**11**), where the co-operative action of both markers of oxidative stress and UV light induced rapid resorption of the polymer under physiological conditions, was explored. Here, the exogenous stimulus (UV light) acted as an on-switch, after which the particles became susceptive to the second, endogenous stimulus, a marker of oxidative stress. The resorbability of bicompartmental microparticles containing the dual-stimuli responsive polymer after exposure to UV light and oxidative stress was confirmed. Particles fabricated from these polymers, with their precisely controlled degradation of select compartments, can potentially be used to establish responsive nanoparticles with distinct release of multiple factors.

CHAPTER 5

Design of Particles for Cochlear Drug Delivery

The material in this chapter has been adapted with minor modifications from the following articles:

(1) S. Rahmani, A. M. Ross, T. H. Park, A. F. Dishman, H. Durmaz, D. Prieskorn, R. Altschuler, J. Lahann, "Multifunctional Microparticles for Cochlear Drug Delivery", *In preparation*.

(2) A. M. Ross, S. Rahmani, D. Prieskorn, N. Wys, A. F. Dishman, C. Martin, J. Lahann, A. Altschuler, "Persistence, Distribution, and Impact of Distinctly Segmented Microparticles on Cochlear Health Following *In Vivo* Infusion", *In preparation*.

5.1 Motivation and Background

Hearing is an integral part of an individual's life and any degree of hearing loss and/or deafness can bring about life-altering changes. In the US alone, over 36 million people, or 17% of the population, have been diagnosed with some level of hearing loss.[194] In fact, deafness is the number one disability in our nation. Based on recent census information, one in three people over the age of 65 and half of those over the age of 75

are affected by hearing loss.[195] Given the large number of people affected, and the foreseeable rise in this number as the elderly population grows, it is of imperative importance to seek medical technologies that restore hearing to these individuals.

In mammals, hearing is achieved by converting sound waves to vibrations that are detected in the inner ear. Within the inner ear, distinct vibration frequencies excite specific hair cells lining the turns of the cochlea. The excited hair cells are able to translate the vibrations to electrical signals and transmit them to the central nervous system for processing through the inner hair cell-auditory nerve synapses.[196] The loss of hearing, whether stemming from noise, ototoxic drugs, and/or aging, is typically caused by oxidative stress, which is the overproduction of reactive oxygen species (ROS) in the cell.[195, 197, 198] Numerous studies have focused on the use of therapeutics to counteract the overproduction of ROS as a means of preventing deafness in individuals, especially since deafness can occur anywhere from hours to weeks, month, or even years after the occurrence of the initial trauma.[199-201] Some of the main therapeutic methods used for the prevention of deafness include antioxidant drugs (salicylate,[201] allopurinol,[202] iron chelators,[203] ebselen,[204] or N-acetylcysteine[205]), heat shock proteins,[206] neurotrophic factors[207] (GDNF,[207-209] NT-3,[210] and BDNF[211]), and gene therapy.[212] While the use of antioxidative drugs and neurotrophic factors (systemically or locally) has been successful,[201, 207] the use of heat shock proteins and/or gene therapy has proven to be more difficult due to the incomplete understanding of the signaling pathways involved or the inability to target the therapies to specific sites in the cochlea.[213, 214]

In events when deafness cannot be adequately prevented, or for those individuals born with this condition, the inner hair cells are either severely damaged or completely

destroyed.[195] In such cases, cochlear implants are the choice method of therapy due to their ability to directly stimulate the auditory nerves and return some level of hearing for most individuals. With the advent of new technologies and a better understanding of cochlear physiology, more advanced cochlear implants with multiple channels have been developed in recent years that can provide a more enhanced and functional level of hearing to most individuals. Due to the success of cochlear implants in individuals with severe to complete hearing loss, individuals with a lower degree of hearing loss have recently qualified to use these devices.[195, 215] In these individuals, a certain percentage of the inner hair cells, and thereby the inner hair cell-auditory nerve synapses, are still functional and are able to translate & transmit sound vibrations to the central nervous system for processing. Unfortunately, studies show that the trauma induced by the insertion of cochlear implants increase the level of ROS[216] and often bring about the death of these remaining hair cells. The death of these hair cells destroy any remaining hearing the individual had maintained and force them to completely rely on the device.[215, 217] Recent studies have focused on the use of ROS preventative therapeutics to reduce the trauma from implant insertion and thereby increase the levels of hearing for these individuals.[216]

Current studies that focus on combining preservative measures and cochlear implant insertion to increase the hearing level of patients use therapeutics for the reduction of ROS as mentioned previously. From among these, the studies that involve neurotrophic factors have been most successful. These studies have used a variety of methods to deliver these factors either prior, during, or after the implant insertion. Kanzaki *et al.* has shown that the infusion of adenoviral vectors encoding a transgene for

GDNF (Glial cell Derived Neurotrophic Factor) at the time of surgery could significantly improve inner hair cell survival over a 43-day period.[218] Similarly, Yamagata *et al.* used a cannula-osmotic pump system loaded with BDNF (Brain Derived Neurotrophic Factor) with similar results. Animals receiving the neurotrophic factor had a higher rate of cell survival and scored significantly lower in the auditory brain stem response (ABR) recordings (where a lower score represents a more physiological state).[211] However, while both of these methods have worked well in animal studies, implementing them on humans has proven to be difficult. As with all gene-therapies, adenoviral vector treatment poses unknown side-effects due to an incomplete understanding of the mechanisms involved and the use of cannula-osmotic pump systems or mini-osmotic pumps is cumbersome and prone to cause infections.[195] The use of a delivery system capable of the continuous release of such neurotrophic factors and antioxidant drugs used in conjunction with the cochlear implant could prove to be a novel solution for this case.

5.2 Experimental Methods

5.2.1 Materials

Dextran, chloroform, dimethylformamide (DMF), dimethyl sulfoxide (DMSO), pyridinium *p*-toluenesulfonate, 2-methoxypropane triethylamine, acetic acid, sodium acetate, phosphate buffered saline (PBS), poly[tris(2,5-bis(hexyloxy)-1,4-phenylenevinylene)-*alt*-(1,3-phenylenevinylene) (PTDPV), poly[(*m*-phenylenevinylene)-

alt-(2,5-dihexyloxy-*p*-phenylenevinylene)] (MEHPV), heparin sulfate, and tween 20 were used as purchased from Sigma Aldrich, USA. Polylactide-*co*-glycolide (PLGA) with a ratio of 50:50 lactide to glycolide and a molecular weight of 44 kDa was purchased from Lactel Corporation. Piribedil was purchased from Ontario Chemicals and Glial Derived Neurotrophic Factor (GDNF) was a generous gift from MedGenesis Therapeutix, Inc.

5.2.2 Fabrication of Multifunctional Particles for Cochlear Delivery

Polymer **13**, a high molecular weight acetal dextran (70 kDa), was graciously synthesized by Dr. Tae-Hong Park and Nathan Jones, following a well established method.[41] Tricompartmental particles with one compartment composed of PLGA (50:50, 40 kDa, 10% w/v) and two compartments composed of polymer **13** and PLGA at a ratio of 65:35 and a total concentration of 7% were fabricated using the EHD co-jetting method. Here a lower overall percentage of polymers were used in the two similar compartments due to the higher molecular weight of the dextran polymer used. For the animal studies, particles with a blue dye in all three compartments were employed that could easily be identified in fluorescent microscopy.

To fabricate particles with piribedil, a 2% w/w amount of the drug was mixed into the jetting solution in the PLGA compartment. For the fabrication of particles with heparin, polymer **4** at a 25% w/w was incorporated in the two similar compartments. The particles were placed in pH 5 for 10 hrs to create porosity on two-thirds of the particles

and were then incubated with heparin overnight. After the incubation, the particles were UV'ed for 2 hours at 365 nm to cross-link the heparin to the benzophenone groups of polymer **4** in the particles via photoreactive chemistry. The particles were washed numerous times to remove the unreacted heparin and were then stored in PBS for further analysis. Zeta potential measuremnts were done to confirm the attachment of the heparin to the microparticles. To determine the optimal loading of GDNF onto the heparin labeled particles, GDNF at three different concentrations (25, 75, and 150 μl) were incubated with particles for 3, 6, and 24 hours (total 9 samples). At each time point, the particles were washed, labeled with primary and secondary antibodies against GDNF, and the samples' fluorescence was measured with a plate reader.

5.2.3 Persistence and Compatibility Testing of Particles *In Vivo*

Animal studies in guinea pigs with microparticles were done in Professor Altschuler's group by Dr. Astin Ross and Diane Prieskorn and the details are included in **Appendix D.**

5.2.4 Release of Therapeutics from Microparticles

To determine the release of Piribedil, the jetted particles were collected into four 20 mg samples and suspended in five ml of pH 5 buffer for 10 hours at 37 ^{o}C to create

pores in the particles. The particles were then washed with PBS and 1% v/v Tween 20, re-suspended in 5 ml of PBS, and placed in a 100-kDa dialysis membrane. The membrane was inserted into a Falcon tube containing 35 mL of the same buffer and gently shaken at 37 ^{o}C. At predetermined intervals, the tubes were removed from the incubator, the membranes were inserted in new tubes with 35 mL of fresh buffer, and replaced back in the incubator. The drug containing buffers in the Falcon tubes were then measured via a UV Visual spectroscopy machine to determine the amount of drug released based on a previously done calibration curve.

To determine the release of GDNF, 12 mg of particles were labeled with heparin and were then divided into 4 groups of 3 mg each. The volume was adjusted to 250 μl and 125 μg of GDNF was added to each sample. The volume was brought to 500 μl to make an effective 250 μg/ml concentration of GDNF for 6 mg/ml of particles. The particles were incubated with the GDNF for 6 hours, followed by multiple washes to remove unbound material. The final buffer solution (sterile PBS with 0.1% tween 20) was brought to a volume of 1 ml and the samples were incubated in a 37 ^{o}C incubator. At predetermined time intervals, the samples were removed and centrifuged at 4000 RPM for 2 min to gently pellet the particles. The supernatant was removed & frozen, the samples were washed to remove the free GDNF in the solution, and the samples were placed back in the incubator. The frozen samples were measured via an ELISA kit for GDNF from Abcam ® by Joel Whitfield.

5.3 Results and Discussion

To design multifunctional particles for cochlear delivery, a combination of the techniques developed in Chapters 2-4 were employed. The parameters for a successful carrier system included (i) the incorporation of piribedil (to reduce trauma-induced apoptosis) and its release over a 2-4 week period; (ii) the encapsulation, protection, and release of GDNF (to help with neural survival & elongation) for a 1-2 month period; (iii) establishment of the general biocompatibility of the particles in the cochlea; (iv) and the persistence of the particles within the time-frame of the study in the cochlea. To this end, tricompartmental particles were engineered through the EHD co-jetting method, where one compartment was composed of PLGA and piribedil, while the other two compartments were composed of PLGA, polymer **4** (benzophenone-functionalized PLGA), and polymer **13** (a high molecular weight acetal dextran) (**Figure 5-1**). The piribedil-containing compartment was designed to meet the first requirement mentioned above, where the release of the therapeutic was expected to span over a 15-20 day period based on previous studies with a similar molecular weight therapeutic (irinotecan) in the same polymer in section 4.3 of this dissertation. The polymers chosen for all compartments were biocompatible or biodegradable and thus should not have caused any MPS signaling or inflammation on their own in the cochlea. Additionally, the large size of the particles (6-8 μm) were chosen to delay uptake in the presence of any potential macrophages (the cochlea does not typically have resident macrophages). Moreover, the polymers, if biodegradable, were chosen to have a degradation rate that exceeded the time requirements for the persistence in the cochlea.

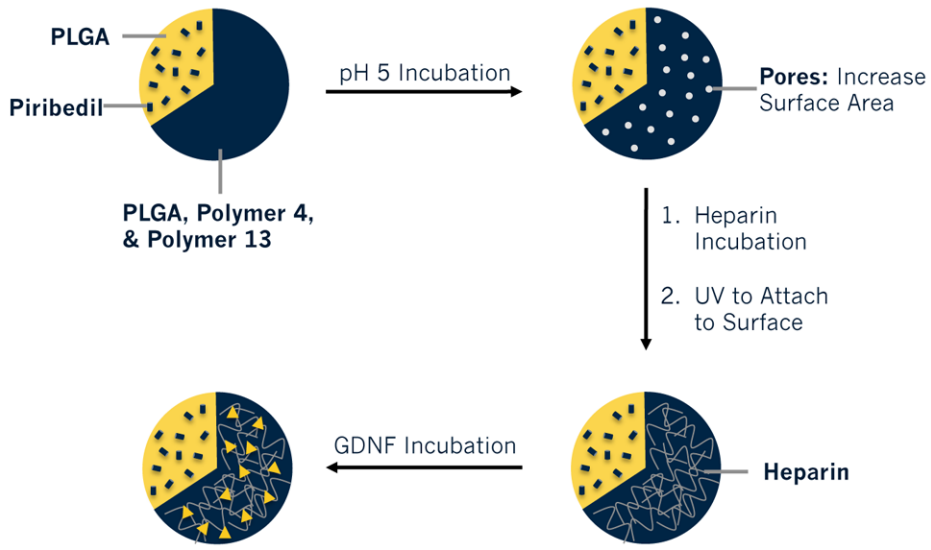

Figure 5-1: Design of multifunctional particles for cochlear delivery.

Lastly, but most importantly, the incorporation and release of GDNF from the particles was designed. This was not a simple matter, as growth factors are easily prone to degradation: the direct incorporation of GDNF in the jetting solutions would result in the denaturation of the growth factor in the organic solutions and, while some studies have successfully incorporated proteins in PLGA particles, the degradation of the polymers and the associated acidic pockets, typically denature the proteins during the release phase.[219] To address this challenge, the particles could be functionalized with heparin, which is well established for its interactions with various growth factors that can be employed for the loading and release of the GDNF, and its ability to shield the GDNF from degradation during this time.[220-223] To accomplish this, particles containing polymer **4** and **13** were designed, where the release of polymer **13** via incubation in a pH 5 buffer would create pores in the particles and increase the surface area, while the benzophenone groups in polymer **4** could potentially be used to cross-link the heparin to the surface of the particles. A full schematic of the designed particles is demonstrated in Figure 5-1.

To begin, the unloaded particles were analyzed to determine their size distribution, release of dextran, and their level of porosity (**Figure 5-2**). Similar to particles in 3.3 with polymer **8** (low molecular weight dextran acetal), the as-fabricated particles have a negative zeta potential measurement (~25.5 mV ± 0.8) due to the free hydroxyl groups available in polymer **13**. Upon pH 5 incubation and the release of the dextran from the particles, the remaining porous particles composed primarily of PLGA have a less negative zeta potential value (-13 mV ± 2.8), which confirms the release of the dextran. Further evidence of the release of polymer **13** from the particles in the acidic environment is shown in Figure 5-2C where SEM images of the particles clearly demonstrate the creation of pores over a period of time in the bulk of the particles. Here, the desired level of porosity (before further degradation of the particles) is achieved at 10 hours in comparison to the 5 hours previously observed with the lower molecular weight

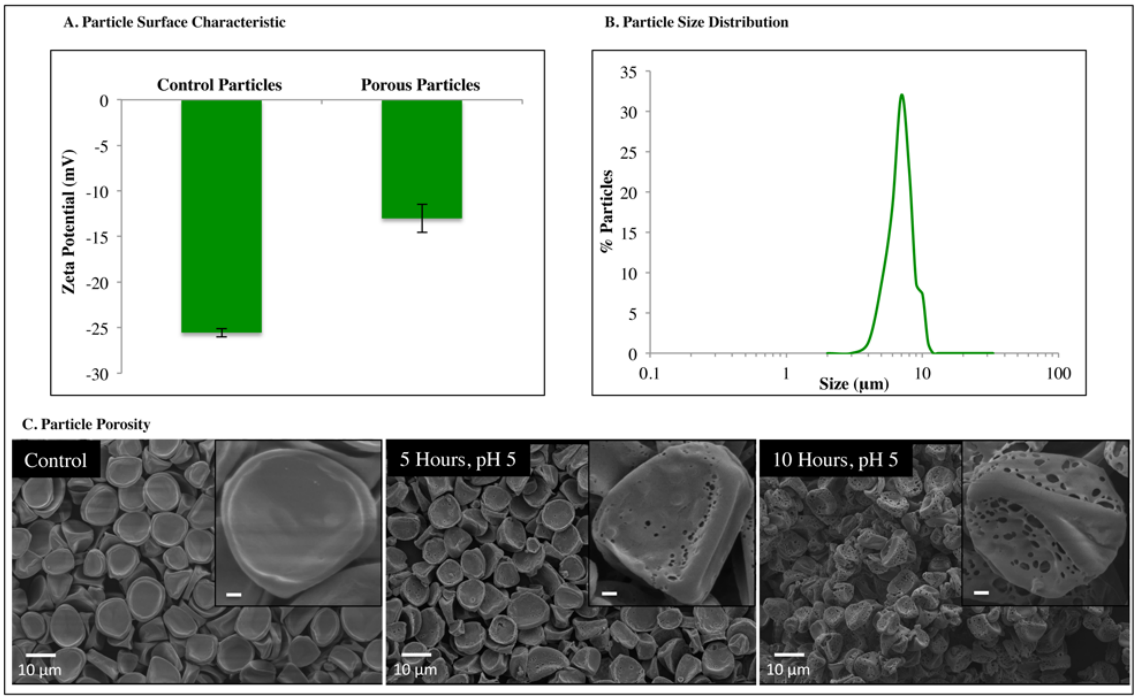

Figure 5-2: Characterization of unloaded particles. (A) The zeta potential measurement of the particles before and after pH 5 incubation, (B) the size distribution of the particles based on SEM images, and (C) the degree of porosity as a function of time.

polymer **8**, which is as expected: the longer chained molecules in this case will move at a slower speed out of the polymer matrix of the particles as compared to the smaller chained molecules in the previous study. The size distribution of the microparticles (Figure 5-2B) demonstrates relatively uniform particles at 7.8 ± 1.4 μm.

Once the characterization of the particles was established, the persistence and general compatibility of the particles on their own within the cochea was examined. This was especially important since the persistence and continuous release of the therapeutics within the cochlea is important for the survival of the hair cells. Here, blue-labeled particles were injected at the base of the cochlea and after one or seven days the animals were sacrificed and their cochlea were dissected and imaged via 2-photon microscopy (**Figure 5-3**). Figure 5-3B-C are the three dimensional reconstruction of the 2-photon

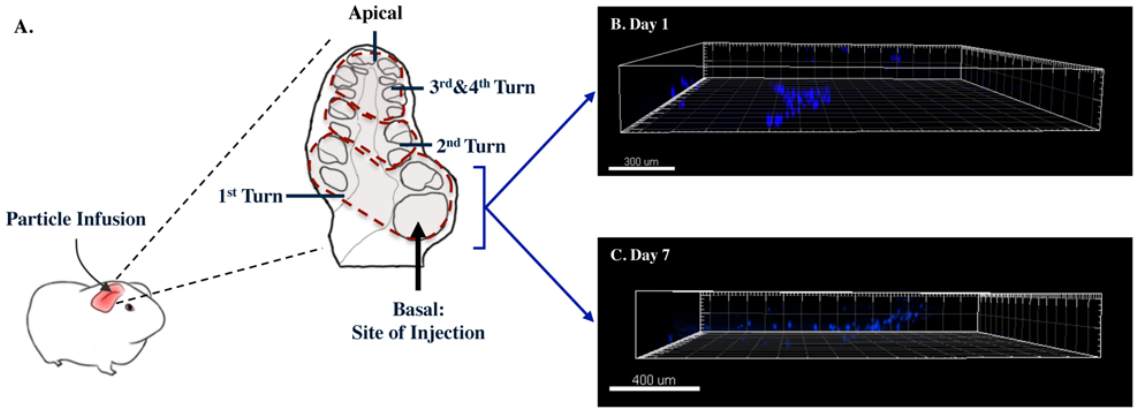

D. Turns	1 Day		7 Days	
1st	3,061 (± 480.4)	87.81% (± 21.84)	3,647 (± 230.7)	93.97% (± 16.7)
2nd	350 (± 34.7)	10.04% (± 2.9)	234 (± 11.5)	6.03% (± 1.5)
3rd & 4th	75 (± 2.6)	2.15% (± 0.2)	0	0%
Total	3486 (± 548)		3881 (± 261)	

Figure 5-3: Persistence of particles within the cochlea. (A) Schematic describing the procedure used to infuse the particles into the cochlea, and a cartoon of a cross section of the cochlea outlining the site of injection and its individual turns. (B-C) 3D reconstruction images of particles within the cochlea after 1 and 7 days, respectively. (D) The particle distribution within the cochlear turns.

images of particles from the basal section of the cochlea, clearly demonstrating the presence of particles within the cochlea after one or seven days. The table (Figure 5-3D) contains individual particle counts from three sections in center of the cochlea, showing a representative distribution of the particles within the cochlear turns for both days. The majority of the particles are located near the base (Turn 1) of the cochlea for both days and at similar concentrations, potentially implying that the particles that survive the first 24 hours post-infusion remain in the cochlea for a prolonged period. Additionally, the distribution of the particles in the first turn is ideal for our case since the majority of the damage to the hair cells occur in this region. **Figure 5-4** contains individual images of particles within each of the cochlear turns at the one-day period for reference. Here again, a similar trend can be observed where the majority of the particles are seen in the fist channel followed by lower percentages in the turns closer to the apex.

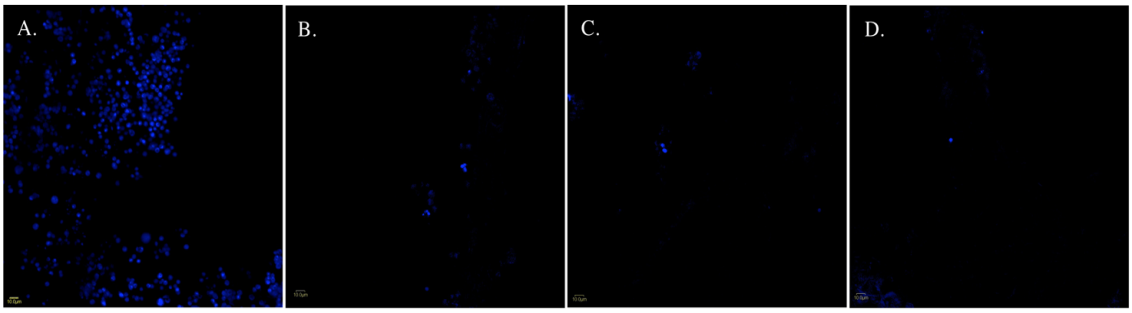

Figure 5-4: Persistence of particles within the cochlea. (A-D) representative images of each of the turns of the cochlea showing the distribution of the particles (blue) in each.

In addition to determining the persistence of the particles within the cochlea, we were also interested in determining whether the presence of the particles altered any detectable functioning abilities of the cochlear components. To test this, an ABR (auditory brainstem response) test was performed (**Figure 5-5**). In this test, sound is

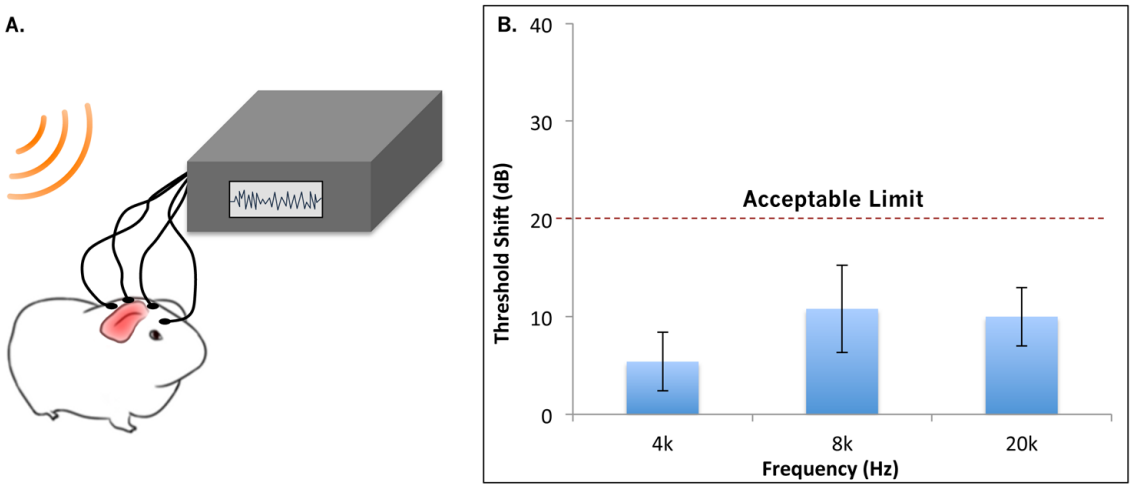

Figure 5-5: ABR testing of guinea pigs after particle infusion into the cochlea. (A) Representative schematic of the procedure and (B) ABR analysis done at various frequencies.

given at various decibels in specific sets of frequencies to animals and their electrical impulses (time response of neurons) are recorded. In these studies, a significant (greater than 15-20 dB) shift in the recorded responses signifies a potential damage to the hair cell functioning and viability. Here, animals were tested at three different frequencies (4, 8, and 20 kHz), infused with particles, and retested after seven days. The shifts at all measured frequencies were well below the acceptable limit, potentially signifying that the presence of particles in the cochlea does not interfere with cochlear components.

Upon characterizing the microparticles and confirming the persistence of the particles in animals, the continuous release of the anti-oxidant therapeutic, piribedil, from the microparticles was assessed. The pH of the fluid within the microenvironment of the cochlea, the perilymph fluid, is at neutral pH and since a continuous release over a 10-20 day period is most optimal for the release of the anti-oxidant therapeutic following surgery and the insertion of the cochlear implant, release from a 44 kDa PLGA polymer was chosen. Particles composed of PLGA and piribedil in one compartment and PLGA and polymer **13** in the other compartments were fabricated following the EHD co-jetting

procedure. The particles contained a green dye in the piribedil containing compartment and a blue dye in the PLGA/polymer **13** compartments. **Figure 5-6A** demonstrates the compartmentalization of these particles. Here, Piribedil auto-fluoresced in the red channel, and this was used as a method to confirm the compartmentalization of the drug. As can be seen in the middle and right images, the red channel overlaps with the green channel (middle) and is completely separate from the blue channel (right), confirming the encapsulation of the therapeutic in the selected compartment. To determine the release kinetics of the piribedil from the therapeutic system, particles were incubated at 37 ^{o}C in a phosphate buffered saline solution and at pre-determined intervals samples were taken of the released material and measured via UV visual spectroscopy to determine the amount of pribedil released. As demonstrated in Figure 5-5B, the release of piribedil

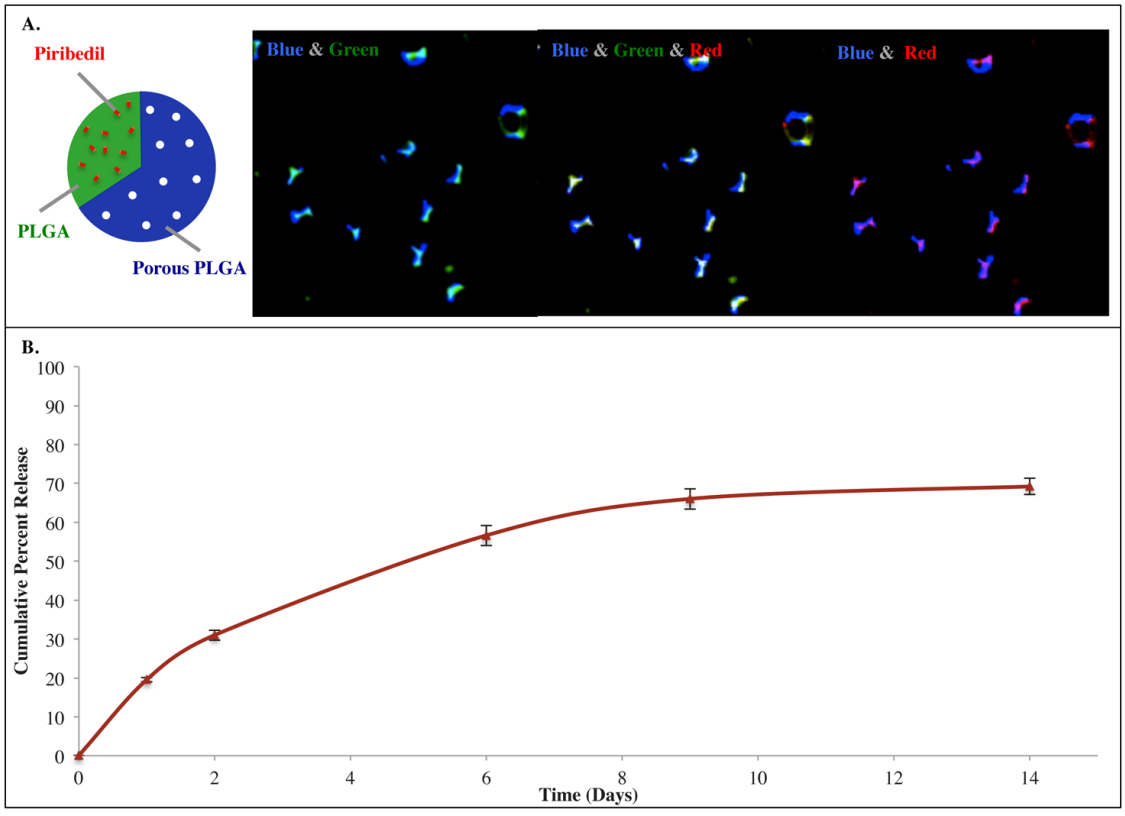

Figure 5-6: Encapsulation and release of piribedil from particles. (A) Schematic showing the location of each component in the particles, and individual channels showing the encapsulation of piribedil (red) in the green compartment. (B) The continuous release of piribedil from particles over a 14-day period.

from the particles is continuous over a 14-day period, which is ideal for the release of the anti-excitotoxic therapeutic.

Next, we were interested in incorporating a neurotrophic factor into our particles. As previously mentioned, a great challenge in this field is the encapsulation and release of the proteins, especially growth factors, without denaturing them in the process. Tri-compartmental particles with PLGA, polymer **4**, and polymer **13** in two compartments and PLGA in one compartment were fabricated according to our original design. The particles were incubated in an acidic environment to create pores in the system, which increased the effective surface area of the particles. The particles were then incubated in a heparin solution, which allowed the heparin molecules to infiltrate into the pores of the microparticles. The particle/heparin mixture was then exposed to UV light, which cross-linked the heparin to the polymer **4** in the particles via photoreactive chemistry (**Figure 5-7**). Zeta potential measurements were done to confirm the attachment of the heparin to the surface of the particles. As shown before, the zeta potential measurements of the particles become less negative after pH 5 incubation and the creation of the pores. After heparin attachment, however, the zeta potential of the particles is more negative again due to the negatively charged groups on the heparin. After heparin attachment, the particles were incubated with GDNF, which is known to associate with heparin. After loading the particles with GDNF, antibody staining was done to confirm the presence of the growth factor selectively on one side of the particles (Figure 5-7B). Here, the PLGA only compartment contained a green dye, the heparin compartment contained a blue dye, and the GDNF is labeled with a magenta dye (Alexa 647 goat anti-rabbit). The three-

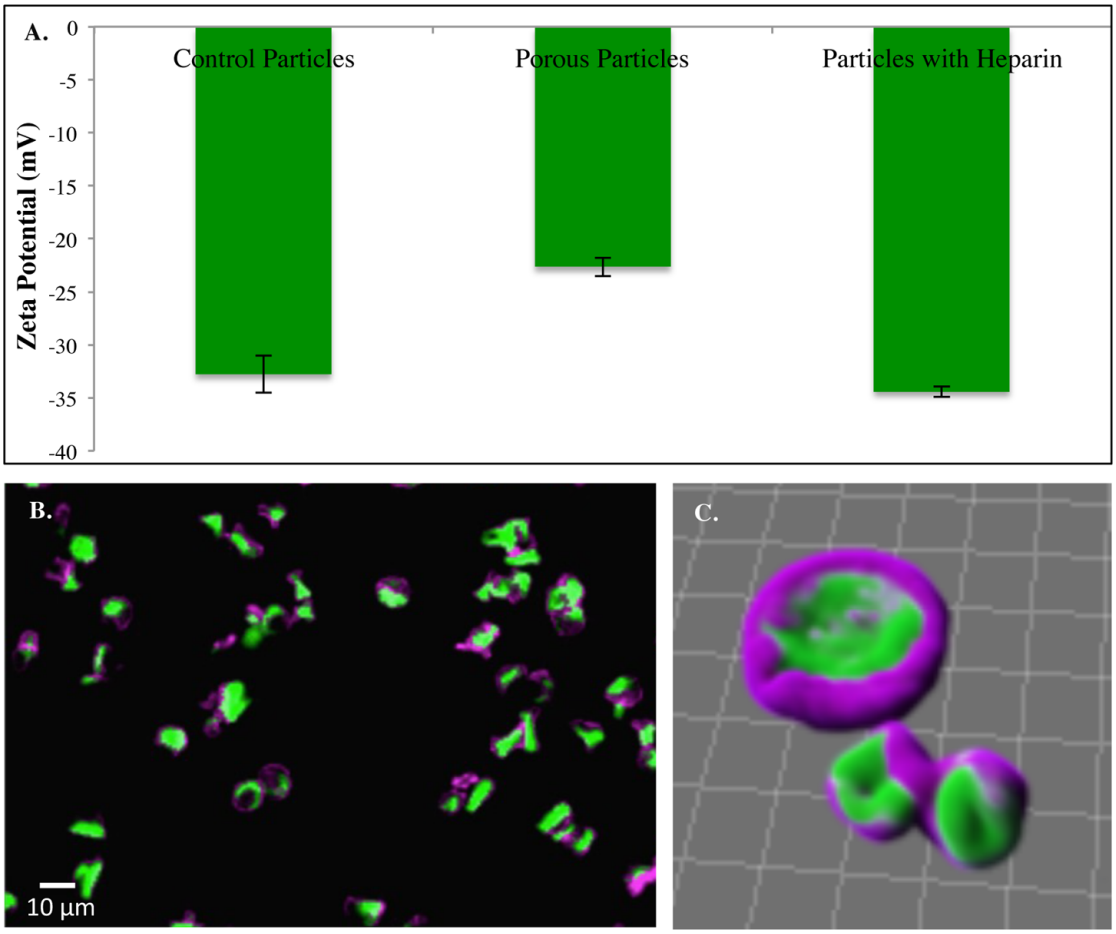

Figure 5-7: Incorporation of heparin and GDNF on the particles. (A) Zeta potential measurements of particles before/after dextran release and after heparin attachment. (B) CLSM images of particles loaded with GDNF and labeled with a magenta secondary antibody and (C) their 3-D reconstruction showing the compartmentalization of the GDNF.

dimensional reconstruction of the particles clearly display the compartmentalization and presence of GDNF on the particles.

Further studies were done to determine the optimal condition for the loading of GDNF into particles (**Figure 5-8**). Here, heparin functionalized particles were incubated with three concentrations of GDNF (25, 75, and 150 µg/ml) and their individual loadings into particles were measured at three incubation time points (3, 6, and 24 hours). To determine the relative amount of GDNF loading, the particles were washed after each incubation, then labeled with primary and secondary antibodies against GDNF, where the

secondary contained a fluorescent molecule. The solutions containing the particles were then measured using a plate reader to determine the relative fluorescent intensity of each sample, which is directly proportional to the concentration of secondary antibody and thereby the GDNF incorporated into each particle set. As expected, increasing the initial concentration of GDNF incubated in the particles resulted in an increase in the amount of GDNF loaded into the particles, where a plateauing effect is not observed for the concentrations tested. Base on this, a high loading of GDNF can be achieved using our designed particles, which is therapeutically desirable as it requires a lower number of particles per injection. Additionally, the optimal incubation time was also determined for this study to potentially be at 6 hours, since shorter incubation times do not allow sufficient time for the incorporation of the GDNF into the particles and longer durations result in the denaturation of the majority of the GDNF, as observed by the significant decrease in the detected amounts at 24 hours.

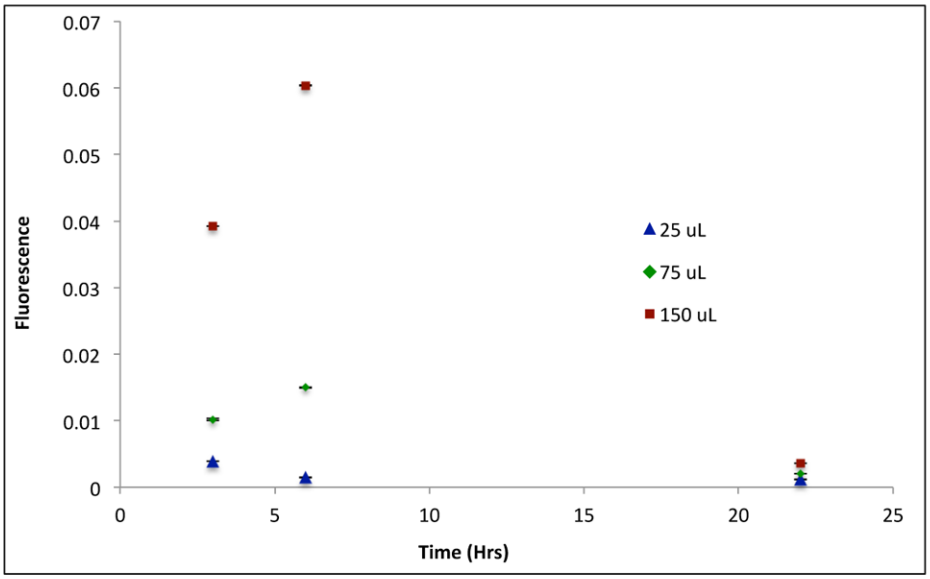

Figure 5-8: Determining the optimal conditions for GDNF loading onto particles. The fluorescent intensity of labeled GDNF at three different concentrations and three incubation time points were measured with a plate reader to determine the optimal conditions for the maximum loading of GDNF into particles.

Once the optimal loading conditions for GDNF had been established, the release of GDNF from particles was investigated. Here, the particles were loaded with GDNF, washed to remove unreacted material, and incubated at physiological conditions. At various time points, the samples were pelleted and the supernatant containing the released GDNF was frozen. These samples were then measured via a GDNF specific ELISA (Enzyme Linked Immunosorbent Assay) to determine the precise amount of GDNF released at each time point. **Figure 5-9** shows the release of GDNF over a 30-day period, which shows the successful and continuous release of the growth factor.

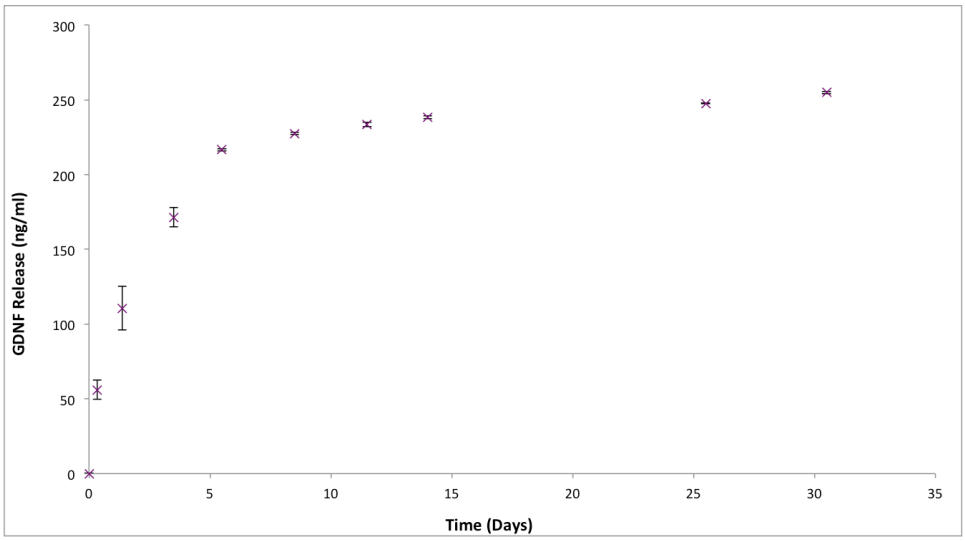

Figure 5-9: Release of GDNF from particles. The release of GDNF as determined based on ELISA measurements over a 50 day period is demonstrated.

5.4 Summary

Multicompartmental particles loaded with multiple therapeutics are an ideal carrier system for delivery to the cochlea where the distinct release of each factor is desired. In this chapter, the design of particles loaded with a small molecule drug and a growth factor for cochlear delivery are explored. The characterization of the base particles and the *In Vivo* persistence and distribution of the microparticles throughout the cochlea after a one- or seven-day period are shown. The selective loading of a small molecule therapeutic and its controlled release is demonstrated. In addition, a novel approach for the loading, protection, and release of a growth factor using heparin functionalized particles is investigated. Together, these results suggest that the methodologies developed in the previous chapters of this dissertation can successfully be employed for the design of multifunctional particles for specific applications.

CHAPTER 6

Conclusions and Future Directions

Throughout this dissertation, the fabrication of multifunctional particles via the EHD co-jetting procedure, methodologies for the programming of specific physical and chemical characteristics, and the use of functional polymers for the responsive release of therapeutics is investigated. Additionally, the application of these techniques for the design of multifunctional particles for the delivery of multiple factors to the cochlea is explored. While these strategies have led to the composition of a toolbox for the design of particles for specific applications, the actual use of these strategies beyond the fabrication of particles for cochlear delivery is yet on-going. Below, specific outlooks for each of this dissertation's chapters are discussed.

6.1 Applications for the Surface Modification of Particles

The attachment of targeting ligands and stealth moieties to the surface of particles was explored in chapter 2, where the attachment of folic acid, iRGD, and PEG to distinct patches was demonstrated. Beyond the simple attachment of these molecules to the surface of particles, further studies into the effect of multi-valency and avidity (multiple

factors of the same targeting molecule or the cooperation of multiple factors, respectively) can also be further studies. Here, the ligand density of the particles can both be controlled based on the concentration of targeting ligands used (up to the saturation point of the functional groups on the surface) or by using different ratios of functional polymers to internally control the maximum number of functional groups present on the surface. By having good control over the ratio of the ligand molecules used, one can establish and sequentially test the effect of ligand concentration on targeting and circulation. Additionally, an important factor in designing the surface of nanoparticles is the ratio between the stealth and targeting molecules. Several design parameters exist, such as: i) isotropic particles with a mixture of both types on the surface using the same ligand chemistry; ii) isotropic particles with a mixture of both types on the surface where the ratio is well established due different ligand chemistries; iii) anisotropic particles with specific patches for each of the ligands; iv) anisotropic particles with specific patches where some have a mixture of the two, and some have just the stealth ligands on the surface. Each of these scenarios has their advantages and disadvantages, and a solid understanding of which system is optimal is lacking based on the current literature. The testing of such particles could lead to not just finding a more effective therapy, but also a better understanding of how opsonization and targeting mechanisms occur in the body.

In addition to controlling the ratios of stealth and targeting ligands on the surface of carrier systems, one could also think about testing the effect of multiple ligands. The cooperative effect of multiple ligands, and the effect of the valency of each, could potentially be tested by using patchy particles where each patch represents a specific ligand. For example, for cancer therapy a ligand could be used for targeting to the

vasculature near the tumors, another could be used for targeting to the cancer cells, and yet another for penetration within the tumor. Additionally, targeting within the cell to the correct site could also be explored. It might be that through the use of such design parameters, particles can be fine-tuned and optimized for their specific applications.

While the design of such systems is very possible using the EHD co-jetting system, the downstream effects of covering the entire surface of these particles with targeting ligands must also be considered. While additional targeting ligands might make the particles more specific and, as a result, potentially more effective systems, if the increase in the targeting ligands results in a decrease in the stealth ligands and compromises the circulation time of the particles, the system might not have sufficient time to get to the target site. As a result, the design of such systems is not an effortless task, but rather can be ambiguous and requires the consideration of various parameters.

In addition to the use of selective surface modification for targeting to specific sites in the body, such surface modification could also potentially be used for the capture of circulating tumor cells. Circulating tumor cells (CTCs) are typically present in extremely low numbers in the blood of most patients suffering from metastatic cancer and have been hypothesized to be the origin of the intractable metastasis of the tumor to other locations in the body.[224] As a result, the capture and study of these cells is an important step in developing a therapy for metastatic cancers. Most CTCs have been noted to overexpress EpCAM (epithelial cell adhesion molecule)[225, 226] and material functionalized with anti-EpCAM antibodies have the potential to target to these rare cells. In collaboration with Professor Nagrath's group in the Chemical Engineering department, we were interested in using particles coated with anti-EpCAM antibodies along with their

well-established microfluidic devices as a means for the capture and further purification of CTCs from patient blood samples.

Here, the surface of particles containing PLGA, polymer **6**, and polymer **8** were sequentially functionalized with azide-PEG-biotin, neutravidin, and biotin conjugated anti-EpCAM (**Figure 6-1**). The particles were then labeled with a secondary antibody and their specific attachment was evaluated against particle that were not incubated with the biotin anti-EpCAM molecule. The particles containing anti-EpCAM were clearly labeled with the secondary antibody (Figure 6-1B, where the inset is a 3D reconstruction of the particles from CLSM images and shows complete coverage by the antibody),

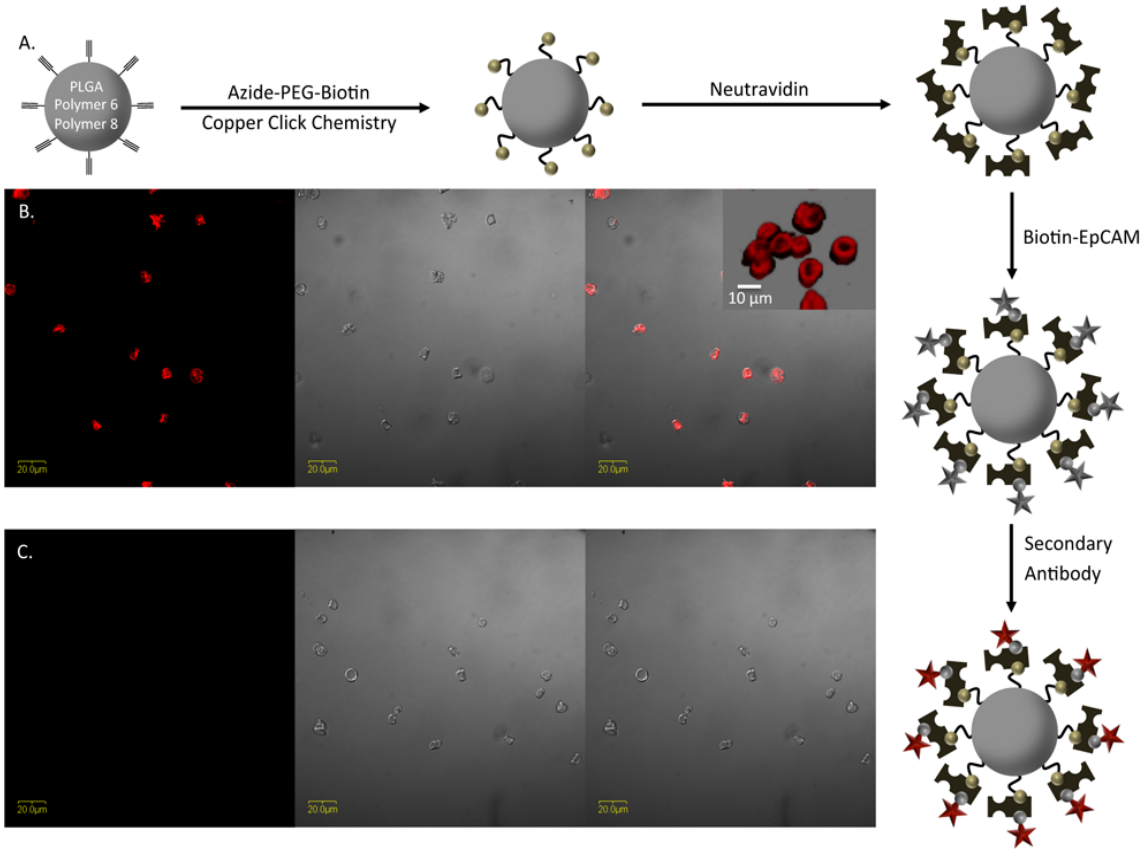

Figure 6-1: Functionalization of particles with anti-EpCAM. (A) Schematic of the steps taken to functionalize the surface with anti-EpCAM and (B-C) secondary antibody labeling of particles to determine the attachment. Here the anti-EpCAM labeled particles fluoresce in the red channel (B), while the control particles are not labeled (C). The inset in (B) is a 3D reconstruction of the particles showing complete coverage by the anti-EpCAM molecule.

while the controls did not have any staining from the secondary antibody (Figure 6-1C).

While the surface functionalization of these particles has been established, the testing of these particles to determine their ability in capturing CTC's is yet to be determined. Additionally, the procedure established here could easily be extended to other targeting molecules that are labeled with biotin. This introduces a method for the functionalization of particles with antibodies that may be prone to denaturation through the common attachment of proteins via EDC/Sulfo-NHS chemistries.

6.2 Testing the Effects of Physical Properties on Particle Functionality

The programming of physical properties of particles such as shape, size, charge, and texture were extensively studied in Chapter 3. Going forward the effect of such physical properties on the functionality of particles in the body need to be tested. While the ability to impart multiple properties has been explored, they each need to be examined to determine their potential suitability for their specific applications, especially how they fair in circulation. This is especially difficult to accomplish without the use of a large number of animals.

A potential method for testing the behavior of particles in blood is the use of Nanoparticle Tracking Analysis (NTA) technology with a Nanosight device, which tracks individual particle sizes based on their diffusion rate. While similar techniques used for size determination would detect both particles and plasma components, the Nanosight will be able to differentiate the particles based on their fluorescent signal. Here a proof of

concept study was done to determine the feasibility of this idea. Purchased, green fluorescent particles were incubated in serum and their size distribution as a function of time was studied (**Figure 6-2**). It can clearly be seen that at longer time-points the average diameter of the particles increase as a layer of proteins attach to the surface (opsonization) and eventually form some aggregate. Going forward, this approach could be applied to the testing of the effect of various physical properties in serum to determine the feasibility of particle sets before testing them animals.

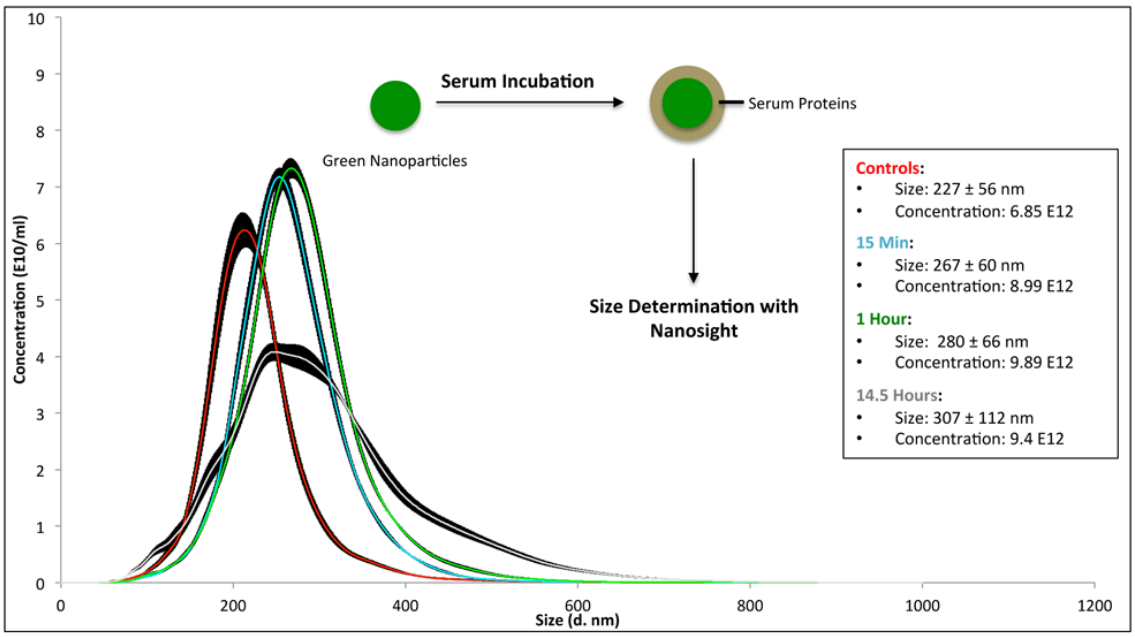

Figure 6-2: Effective size of nanoparticles in serum. Nanoparticles were incubated in serum for 15 min, 1 and 14.5 hours and their effective size range was determined using Nanosight. The colored lines signify the average size while the black lines are the standard deviations per size derived from 6 runs of over 3-4 thousand tracked particles.

6.3 Toward Dual Release of Therapeutics

In chapter 4, the on-demand degradation and responsive release of therapeutics using functional polymers was explored. However, while both the degradation and release of therapeutics from polymer **2** and polymer **8** were established, dual responsive release of therapeutics from polymer **11** has not been explored. In addition, the release of more than one small molecular weight therapeutic with distinct kinetics from the same particle set is yet to be determined. Here, one of the major challenges was the encapsulation of small molecular therapeutics in select compartments. While these therapeutics stay compartmentalized at lower concentrations (for example irinotecan and piribedil at 2% w/w), most therapeutics will diffuse into the second compartment during the jetting procedure due to their small size. While an exception to this in a specific case (section 3.3) has been studied, the majority of therapeutics, especially in PLGA polymers, are not compartmentalized at higher concentrations (**Figure 6-3A**). To this end, a particle system with a third, middle compartment composed of a high molecular weight,

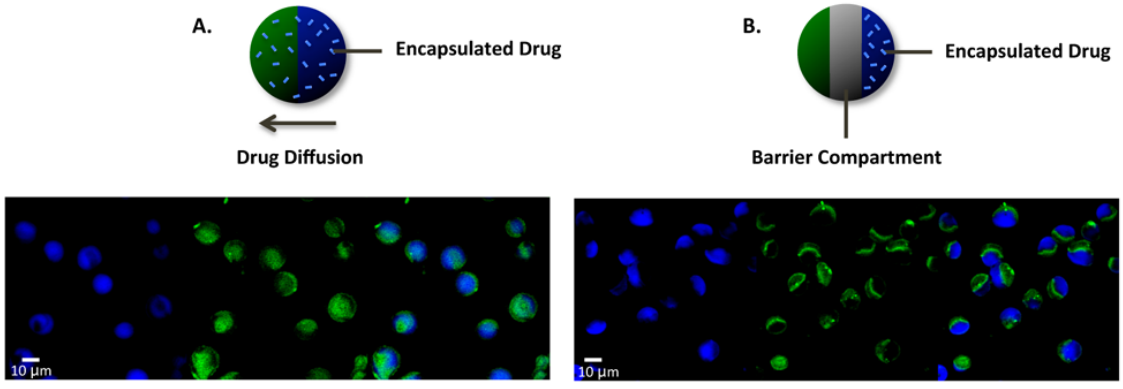

Figure 6-3: Compartmentalization of therapeutics in particles. In bi-compartmental particles, therapeutics at high encapsulation rates (here 25% w/w) diffuse to the other compartment during the jetting process (A). Incorporation of a 'barrier' compartment composed of a high molecular weight, hydrophobic polymer reduces the rate of diffusion and results in compartmentalized therapeutics even at high concentrations.

hydrophobic polymers was fabricated. Here, this compartment acted as a "barrier" to prevent the diffusion of the therapeutic to the other compartment. As shown in Figure 6-3, irinotecan (autofluorescing in the blue compartment) is not compartmentalized in the bi-compartmental particles, meaning that blue is also seen in the green compartment, while it is compartmentalized in the tri-compartmental particles with a barrier compartment in between, signified by the blue and green dyes that do not overlap. This technique could potentially be used for the fabrication of particles with multiple drugs encapsulated in separate compartments for the establishment of dual, distinct release of therapeutics.

6.4 Towards Multiple Protein Delivery

The design of multifunctional particles for cochlear delivery was examined in detail in Chapter 4, and the fabrication of such particles and their testing for release of multiple factors was established. Looking forward, the feasibility of such drug loaded particles in animals needs to be explored. Such testing needs to include appropriate controls and examine the effect of the release of each therapeutic individually, combined, and delivered in a different method as a control (for example via an osmotic pump) to determine the advantages and disadvantages of the multifunctional particles.

In addition, while the techniques established for the incorporation of GDNF in particles using heparin works well because of the strong interaction between heparin and the growth factor, this strategy cannot always be applied to other growth factors and

proteins, especially if they do not have the appropriate binding sites to establish interactions with heparin. As such, other techniques for the incorporation of growth factors should be investigated. A possible strategy is the development of core-shell type particles where the center compartment is composed of a water-soluble core and the shell is composed of PLGA (**Figure 6-4**). This could potentially allow for the incorporation of a small molecule therapeutic, like piribedil, in the shell of the particles, while allowing for the incorporation and protection of the protein in the core. The release of the therapeutics would then depend on their diffusion through shell compartment. Here preliminary studies with core-shell particles and their characterization (Figure 6-4B-C, SEM & TEM (transmission electron microscopy), respectively) are demonstrated. Further analysis with regards to the encapsulation and release of proteins is needed to determine the feasibility of this system as an alternative method to the current established use of heparin. Additionally, the combination of both techniques could potentially result in particles with multiple protein release kinetics both for heparin binding growth factors and other types of proteins.

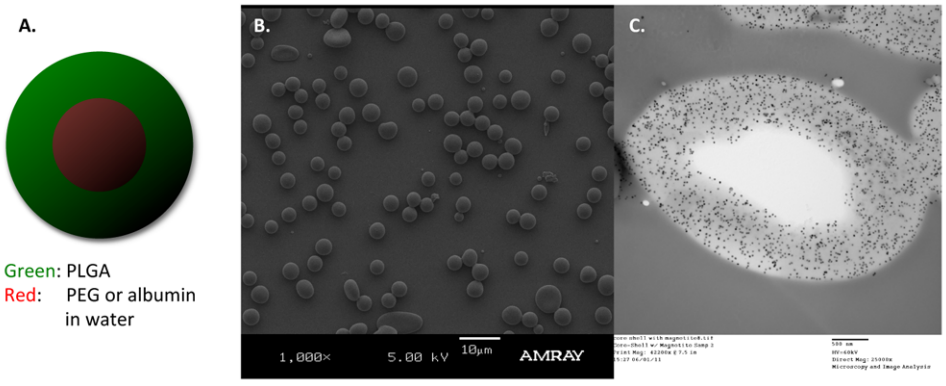

Figure 6-4: Fabrication of core-shell particles. (A) Here the shell is composed of PLGA and the core is composed of a water-soluble compound, such as PEG or albumin. (B-C) SEM and TEM analysis of the particles. For the TEM images, iron oxide nanoparticles were encapsulated in the shell to provide a contrast for the imaging. The particles were embedded in paraffin, then sections at 100 nm before mounting for TEM analysis.

6.5 Future Outlook

The work established in this dissertation has lead to the formation of a toolbox that can be used for the design of multifunctional particles with programmable properties for individual applications. While this work explored the design of particles for cochlear delivery, future investigations could focus on the use of these parameters for the design of multifunctional particles for applications such as cancer therapy, cardiovascular disease diagnosis, and Alzheimer therapy. Each of these individual applications has their own unique requirements and particles need to be optimized for each separately. More importantly, each particle set needs to be validated for their specific desired parameters. Certain tools already exist, however, the majority relies on the injection of particle into animals to determine their fate. While this is a valid method for characterizing a particle system's functionality as a whole, it does not allow for the understanding of which specific physical properties are determining its functionality. To validate the particles for such applications, *In Situ* tools that eliminate the use of a large number of animals and delays in deciphering the optimal properties for particles need to be developed.

Appendix A

Synthesis and Characterization of Functional Poly (Lactide -*co*-Glycolides)

The synthesis and full characterization of functional polymers used were graciously done by Dr. Sampa Saha and Dr. Hakan Durmaz.

Monomer A Synthesis:

Monomer **A** has been synthesized using the literature reported procedure.[131]

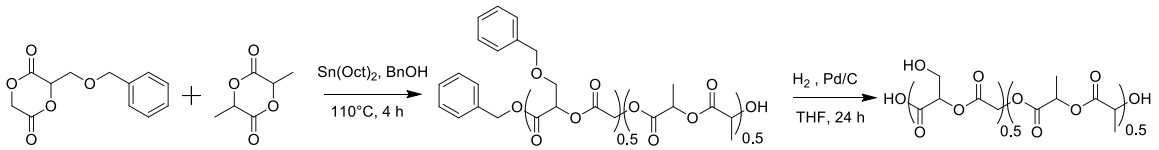

Scheme 2-1: Synthesis of the hydroxylated poly (lactide-*co*-glycolide)

Random copolymer synthesis (Scheme 2-1):

Ring-opening co-polymerizations of monomer **A** and l-lactide were performed in the melt using benzyl alcohol (BnOH) and $Sn(Oct)_2$ as the initiator and catalyst, respectively. Briefly, monomer **A** (4.56 g, 19.3 mmol) and recrystallized l-lactide (2.78 g, 19.3 mmol) were placed in an oven dried Schlenk flask equipped with a small stirring bar under a dry argon atmosphere. BnOH (10.5 mg, 0.1 mmol) and catalyst $Sn(Oct)_2$ (39.6 mg, 0.1 mmol) were added by an argon purged dry syringe, and the flask was kept under

vacuum for 2 hours. The flask was then closed and immersed in an oil bath thermostated at 110 °C for 4 hours. The resulting polymer **A** was dissolved in dichloromethane, precipitated in cold methanol, and dried in vacuum. Polymerizations proceeded in good yield (90%). *^{1}H NMR:* ($CDCl_3$) δ: 1.5-1.7 (m, 6H), 3.8-4.0 (m, 2H), 4.5-4.6 (m, 2H), 4.6-5.0 (m, 2H), 5.1-5.3 (m, 2H), 5.4-5.5 (m, 1H), 7.2-7.4 (m, 5H).

Deprotection of Polymer A to yield Polymer 2 has been done using literature reported procedure.[131] The yield of the final polymer **2** was around 80%. Found Mn: 46333; Mw: 52883; PDI: 1.14; (Molecular weight has been determined by GPC using polystyrene as calibration standard). *Polymer 2 characterizations: ^{1}H NMR:* ($CDCl_3$) δ: 1.5-1.7 (m, 6H), 3.8-4.0 (m, 2H), 4.6-5.0 (m, 2H), 5.1-5.3 (m, 2H), 5.4-5.5 (m, 1H). *FT-IR:* ν = [1100, 1300, 1190, 1200, 1260, 1350, 1380, 1400, 1450, 1770, 2920, and 2980 cm^{-1}]. *Raman:* ν = [1440, 1750, 2876, 2900, 2943, 3000 cm^{-1}].

Functionalization and characterization of polymers 3, 4, and 5 (Scheme 2):

Functionalized poly-lactide derivative 3: Compound **2** (3-(diphenylphosphino)-4-(methoxycarbonyl) benzoic acid) was synthesized according to the literature reported protocol.[132] 56 mg of compound **2** was dissolved in 1 ml of dry dichloromethane under dry argon atmosphere. Then 42 mg of DCC (dicyclohexyl carbodiimide) and 12.5 mg of DMAP (N,N dimethyl amino pyridine) was added to this solution. The solution was stirred for 10 min, then 15 mg of polymer **2** was added under argon and stirred for overnight at RT. Next, all the solvents were evaporated to dryness. Then the resulting

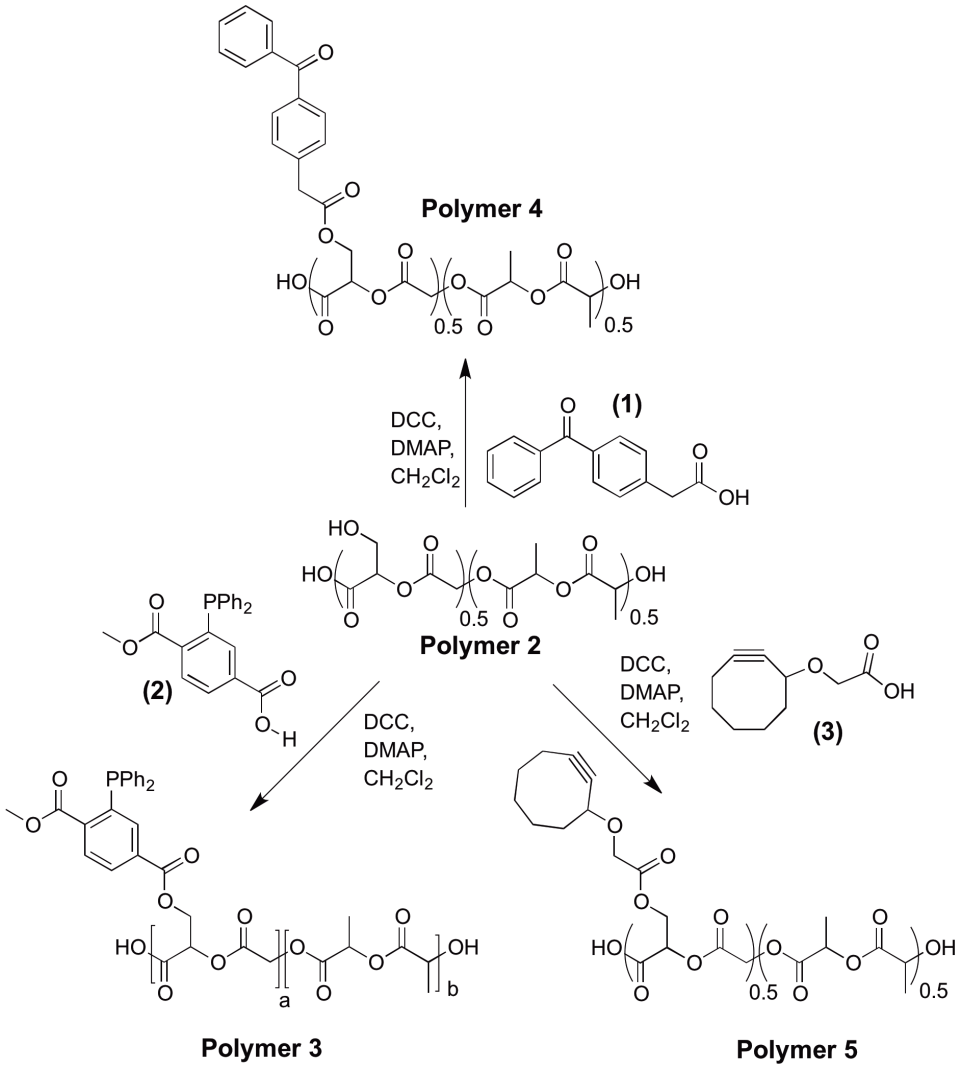

Scheme 2: Synthesis of poly (lactide-*co*-glycolide) derivatives.

polymer **3** was dissolved in minimal amount of dichloromethane, precipitated in cold methanol, and dried in vacuum. Functionalization proceeded in good yield at 90% conversion. This polymer is air sensitive and after work up we found that around 20% of triphenyl phosphine functionality of polymer **3** was converted to its phosphine oxide analogues. Hence, we stored the polymer in oxygen free atmosphere (vacuum dessicator) for future use. We have used this mixture of polymers (70% polymer **3**, 20% phosphine oxide analogue of polymer **3** and 10% polymer **2**) for subsequent study.

Polymer 3 characterization: ^{1}H *NMR:* ($CDCl_3$) δ 1.42-1.67 (bs, 6H), 3.62-3.82 (s, 3H), 4.42-4.97 (m, 4H), 5.02-5.3 (m, 2H), 5.38-5.58 (bs, 1H), 7.18-7.78 (m, 13H). ^{31}P *NMR*: ($CDCl_3$) δ: -4.3 ppm. *FT-IR*: ν = [1100, 1200, 1180, 1260, 1280, 1350, 1380, 1430, 1580, 1730, 1760, 2940, and 2980 cm^{-1}]. *Raman*: ν = [1430, 1596, 1732, 2896, 2900, 2943, 2977, 3057 cm^{-1}].

Functionalized poly-lactide derivative 4: Compound **1** (2-(4-benzoylphenyl) acetic acid) was synthesized according to the literature reported protocol.[133] 35 mg of compound **1** was dissolved in 1 ml of dry dichloromethane under argon atmosphere. Then 42 mg of DCC and 12.5 mg of DMAP was added to this solution. The solution was stirred for 10 min, then 15 mg of polymer **2** was added under argon and stirred for overnight at RT. All solvents were evaporated to dryness, then the resulting polymer **4** was dissolved in minimal amount of dichloromethane, precipitated in cold methanol, and dried in vacuum. Functionalization proceeded in good yield at 100% conversion. *Polymer 4 characterization:* ^{1}H *NMR:* ($CDCl_3$) δ 1.42-1.71 (bs, 6H), 4.58-4.97 (m, 4H), 5.05-5.25 (m, 2H), 5.5-5.7 (bs, 1H), 7.39-7.55 (bs, 2H), 7.55-7.65 (bs, 1H), 7.70-7.9 (bs, 4H), 8.05-8.25 (bs, 2H). *FT-IR*: ν = [1090, 1120, 1180, 1270, 1300, 1350, 1380, 1450, 1580, 1660, 1760, 2930, and 2980 cm^{-1}]. *Raman*: ν = [1440, 1610, 1660, 1730, 2865, 2943, 2983, 3067 cm^{-1}].

Functionalized poly-lactide derivative 5*:* Compound **3** (2-(cyclooct-2-yn-l-yloxy) acetic acid) has been synthesized according to the literature reported protocol.[134] 28 mg of compound **3** was dissolved in 1 ml of dry dichloromethane under dry argon atmosphere. Then 42 mg of DCC and 12.5 mg of DMAP was added to this solution. The solution was stirred for 10 min, then 15 mg of polymer **2** was added under argon and

stirred for overnight at RT. All solvents were evaporated to dryness, then the resulting polymer **5** was dissolved in minimal amount of dichloromethane, precipitated in cold methanol, and dried in vacuum. Functionalization proceeded in good yield at around 90% conversion. *Polymer 5 characterization:* ^{1}H *NMR* ($CDCl_3$) δ 0.9-1.4 (m, 8H), 1.45-1.95 (m, 4H), 1.95-2.1 (m, 1H), 2.1-2.2 (m, 2H), 2.2-2.3 (m, 1H), 4.05-4.25 (m, 2H), 4.33 – 4.42 (m, 1H), 4.5-4.95 (m, 4H), 5.11-5.25 (m, 2H), 5.4-5.6 (m, 1H). *FT-IR*: ν = [1100, 1130, 1190, 1200, 1240, 1350, 1380, 1400, 1450, 1770, 2920, and 2980 cm^{-1}]. *Raman*: ν = [1440, 1750, 2200, 2852, 2876, 2943, 2973 cm^{-1}].

Synthesis of Acrylate and Alkyne Functionalized PLGA (PLGA-acrylate-alkyne):

PLGA-OH (4.0 g, 0.49 mmol, $M_{n,theo}$= 8100 g/mol) was dissolved in 100 mL of THF. To this solution was added triethylamine (0.68 mL, 4.90 mol) and the reaction mixture was cooled to 0 ^{o}C. Acryloyl chloride (0.20 mL, 2.47 mmol) in 20 mL of THF was added dropwise over 30 min to this solution under nitrogen. The mixture was stirred at 0 ^{o}C for 1 h then overnight at room temperature under nitrogen atmosphere. The solvent was evaporated and the remaining viscous polymer was dissolved in $CHCl_3$ and precipitated into large amount of methanol. The dissolution-precipitation procedure was repeated two times. After decantation of methanol, remaining sticky polymer was dissolved in $CHCl_3$ and evaporated to dryness to give 3 g polymer as a pale yellow solid. The obtained polymer was immediately dissolved in 100 mL of CH_2Cl_2. To this solution were added 4-pentynoic acid (1.09 g, 0.011 mol) and DMAP (0.135 g, 1.11 mmol), respectively. After stirring 10 min at room temperature, DCC (2.27 g, 0.011 mol)

dissolved in 20 mL of CH_2Cl_2 was added to the mixture. Reaction mixture was stirred overnight at room temperature under nitrogen. Next, urea by-product was filtered and the solvent was removed by rotary evaporation. Remaining viscous polymer was dissolved in $CHCl_3$ and precipitated into large amount of methanol. The dissolution-precipitation procedure was repeated two times. After decantation of methanol, remaining sticky polymer was dissolved in $CHCl_3$ and evaporated to dryness to give the polymer as a light brown solid. Yield: 2.5 g (70%). $M_{n,GPC}$= 9600 g/mol, $M_w/M_{n=}$ 1.52 (based on PS standarts). ^{1}H NMR (400 MHz, $CDCl_3$, δ): ^{1}H NMR (400 MHz, $CDCl_3$, δ): 6.44 (d, CH_2=C*H*C=O), 6.11 (m, C*H*$_2$=CHC=O), 5.9 (d, C*H*$_2$=CHC=O), 5.4-5.3 (m, C*H*CH_2O), 5.2-5.0 (m, C=OC*H*CH_3O), 4.9-4.4 (m, CHC*H*$_2$OC=O and C=OC*H*$_2$OC=O), 2.8-2.4 (m, CH≡CC*H*$_2$C*H*$_2$C=O), 1.96 (s, C*H*≡CCH$_2$CH$_2$C=O), 1.7-1.5 (m, C=OCHC*H*$_3$O).

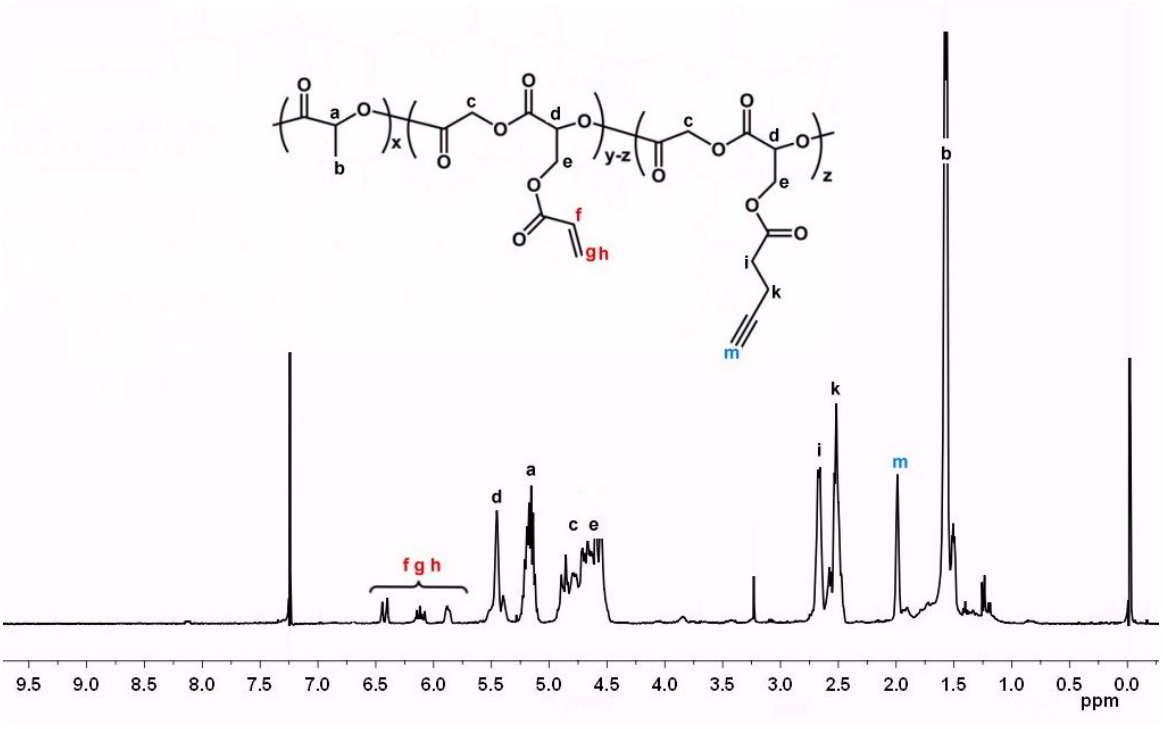

Figure 4. ^{1}H NMR spectrum of PLGA-acrylate-alkyne in $CDCl_3$ (400 MHz).

^{1}H NMR spectrum of PLGA- acrylate-alkyne is given in Figure 4, from ^{1}H NMR spectrum it is clear that methylene protons adjacent to hydroxyl between δ 4.2-3.8 ppm shifted to δ 4.5 ppm and acrylate protons can be seen between δ 6.5-5.8 ppm after esterification. In addition, methine proton next to triple bond at δ 1.96 ppm and methylene protons next to carbonyl between δ 2.8-2.4 ppm confirmed the structure. Besides, the mol percentages of acrylate and alkyne were found to be 16% and 84%, respectively from ^{1}H NMR.

References:

[1] M. Leemhuis, C. F. van Nostrum, J. A. W. Kruijtzer, Z. Y. Zhong, M. R. ten Breteler, P. J. Dijkstra, J. Feijen, W. E. Hennink, *Macromolecules* **2006**, *39*, 3500-3508.

[2] K. L. Kiick, E. Saxon, D. A. Tirrell, C. R. Bertozzi, *P Natl Acad Sci USA* **2002**, *99*, 19-24.

[3] M. S. Xu, M. Lukeman, P. Wan, *J Photoch Photobio A* **2009**, *204*, 52-62.

[4] N. J. Agard, J. M. Baskin, J. A. Prescher, A. Lo, C. R. Bertozzi, *Acs Chem Biol* **2006**, *1*, 644-648.

[5] S. Bhaskar, J. Hitt, S. W. L. Chang, J. Lahann, *Angew Chem Int Edit* **2009**, *48*, 4589-4593.

[6] K. J. Lee, J. Yoon, S. Rahmani, S. Hwang, S. Bhaskar, S. Mitragotri, J. Lahann, *P Natl Acad Sci USA* **2012**, *109*, 16057-16062.

Appendix B

Raman Spectroscopy Analysis

Appendix B-1: Full Raman spectra of polymer **4** containing compartment.

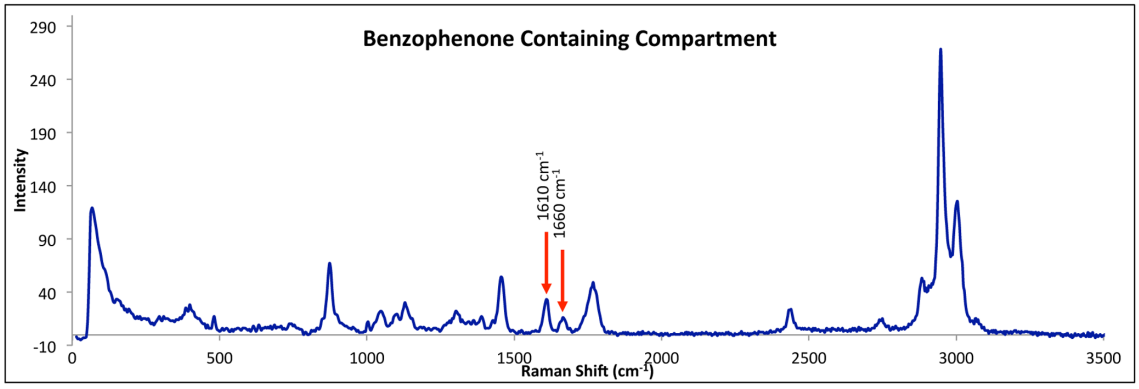

Appendix B-1: The full Raman spectra of the compartment containing polymer **4** and PLGA**.** Here, the 1610 and 1660 nm signals (shown with red arrows) signify the benzophenone functional groups present in this polymer.

Appendix B-2: Full Raman spectra of polymer **4** and **5** containing compartments

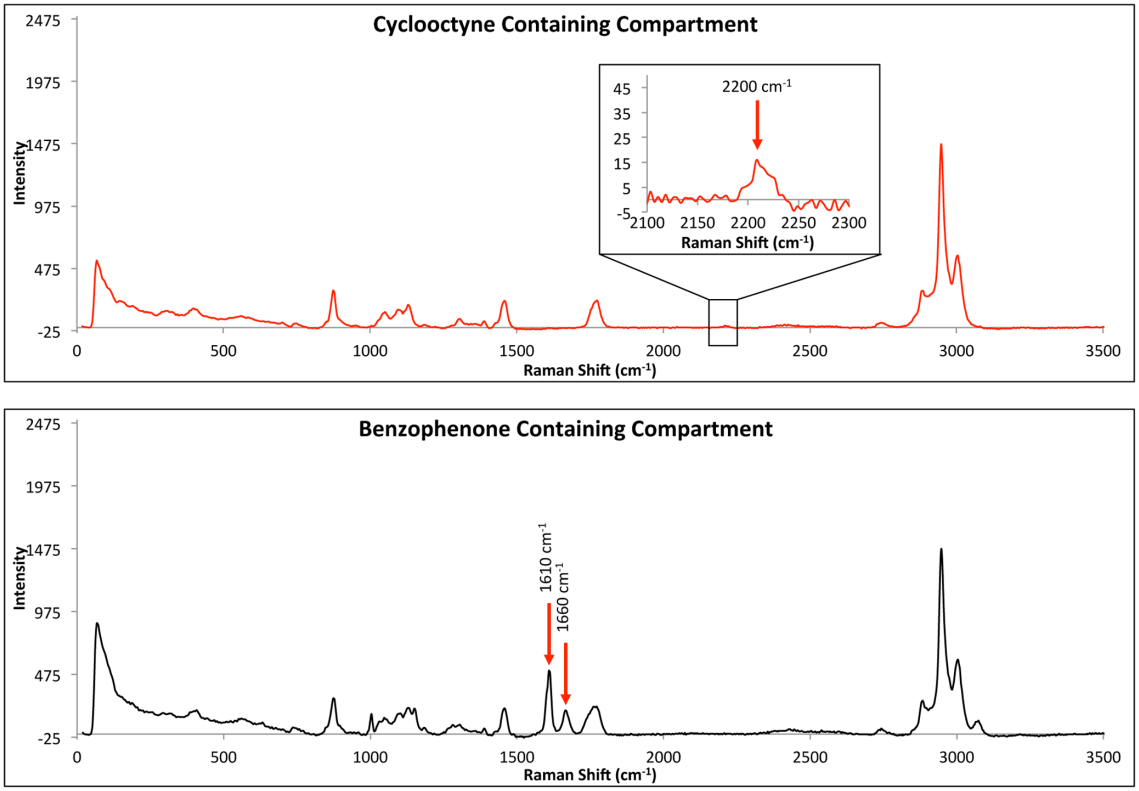

Appendix B-2 4: The full Raman spectra of the compartments containing polymer **4** or **5** in tricompartmental microparticles in **Figure 2-6.** Here, the top spectra is of the compartment containing polymer **5** and PLGA, with the appropriate signals at 2200 cm^{-1} for cyclooctyne, and the bottom spectra is of the compartment containing polymer **4** and PLGA, with the peaks at 1610 and 1660 cm^{-1} for benzophenone.

Appendix C

Synthesis and Characterization of Dual Functional Polymers

Characterization

^{1}H NMR and ^{13}C NMR spectra were recorded using a *Bruker* Avance III 500 spectrometer in $CDCl_3$ and DMSO-d_6. Working frequencies were 500 MHz for ^{1}H and 125 MHz for ^{13}C NMR. Infrared (IR) spectrum of compound **2** was recorded on *Bruker* Alpha spectrometer. The sample was measured as a pure compound using ATR-technique (ATR = Attenuated Total Reflection). Analysis of the polymer structures was undertaken with a *Thermo* Nicolet 6700 spectrometer with an 85° grazing angle and 128 scans for each sample at a resolution of 4 cm^{-1} or with *Bruker* Vertex 80 spectrometer, detector: LN2 cooled narrow band MCT with an 80° grazing angle and 1024 scans for each sample at a resolution of 2 cm^{-1}. Reference: deuterated 1-hexadecanethiol self-assembled monolayer on a gold wafer. Samples were prepared by spin coating of polymer solutions (in dry THF or chloroform) on gold wafers. Electron ionization (EI) mass spectra were recorded on a *Finnigan* MAT 95 spectrometer. Gel permeation chromatography (GPC) using THF as mobile phase was performed on a Toson EcoSEC GPC system with autosampler and a differential refractive index detector at 30 °C and at an elution rate of 1.0 mL/min. Three PSS SDV columns (100 Å, 5 μ, 8.0 x 300 mm 1000

Å, 5 µ, 8.0 x 300 mm and 100000 Å, 5 µ, 8.0 x 300 mm) were calibrated by linear polystyrene standards. GPC using DMAc with 0.03 w/w% LiBr as mobile phase was performed on *Polymer Laboratories* PL-GPC 50 Plus Integrated System with autosampler and a differential refractive index detector, at 50 °C with an elution rate of 1.0 mL/min. A *Polymer Laboratories* PLgel 5 µm bead-size guard column (7.5 × 50 mm) and three *Polymer Laboratories* PLgel 5 µm MixedC columns (7.5 × 300 mm) were calibrated by linear polystyrene standards.

The particles were visualized using a confocal laser scanning microscopy (CLSM) (*Olympus*, FluoView 500). For this purpose, the particles were deposited on a glass cover slip during the jetting process and a drop of water was placed on the cover slip. 405 nm laser, 488 nm argon laser, and 533 nm helium-neon green (HeNeG) laser were used to excite MEHPV, PTDPV, and TRITC, respectively. The barrier filters were set to 430–460 nm for MEHPV, 505–525 nm for PTDPV, and >560nm for TRITC. The particles were imaged using an *Amray* 1910 field emission scanning electron microscope (FE-SEM). To do this, the particles were suspended in water, deposited on silicon wafers and left to dry overnight, after which the wafers were sputter coated with gold and imaged. The confocal Raman microscopy images were obtained using *WITec* alpha 300R microscope utilizing 532 nm laser. To remove any remaining solvents particles were dried *in vacuo* overnight prior to measurements. Spectra were acquired using an integration time of 0.5 sec per pixel with image scan area of 100 pixels x 100 pixels.

(4-Nitrophenyl)methyl mercaptoacetate (2)

Thioglycolic acid (8.3 mL, 0.12 mol, 2 eq) and *o*-nitrobenzyl alcohol (9.18 g, 0.06 mol, 1 eq) were dissolved in toluene (90 mL) and concentrated sulfuric acid (0.3 mL) was added thereto. The reaction was refluxed for 2 days and solvent was removed *in vacuo*. The crude product was purified chromatographically on silica gel with hexane/ethyl acetate (4:1 v/v) mixture as eluent to yield 8.69 g (64%) of the title compound as a yellow liquid, which solidified after some time. ^{1}H NMR (500 MHz, $CDCl_3$): δ = 8.09 (dd, J = 8.3 Hz, J = 0.9 Hz, 1H, H_{Ar}), 7.69–7.60 (m, 2H, H_{Ar}), 7.49 (td, J = 8.3 Hz, J = 1.7 Hz, 1H, H_{Ar}), 5.55 (s, 2H, $ArCH_2O$), 3.34 (d, J = 8.4 Hz, 2H, $C\underline{H}_2SH$), 2.05 (t, J = 8.4 Hz, 1H, $CH_2S\underline{H}$) ppm; ^{13}C NMR (125 MHz, $CDCl_3$): δ = 170.3 (C=O), 147.5 (C_{Ar}), 133.9 (CH_{Ar}), 131.6 (C_{Ar}), 129.1 (2C, CH_{Ar}), 125.2 (CH_{Ar}), 63.9 ($Ar\underline{C}H_2O$), 26.4 ($\underline{C}H_2SH$) ppm; IR (Platinum ATR): υ = 3113, 2957, 2854, 2562, 1842, 1724, 1611, 1575, 1517, 1439, 1414, 1375, 1340, 1309, 1280, 1224, 1142, 1080, 1048, 1023, 979, 965, 936, 860, 795, 730, 671, 600, 587 cm^{-1}; HRMS (EI) *m/z* calculated for $C_9H_9NSO_4$ ($[M]^+$): 227.0252, found 227.0255.

Poly(allyl glycidyl ether) (1)

Polymerization was performed in flame dried Schlenk flasks under an argon atmosphere. Initiating alkoxide was prepared *in situ* from 2-methoxyethanol (23.6 µL, 0.3 mmol, 1 eq) and potassium naphthalenide in THF solution. Complete formation of 2-methoxyethanolate was indicated by the maintenance of the solution's green color. Allyl glycidyl ether (3.5 mL, 0.03 mol, 100 eq) was introduced into the reaction vessel with a gastight syringe and the reaction was stirred for 72 h at 30°C. Polymerization was terminated by the addition of acidified methanol and solvent was removed *in vacuo*.

Monomer conversion was 98% as calculated based on ^{1}H NMR spectrum of crude polymer. The crude polymer was purified chromatographically on a silica gel column with gradient elution (chloroform to chloroform/methanol 10:0.7 v/v mixture as an eluent) yielding 3.35 g (98%) of slightly yellow oil. GPC (THF): M_n 11600 g/mol, M_w 13100 g/mol, PDI 1.12. ^{1}H NMR (500 MHz, $CDCl_3$): δ = 5.93–5.82 (m, 1H, C<u>H</u>=CH_2), 5.25 (d, 1H, CH=C<u>H</u>$_2$), 5.14 (d, 1H, CH=C<u>H</u>$_2$), 3.98 (d, 2H, OC<u>H</u>$_2$CH=CH_2), 3.67–3.43 (m, 5H, $CH_{2\text{-PEG}}$ + CH_{PEG} + CH_{PEG}C<u>H</u>$_2$O), 3.36 (s, 3H, CH_3O) ppm; ^{13}C NMR (125 MHz, $CDCl_3$): δ = 135.1 (CH_2=<u>C</u>H), 116.9 (<u>C</u>H_2=CH), 79.0–78.8 (CH_{PEG}), 72.4 (O<u>C</u>H_2CH=CH_2), 70.4–69.9 (2C, $CH_{2\text{-PEG}}$ + CH_{PEG}<u>C</u>H_2O), 59.2 (CH_3O).

o-Nitrobenzyl poly(ethylene glycol) (10)

Purified polymer **1** (0.8 g, 7 mmol of C=C, 1 eq) was dissolved in 3 ml of dry THF under an argon atmosphere, **2** (4.9 g, 22 mmol, 3 eq) and AIBN (0.178 g, 1.1 mmol, 0.15 eq) were added thereto and the reaction was refluxed for 5 h. Completion of the reaction was confirmed by ^{1}H NMR spectrometry by the disappearance of allyl group signal. The solvent was removed *in vacuo* and the residue was purified on a silica gel column with gradient elution (chloroform to chloroform/methanol 10:0.7 v/v mixture as an eluent) to yield 1.71 g (72%) of the title polymer as a yellow viscous oil. GPC (DMAc): M_n 22100 g/mol, M_w 27500 g/mol, PDI 1.24. ^{1}H NMR (500 MHz, $CDCl_3$): δ = 8.07 (d, 1H, H_{Ar}), 7.68–7.62 (m, 2H, H_{Ar}), 7.52–7.45 (m, 1H, H_{Ar}), 5.52 (s, 2H, $ArCH_2O$), 3.70–3.35 (m, 7H, $CH_{2\text{-PEG}}$ + CH_{PEG} + CH_{PEG}C<u>H</u>$_2$O + OC<u>H</u>$_2$CH$_2$), 3.28 (s, 2H, SCH_2C=O), 2.68 (t, 2H, SC<u>H</u>$_2$CH$_2$), 1.82 (m, 2H, CH_2C<u>H</u>$_2$CH$_2$) ppm; ^{13}C NMR (125 MHz, $CDCl_3$): δ = 169.9 (C=O), 147.6 (C_{Ar}), 134.1 (CH_{Ar}), 132.0 (C_{Ar}), 129.2 (CH_{Ar}), 129.1 (CH_{Ar}), 125.2 (CH_{Ar}), 79.2–78.4 (CH_{PEG}), 71.4–70.8 ($CH_{2\text{-PEG}}$), 70.3–70.0 (CH_{PEG}<u>C</u>H_2O), 69.7 (O<u>C</u>H_2CH$_2$),

63.6 (Ar<u>C</u>H_2O), 33.4 (S<u>C</u>H_2C=O), 29.5 (S<u>C</u>H_2CH_2), 29.1 (CH_2<u>C</u>H_2CH_2) ppm; IR (spin coated film on a gold wafer): υ = 2922, 2868, 1741, 1614, 1579, 1530, 1448, 1373, 1346, 1272, 1132, 1007, 860 cm^{-1}.

Oxidized o-Nitrobenzyl poly(ethylene glycol) (11)

Polymer **3** (M_n 22100 g/mol, 150 mg, 0.44 mmol of thioether groups, 1 eq) was dissolved in 6 ml of acetic acid and 2 ml of acetonitrile and cooled down to 0 °C. Next, hydrogen peroxide solution (30%, 0.4 ml, 3.9 mmol, 9 eq) was added thereto dropwise and the reaction was stirred at 0 °C for 6 h. The reaction was slowly poured into 5% sodium bicarbonate solution, extracted with dichloromethane, dried over anhydrous sodium sulfate, filtered and concentrated *in vacuo* to yield 147 mg (94%) of the title polymer as a yellow viscous oil. GPC (DMAc): M_n 26100 g/mol, M_w 34200 g/mol, PDI 1.31. ^{1}H NMR (500 MHz, $CDCl_3$): δ = 8.07 (d, 1H, H_{Ar}), 7.71–7.62 (m, 2H, H_{Ar}), 7.47 (m, 1H, H_{Ar}), 5.57 (s, 2H, ArCH_2O), 3.81 (dd, 2H, SCH_2C=O), 3.70–3.40 (m, 7H, $CH_{2\text{-PEG}}$ + CH_{PEG} + CH_{PEG}C<u>H</u>$_2$O + OC<u>H</u>$_2CH_2$), 2.96 (m, 2H, SC<u>H</u>$_2CH_2$), 2.0 (m, 2H, CH_2C<u>H</u>$_2CH_2$) ppm; ^{13}C NMR (125 MHz, $CDCl_3$): δ = 165.2 (C=O), 147.4 (C_{Ar}), 134.3 (CH_{Ar}), 131.2 (C_{Ar}), 129.6 (CH_{Ar}), 129.3 (CH_{Ar}), 125.2 (CH_{Ar}), 79.0–78.5 (CH_{PEG}), 71.1–70.8 ($CH_{2\text{-PEG}}$), 70.2–69.9 (CH_{PEG}<u>C</u>H_2O), 69.7 (O<u>C</u>H_2CH_2), 64.4 (Ar<u>C</u>H_2O), 55.8 (O=S<u>C</u>H_2C=O), 49.9 (O=S<u>C</u>H_2CH_2), 23.2 (CH_2<u>C</u>H_2CH_2) ppm; IR (spin coated film on a gold wafer): υ = 3243, 2924, 2870, 2375, 1742, 1653, 1613, 1578, 1530, 1447, 1374, 1346, 1276, 1121, 1057, 860 cm^{-1}.

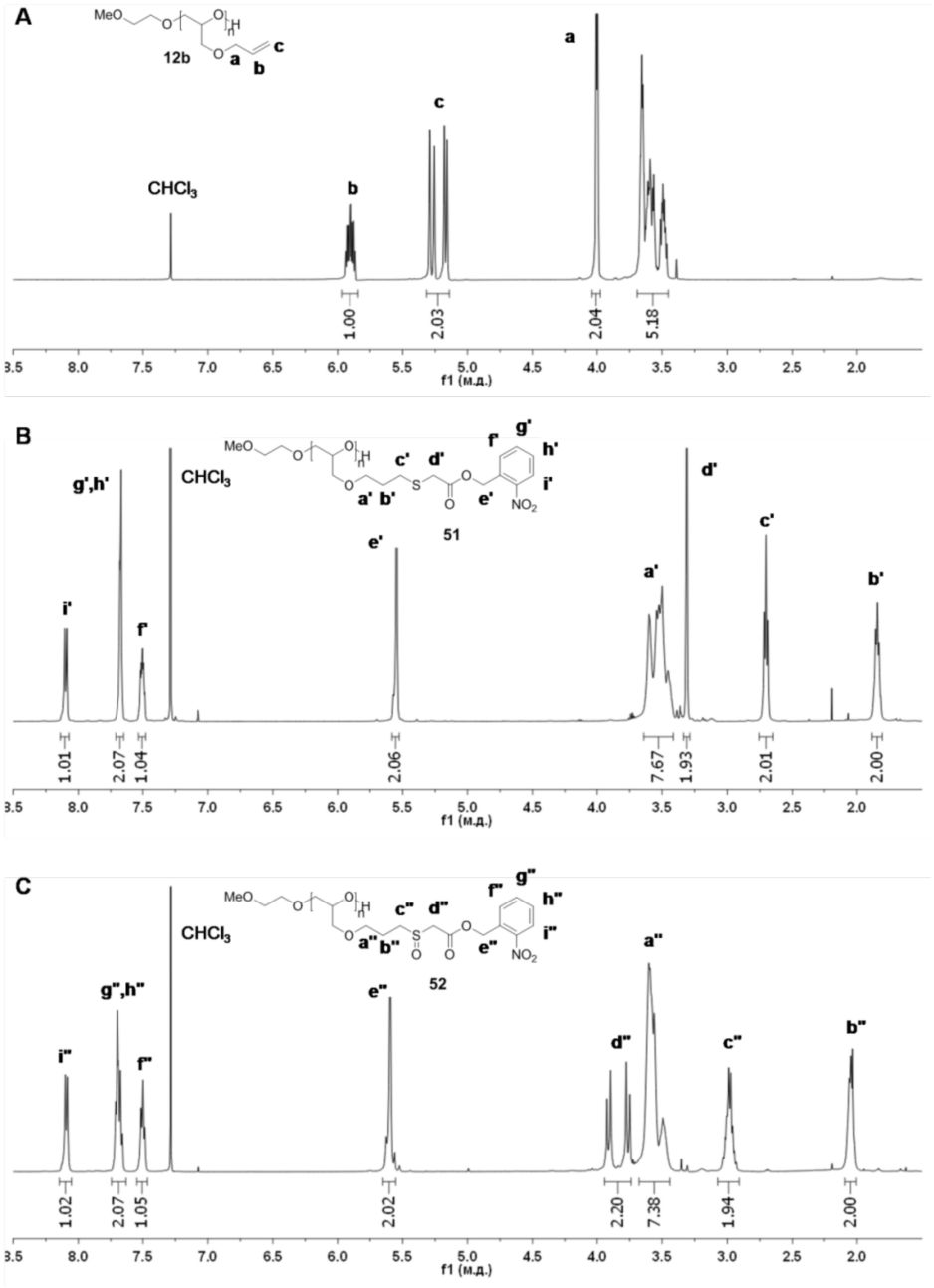

Figure Appendix C-1. Comparative ^{1}H NMR spectra of polymers **1** (A), **10** (B) and **11** (C). Solvent $CDCl_3$.

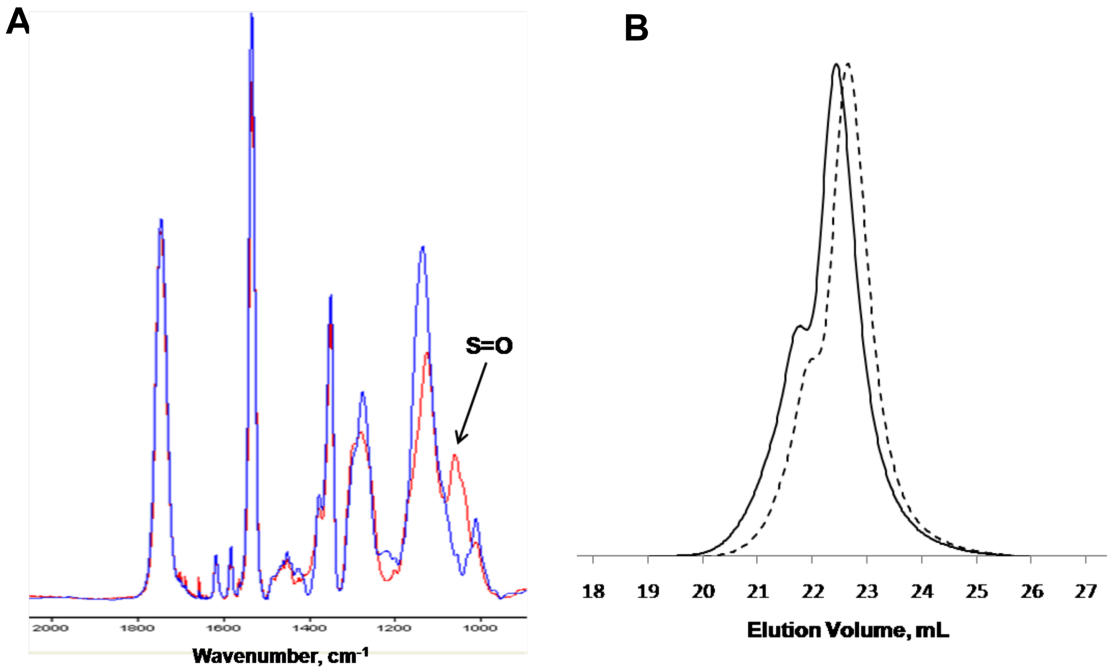

Figure Appendix C-2. Comparative IR spectra of polymers **10** (blue line) and **11** (red line) (A) and their gel permeation chromatograms (polymer **10** (dashed line), polymer **11** (solid line)) (B).

Appendix D

Experimental Procedures for Cochlear Analysis

In vivo infusion: Surgeries were conducted in a sterile environment and utilized aseptic technique. For *in vivo* infusions, Hartley guinea pigs (Charles River Laboratory, Wilmington, MA) were anesthetized and a post auricular approach was used to provide access to the middle ear. The temporal bone was drilled to visualize the cochlea and a fine pick was used to create a small hole in the basal turn of the cochlea near the round window. A micro-cannula with a silastic ball was inserted 0.5mm into the basal turn of the scala tympani and cyanoacrylate was used to seal the cannula in place as outlined previously (Prieskorn & Miller, 2000). The microcannula was made from polyethylene 10 (PE10) tubing and polyimide (I.D. = 0.12 mm, O.D. =0.16 mm, # 049, MicroLumen, Tampa, FL, USA). The silastic ball was made from Sylgard (Dow Corning,Midland, MI). A syringe infusion pump (Harvard Apparatus, Holliston, Maine) was used to deliver particles into the scala tympani at a flow rate of 1 μl/minute over 5 minutes. Infusions were always performed on the left ear and the right ear was used as needed for a contralateral control. All animal procedures had been approved by the University Committee for the Use and Care of Animals.

Harvesting, cryoprotection, and decalcification of cochlear specimens: Guinea pigs were anesthetized and euthanized by injection of sodium pentobarbital (FatalPlus; Vortech Pharmaceuticals, Dearborn, MI). In all cases, secondary euthanasia was performed by transecting the aorta and the ventricle. Animals were then decapitated and

the temporal bones that encase the cochleae were detached. Excess bullar bone was removed to facilitate visualization of each cochlea and then the middle ear bones were also detached. Specimens were fixed in 4% paraformaldehyde for 1-2 hours. Following fixation, cochleae were decalcified in a solution that was two-thirds formic acid (Immunocal; Decal Chemical Corporation,Tallman, NY) and one-third 7% sucrose overnight. Prior to freezing, specimens were placed in aluminum containers and immersed in a 30% sucrose solution. Freezing was performed by placing the bottom of the container in contact with liquid nitrogen cooled 2-methyl-butane (Fisher Scientific, Pittsburgh, PA). Specimens were wrapped in parafilm and stored at -80°C until sectioning.

Cryostat Sectioning: Samples were cut into 14 μm sections. Slides were generated for each animal and samples of the same representative depths from each animal were assessed to ascertain particle persistence and distribution. For immunohistochemistry, up to 4 midmodiolar sections were taken from the MP infused cochlea of each animal. These sections were stained with CD45, a leukocyte antigen, to denote immune cell activity, and propidium iodide to indicate the presence of more general cell structures such as nuclei. Cryosections of the liver of one of the guinea pigs were also made for use as positive and negative (in the absence of primary antibody) controls.

Infused particle number and persistence: A sample of the particle solution was counted before the infusions using a hemacytometer. Persistence and distribution assessments were conducted using cryosections from cochleae that had particle infusions 7 days prior

to harvest of the cochlea (n=3 for each timepoint). Sections from various depths of the cochlea were sampled for particle number. The guinea pig cochlea consists of four turns with 2 perilymphatic compartments, the scala tympani and scala vestibule. During assessment the location of particles within cochlear cross sections was noted and their distribution within the cochlea determined.

Auditory Brainstem Response (ABR): Animals were anesthetized with xylazine (10 mg/kg intramuscularly) and ketamine (40 mg/kg intramuscularly). Needle electrodes (active, reference, and ground) were inserted subcutaneously at the vertex and below each pinna and used to record the neurologic response. Up to 1024 responses were averaged for each stimulus level, with the stimulus consisting of a 15-msec tone burst, provided at 10/sec. Pure tones were delivered via a transducer coupled to the external auditory canal at 4, 8, and 20 kHz. Initial sound levels were set at 80 dB for pre- and post- infusion tests. Threshold determination was based on the visual detection of maximum peak–peak amplitude of the resulting waveforms. ABRs were given prior to infusion to enable exclusion of animals with abnormal hearing, and to enable detection, if present, of threshold shifts post infusion.

Hair cell counts: To prepare specimens for hair cell analysis, ears were harvested in the same manner as those used for cryosection preparation with a few notable differences. Following removal of the middle ear bones, the apex was visualized under stereoscopic magnification and slightly perforated with a 28G needle to create a small hole. Then the round window was opened and approximately 300 μL of 4% PFA was infused directly

into the cochlea via the hole in the apex. Specimens were postfixed by immersion in 4% PFA overnight. The following day, cochleae were rinsed and the otic capsule, lateral wall, and tectorial membrane were carefully removed. Phalloidin was used to stain the modiolous and the attached organ of Corti. Following rinsing to remove excess stain, the organ of Corti was dissected from the modiolous and each turn was mounted onto a microscope slide and coverslipped. Phalloidin staining of the organ of Corti enabled visualization and counting of both inner and outer hair cells (as indicated by the presence of nuclei and/or stereocillia). The counts were performed as described in [Schacht, 2012] Counts were then plotted using Cytogram, a custom software, and presented as percentage hair cell loss at a particular distance from the apex as compared to a database of normal guinea pigs (those not exposed to any external stimuli or agents that could induce hearing loss). The tracking of distance along the cochlear spiral also facilitated the correlation of areas of loss with known frequency maps of the guinea pig cochlea. This provided insight on areas that may be functionally affected by the treatment.

REFERENCES

1. Bertrand, N. & Leroux, J.C. The journey of a drug-carrier in the body: An anatomo-physiological perspective. *J Control Release* **161**, 152-163 (2012).
2. Sun, T.M. et al. Engineered Nanoparticles for Drug Delivery in Cancer Therapy. *Angew Chem Int Edit* **53**, 12320-12364 (2014).
3. Lee, K.J. et al. Compartmentalized Photoreactions within Compositionally Anisotropic Janus Microstructures. *Macromolecular Rapid Communications* **32**, 431-437 (2011).
4. Peer, D. et al. Nanocarriers as an emerging platform for cancer therapy. *Nat Nanotechnol* **2**, 751-760 (2007).
5. Morachis, J.M., Mahmoud, E.A. & Almutairi, A. Physical and Chemical Strategies for Therapeutic Delivery by Using Polymeric Nanoparticles. *Pharmacol Rev* **64**, 505-519 (2012).
6. Pearce, T.R., Shroff, K. & Kokkoli, E. Peptide Targeted Lipid Nanoparticles for Anticancer Drug Delivery. *Adv Mater* **24**, 3803-3822 (2012).
7. Shapira, A., Livney, Y.D., Broxterman, H.J. & Assaraf, Y.G. Nanomedicine for targeted cancer therapy: Towards the overcoming of drug resistance. *Drug Resist Update* **14**, 150-163 (2011).
8. Allen, T.M. Ligand-targeted therapeutics in anticancer therapy. *Nat Rev Cancer* **2**, 750-763 (2002).
9. Hauert, S. & Bhatia, S.N. Mechanisms of cooperation in cancer nanomedicine: towards systems nanotechnology. *Trends Biotechnol* **32**, 448-455 (2014).

10. Barreto, J.A. et al. Nanomaterials: Applications in Cancer Imaging and Therapy. *Adv Mater* **23**, H18-H40 (2011).

11. Quaglia, F. Bioinspired tissue engineering: The great promise of protein delivery technologies. *Int J Pharmaceut* **364**, 281-297 (2008).

12. Duncan, R. The dawning era of polymer therapeutics. *Nat Rev Drug Discov* **2**, 347-360 (2003).

13. Langer, R. & Tirrell, D.A. Designing materials for biology and medicine. *Nature* **428**, 487-492 (2004).

14. Ferrari, M. Cancer nanotechnology: Opportunities and challenges. *Nat Rev Cancer* **5**, 161-171 (2005).

15. Loomis, K., McNeeley, K. & Bellamkonda, R.V. Nanoparticles with targeting, triggered release, and imaging functionality for cancer applications. *Soft Matter* **7**, 839-856 (2011).

16. Xie, J., Lee, S. & Chen, X.Y. Nanoparticle-based theranostic agents. *Adv Drug Deliver Rev* **62**, 1064-1079 (2010).

17. Allen, T.M. & Cullis, P.R. Drug delivery systems: Entering the mainstream. *Science* **303**, 1818-1822 (2004).

18. Heidel, J.D. & Davis, M.E. Clinical Developments in Nanotechnology for Cancer Therapy. *Pharm Res-Dordr* **28**, 187-199 (2011).

19. Soundararajan, V., Warnock, K. & Sasisekharan, R. Multifunctional Nanoscale Platforms for Targeting of the Cancer Cell Immortality Spectrum. *Macromol Rapid Comm* **31**, 202-216 (2010).

20. S. Jiang, S.G. Janus Particle Synthesis, Self-Assembly, and Applications. *RSC Publishing, London* (2012).

21. Grzelczak, M., Vermant, J., Furst, E.M. & Liz-Marzan, L.M. Directed Self-Assembly of Nanoparticles. *Acs Nano* **4**, 3591-3605 (2010).

22. Glotzer, S.C., Solomon, M.J. & Kotov, N.A. Self-assembly: From nanoscale to microscale colloids. *Aiche J* **50**, 2978-2985 (2004).

23. Park, T.H. & Lahann, J. Janus Particles with Distinct Compartments via Electrohydrodynamic Co-jetting. *Janus Particle Synthesis, Self-Assembly and Applications*, 54-73 (2012).

24. Glotzer, S.C. & Solomon, M.J. Anisotropy of building blocks and their assembly into complex structures. *Nat Mater* **6**, 557-562 (2007).

25. Yang, S.M., Kim, S.H., Lim, J.M. & Yi, G.R. Synthesis and assembly of structured colloidal particles. *J Mater Chem* **18**, 2177-2190 (2008).

26. Walther, A. & Muller, A.H.E. Janus particles. *Soft Matter* **4**, 663-668 (2008).

27. Mitragotri, S. & Lahann, J. Physical approaches to biomaterial design. *Nature Materials* **8**, 15-23 (2009).

28. Dendukuri, D. & Doyle, P.S. The Synthesis and Assembly of Polymeric Microparticles Using Microfluidics. *Adv Mater* **21**, 4071-4086 (2009).

29. Yoon, J., Lee, K.J. & Lahann, J. Multifunctional polymer particles with distinct compartments. *Journal of Materials Chemistry* **21**, 8502-8510 (2011).

30. Lee, K.J., Yoon, J. & Lahann, J. Recent advances with anisotropic particles. *Current Opinion in Colloid & Interface Science* **16**, 195-202 (2011).

31. Lee, K.J. & Lahann, J. Preparation of shape-switching colloids using electrohydrodynamic co-jetting. *Abstr Pap Am Chem S* **242** (2011).

32. Sacanna, S., Irvine, W.T.M., Chaikin, P.M. & Pine, D.J. Lock and key colloids. *Nature* **464**, 575-578 (2010).

33. Chen, Q. et al. Supracolloidal Reaction Kinetics of Janus Spheres. *Science* **331**, 199-202 (2011).

34. Chen, Q., Bae, S.C. & Granick, S. Directed self-assembly of a colloidal kagome lattice. *Nature* **469**, 381-384 (2011).

35. Pregibon, D.C., Toner, M. & Doyle, P.S. Multifunctional encoded particles for high-throughput biomolecule analysis. *Science* **315**, 1393-1396 (2007).

36. Sengupta, S. et al. Temporal targeting of tumour cells and neovasculature with a nanoscale delivery system. *Nature* **436**, 568-572 (2005).

37. Yoshida, M. et al. Structurally Controlled Bio-hybrid Materials Based on Unidirectional Association of Anisotropic Microparticles with Human Endothelial Cells. *Adv Mater* **21**, 4920-+ (2009).

38. Kim, J. et al. Programming magnetic anisotropy in polymeric microactuators. *Nat Mater* **10**, 747-752 (2011).

39. Higuchi, T., Tajima, A., Motoyoshi, K., Yabu, H. & Shimomura, M. Frustrated Phases of Block Copolymers in Nanoparticles. *Angew Chem Int Edit* **47**, 8044-8046 (2008).

40. Yoon, J., Kota, A., Bhaskar, S., Tuteja, A. & Lahann, J. Amphiphilic Colloidal Surfactants Based on Electrohydrodynamic Cojetting. *Acs Appl Mater Inter* **5**, 11281-11287 (2013).

41. Rahmani, S., Park, T.H., Dishman, A.F. & Lahann, J. Multimodal delivery of irinotecan from microparticles with two distinct compartments. *J Control Release* **172**, 239-245 (2013).

42. Park, T.H. et al. Photoswitchable Particles for On-Demand Degradation and Triggered Release. *Small* **9**, 3051-3057 (2013).

43. Misra, A.C., Bhaskar, S., Clay, N. & Lahann, J. Multicompartmental Particles for Combined Imaging and siRNA Delivery. *Advanced Materials* **24**, 3850-3856 (2012).

44. Chou, T.C. Theoretical basis, experimental design, and computerized simulation of synergism and antagonism in drug combination studies. *Pharmacol Rev* **58**, 621-681 (2006).

45. Pelicano, H. et al. Targeting Hsp90 by 17-AAG in leukemia cells: mechanisms for synergistic and antagonistic drug combinations with arsenic trioxide and Ara-C. *Leukemia* **20**, 610-619 (2006).

46. Jia, J. et al. Mechanisms of drug combinations: interaction and network perspectives. *Nat Rev Drug Discov* **8**, 111-128 (2009).

47. Kim, J.W., Larsen, R.J. & Weitz, D.A. Synthesis of nonspherical colloidal particles with anisotropic properties. *J Am Chem Soc* **128**, 14374-14377 (2006).

48. Walther, A., Andre, X., Drechsler, M., Abetz, V. & Muller, A.H.E. Janus discs. *J Am Chem Soc* **129**, 6187-6198 (2007).

49. Kraft, D.J. et al. Patchy Polymer Colloids with Tunable Anisotropy Dimensions. *J Phys Chem B* **115**, 7175-7181 (2011).

50. Rolland, J.P. et al. Direct fabrication and harvesting of monodisperse, shape-specific nanobiomaterials. *J Am Chem Soc* **127**, 10096-10100 (2005).

51. Badaire, S., Cottin-Bizonne, C., Woody, J.W. & Stroock, A.D. COLL 294-Shape selectivity in the assembly of lithographically-designed particles. *Abstr Pap Am Chem S* **232** (2006).

52. Merkel, T.J. et al. Scalable, Shape-Specific, Top-Down Fabrication Methods for the Synthesis of Engineered Colloidal Particles. *Langmuir* **26**, 13086-13096 (2010).

53. Nisisako, T., Torii, T., Takahashi, T. & Takizawa, Y. Synthesis of monodisperse bicolored janus particles with electrical anisotropy using a microfluidic co-flow system. *Adv Mater* **18**, 1152-+ (2006).

54. Chen, C.H., Abate, A.R., Lee, D.Y., Terentjev, E.M. & Weitz, D.A. Microfluidic Assembly of Magnetic Hydrogel Particles with Uniformly Anisotropic Structure. *Adv Mater* **21**, 3201-+ (2009).

55. Bong, K.W., Bong, K.T., Pregibon, D.C. & Doyle, P.S. Hydrodynamic Focusing Lithography. *Angew Chem Int Edit* **49**, 87-90 (2010).

56. Greiner, A. & Wendorff, J.H. Electrospinning: A fascinating method for the preparation of ultrathin fibres. *Angew Chem Int Edit* **46**, 5670-5703 (2007).

57. Lv, W.P. et al. A Facile Route Towards Inorganic Particles with Two Distinct Compartments Based on Electro-Hydrodynamic Co-Jetting. *Part Part Syst Char* **30**, 936-939 (2013).

58. Lv, W.P. et al. Anisotropic Janus Catalysts for Spatially Controlled Chemical Reactions. *Small* **8**, 3116-3122 (2012).

59. Gupta, P. & Wilkes, G.L. Some investigations on the fiber formation by utilizing a side-by-side bicomponent electrospinning approach. *Polymer* **44**, 6353-6359 (2003).

60. Loscertales, I.G. et al. Micro/nano encapsutation via electrified coaxial liquid jets. *Science* **295**, 1695-1698 (2002).

61. Larsen, G., Velarde-Ortiz, R., Minchow, K., Barrero, A. & Loscertales, I.G. A method for making inorganic and hybrid (organic/inorganic) fibers and vesicles with diameters in the submicrometer and micrometer range via sol-gel chemistry and electrically forced liquid jets. *J Am Chem Soc* **125**, 1154-1155 (2003).

62. Loscertales, I.G. et al. Electrically forced coaxial nanojets for one-step hollow nanofiber design. *J Am Chem Soc* **126**, 5376-5377 (2004).

63. Sun, Z.C., Zussman, E., Yarin, A.L., Wendorff, J.H. & Greiner, A. Compound core-shell polymer nanofibers by co-electrospinning. *Adv Mater* **15**, 1929-+ (2003).

64. Roh, K.H., Martin, D.C. & Lahann, J. Biphasic Janus particles with nanoscale anisotropy. *Nat Mater* **4**, 759-763 (2005).

65. Roh, K.H., Yoshida, M. & Lahann, J. Water-stable biphasic nanocolloids with potential use as anisotropic imaging probes. *Langmuir* **23**, 5683-5688 (2007).

66. Bhaskar, S., Roh, K.H., Jiang, X.W., Baker, G.L. & Lahann, J. Spatioselective Modification of Bicompartmental Polymer Particles and Fibers via Huisgen 1,3-Dipolar Cycloaddition. *Macromol Rapid Comm* **29**, 1655-1660 (2008).

67. Mandal, S., Bhaskar, S. & Lahann, J. Micropatterned Fiber Scaffolds for Spatially Controlled Cell Adhesion. *Macromolecular Rapid Communications* **30**, 1638-1644 (2009).

68. Bhaskar, S., Pollock, K.M., Yoshida, M. & Lahann, J. Towards Designer Microparticles: Simultaneous Control of Anisotropy, Shape, and Size. *Small* **6**, 404-411 (2010).

69. Roh, K.H., Martin, D.C. & Lahann, J. Triphasic nanocolloids. *J Am Chem Soc* **128**, 6796-6797 (2006).

70. Bhaskar, S., Pollock, K.M., Yoshida, M., Roh, K.H. & Lahann, J. COLL 307-Multicompartmental biodegradable microparticles via electrohydrodynamic co-jetting: Control over shape, anisotropy, and surface chemistry. *Abstr Pap Am Chem S* **238** (2009).

71. Bhaskar, S., Hitt, J., Chang, S.W.L. & Lahann, J. Multicompartmental Microcylinders. *Angewandte Chemie-International Edition* **48**, 4589-4593 (2009).

72. Bhaskar, S. et al. Engineering, Characterization and Directional Self-Assembly of Anisotropically Modified Nanocolloids. *Small* **7**, 812-819 (2011).

73. Lee, K.J. et al. Spontaneous shape reconfigurations in multicompartmental microcylinders. *P Natl Acad Sci USA* **109**, 16057-16062 (2012).

74. de las Heras, D., Tavares, J.M. & da Gama, M.M.T. Bicontinuous and mixed gels in binary mixtures of patchy colloidal particles. *Soft Matter* **8**, 1785-1794 (2012).

75. Russo, J., Tartaglia, P. & Sciortino, F. Reversible gels of patchy particles: Role of the valence. *J Chem Phys* **131** (2009).

76. Doppelbauer, G., Bianchi, E. & Kahl, G. Self-assembly scenarios of patchy colloidal particles in two dimensions. *J Phys-Condens Mat* **22** (2010).

77. Yi, G.R., Pine, D.J. & Sacanna, S. Recent progress on patchy colloids and their self-assembly. *J Phys-Condens Mat* **25** (2013).

78. Pawar, A.B. & Kretzschmar, I. Fabrication, Assembly, and Application of Patchy Particles. *Macromol Rapid Comm* **31**, 150-168 (2010).

79. Hermans, T.M. et al. Self-assembly of soft nanoparticles with tunable patchiness. *Nat Nanotechnol* **4**, 721-726 (2009).

80. Jones, M.R. et al. DNA-nanoparticle superlattices formed from anisotropic building blocks. *Nat Mater* **9**, 913-917 (2010).

81. Rodriguez-Fernandez, D. & Liz-Marzan, L.M. Metallic Janus and Patchy Particles. *Part Part Syst Char* **30**, 46-60 (2013).

82. Nel, A.E. et al. Understanding biophysicochemical interactions at the nano-bio interface. *Nat Mater* **8**, 543-557 (2009).

83. Udit, A.K. et al. Heparin Antagonism by Polyvalent Display of Cationic Motifs on Virus-Like Particles. *Chembiochem* **10**, 503-510 (2009).

84. Schmidt, R.C. & Healy, K.E. Controlling biological interfaces on the nanometer length scale. *J Biomed Mater Res A* **90A**, 1252-1261 (2009).

85. Torres, A.J., Wu, M., Holowka, D. & Baird, B. Nanobiotechnology and cell biology: Micro- and nanofabricated surfaces to investigate receptor-mediated signaling. *Annu Rev Biophys* **37**, 265-288 (2008).

86. Alves, N.M., Pashkuleva, I., Reis, R.L. & Mano, J.F. Controlling Cell Behavior Through the Design of Polymer Surfaces. *Small* **6**, 2208-2220 (2010).

87. Ross, A.M., Jiang, Z.X., Bastmeyer, M. & Lahann, J. Physical Aspects of Cell Culture Substrates: Topography, Roughness, and Elasticity. *Small* **8**, 336-355 (2012).

88. Zheng, W.F., Zhang, W. & Jiang, X.Y. Precise Control of Cell Adhesion by Combination of Surface Chemistry and Soft Lithography. *Adv Healthc Mater* **2**, 95-108 (2013).

89. Jiang, X.W., Chen, H.Y., Galvan, G., Yoshida, M. & Lahann, J. Vapor-based initiator coatings for atom transfer radical polymerization. *Adv Funct Mater* **18**, 27-35 (2008).

90. Pontani, L.L., Haase, M.F., Raczkowska, I. & Brujic, J. Immiscible lipids control the morphology of patchy emulsions. *Soft Matter* **9**, 7150-7157 (2013).

91. Walker, D.A., Leitsch, E.K., Nap, R.J., Szleifer, I. & Grzybowski, B.A. Geometric curvature controls the chemical patchiness and self-assembly of nanoparticles. *Nat Nanotechnol* **8**, 676-681 (2013).

92. Shah, A.A., Schultz, B., Kohlstedt, K.L., Glotzer, S.C. & Solomon, M.J. Synthesis, Assembly, and Image Analysis of Spheroidal Patchy Particles. *Langmuir* **29**, 4688-4696 (2013).

93. Zhang, Z.L. & Glotzer, S.C. Self-assembly of patchy particles. *Nano Lett* **4**, 1407-1413 (2004).

94. Sacanna, S. et al. Shaping colloids for self-assembly. *Nat Commun* **4** (2013).

95. Scotchford, C.A. et al. Chemically patterned, metal-oxide-based surfaces produced by photolithographic techniques for studying protein- and cell-

interactions. II: Protein adsorption and early cell interactions. *Biomaterials* **24**, 1147-1158 (2003).

96. Kim, M. et al. Addressable Micropatterning of Multiple Proteins and Cells by Microscope Projection Photolithography Based on a Protein Friendly Photoresist. *Langmuir* **26**, 12112-12118 (2010).

97. Lee, K.J., Park, T.H., Hwang, S., Yoon, J. & Lahann, J. Janus-Core and Shell Microfibers. *Langmuir* **29**, 6181-6186 (2013).

98. Kaufmann, T. et al. Chemically orthogonal trifunctional Janus beads by photochemical "sandwich" microcontact printing. *Chem Commun* **49**, 63-65 (2013).

99. Kaufmann, T. et al. Bifunctional Janus beads made by "sandwich" microcontact printing using click chemistry. *J Mater Chem* **22**, 6190-6199 (2012).

100. Perry, J.L. et al. PEGylated PRINT Nanoparticles: The Impact of PEG Density on Protein Binding, Macrophage Association, Biodistribution, and Pharmacokinetics. *Nano Lett* **12**, 5304-5310 (2012).

101. Nie, Z.H., Li, W., Seo, M., Xu, S.Q. & Kumacheva, E. Janus and ternary particles generated by microfluidic synthesis: Design, synthesis, and self-assembly. *J Am Chem Soc* **128**, 9408-9412 (2006).

102. Rycenga, M., Langille, M.R., Personick, M.L., Ozel, T. & Mirkin, C.A. Chemically Isolating Hot Spots on Concave Nanocubes. *Nano Lett* **12**, 6218-6222 (2012).

103. Zhou, T., Wang, B.B., Dong, B. & Li, C.Y. Thermoresponsive Amphiphilic Janus Silica Nanoparticles via Combining "Polymer Single-Crystal Templating" and "Grafting-from" Methods. *Macromolecules* **45**, 8780-8789 (2012).

104. Wang, B.B., Dong, B., Li, B., Zhao, B. & Li, C.Y. Janus gold nanoparticle with bicompartment polymer brushes templated by polymer single crystals. *Polymer* **51**, 4814-4822 (2010).

105. Chen, R.T. et al. Fabrication of asymmetric "Janus" particles via plasma polymerization. *Chem Commun* **46**, 5121-5123 (2010).

106. Tang, J.L., Schoenwald, K., Potter, D., White, D. & Sulchek, T. Bifunctional Janus Microparticles with Spatially Segregated Proteins. *Langmuir* **28**, 10033-10039 (2012).

107. Jiang, S. & Granick, S. A simple method to produce trivalent colloidal particles. *Langmuir* **25**, 8915-8918 (2009).

108. Eriksson, K., Johansson, L., Gothelid, E., Nyholm, L. & Oscarsson, S. Manufacturing of anisotropic particles by site specific oxidation of thiols. *J Mater Chem* **22**, 7681-7683 (2012).

109. Saha, S. et al. Chemically Controlled Bending of Compositionally Anisotropic Microcylinders. *Angewandte Chemie-International Edition* **51**, 660-665 (2012).

110. Yoshida, M., Roh, K.H. & Lahann, J. Short-term biocompatibility of biphasic nanocolloids with potential use as anisotropic imaging probes. *Biomaterials* **28**, 2446-2456 (2007).

111. Zhang, J., Wang, X.J., Wu, D.X., Liu, L. & Zhao, H.Y. Bioconjugated Janus Particles Prepared by in Situ Click Chemistry. *Chem Mater* **21**, 4012-4018 (2009).

112. Zhang, J., Jin, J. & Zhao, H.Y. Surface-Initiated Free Radical Polymerization at the Liquid-Liquid Interface: A One-Step Approach for the Synthesis of Amphiphilic Janus Silica Particles. *Langmuir* **25**, 6431-6437 (2009).

113. Cho, Y.S. et al. Particles with coordinated patches or windows from oil-in-water emulsions. *Chem Mater* **19**, 3183-3193 (2007).

114. Deng, X.P. & Lahann, J. A Generic Strategy for Co-Presentation of Heparin-Binding Growth Factors Based on CVD Polymerization. *Macromol Rapid Comm* **33**, 1459-1465 (2012).

115. Deng, X.P., Eyster, T.W., Elkasabi, Y. & Lahann, J. Bio-Orthogonal Polymer Coatings for Co-Presentation of Biomolecules. *Macromol Rapid Comm* **33**, 640-645 (2012).

116. Elkasabi, Y., Yoshida, M., Nandivada, H., Chen, H.Y. & Lahann, J. Towards multipotent coatings: Chemical vapor deposition and biofunctionalization of carbonyl-substituted copolymers. *Macromol Rapid Comm* **29**, 855-870 (2008).

117. Elkasabi, Y., Chen, H.Y. & Lahann, J. Multipotent polymer coatings based on chemical vapor deposition copolymerization. *Adv Mater* **18**, 1521-+ (2006).

118. Jung, C.Y. et al. One-pot synthesis and surface modifications of organically modified silica (ORMOSIL) particles having multiple functional groups. *J Colloid Interf Sci* **367**, 67-73 (2012).

119. Nicolas, J., Mura, S., Brambilla, D., Mackiewicz, N. & Couvreur, P. Design, functionalization strategies and biomedical applications of targeted biodegradable/biocompatible polymer-based nanocarriers for drug delivery. *Chem Soc Rev* **42**, 1147-1235 (2013).

120. Petrie, T.A., Stanley, B.T. & Garcia, A.J. Micropatterned surfaces with controlled ligand tethering. *J Biomed Mater Res A* **90A**, 755-765 (2009).

121. Chan, E.W.L. & Yousaf, M.N. Immobilization of ligands with precise control of density to electroactive surfaces. *J Am Chem Soc* **128**, 15542-15546 (2006).

122. Jiang, S. & Granick, S. A Simple Method to Produce Trivalent Colloidal Particles. *Langmuir* **25**, 8915-8918 (2009).

123. Sletten, E.M. & Bertozzi, C.R. Bioorthogonal Chemistry: Fishing for Selectivity in a Sea of Functionality. *Angew Chem Int Edit* **48**, 6974-6998 (2009).

124. Bertozzi, C.R. Guest Editorial a Decade of Bioorthogonal Chemistry. *Accounts Chem Res* **44**, 651-653 (2011).

125. Sletten, E.M. & Bertozzi, C.R. From Mechanism to Mouse: A Tale of Two Bioorthogonal Reactions. *Accounts Chem Res* **44**, 666-676 (2011).

126. Nandivada, H., Jiang, X.W. & Lahann, J. Click chemistry: Versatility and control in the hands of materials scientists. *Adv Mater* **19**, 2197-2208 (2007).

127. Lahann, J. Click chemistry for biotechnology and materials science. (Wiley, Chichester, West Sussex; 2009).

128. Deng, X.P., Friedmann, C. & Lahann, J. Bio-orthogonal "Double-Click" Chemistry Based on Multifunctional Coatings. *Angewandte Chemie-International Edition* **50**, 6522-6526 (2011).

129. Wang, Y. et al. Patchy particle self-assembly via metal coordination. *J Am Chem Soc* **135**, 14064-14067 (2013).

130. Groschel, A.H. et al. Facile, solution-based synthesis of soft, nanoscale Janus particles with tunable Janus balance. *J Am Chem Soc* **134**, 13850-13860 (2012).

131. Groschel, A.H. et al. Precise hierarchical self-assembly of multicompartment micelles. *Nat Commun* **3**, 710 (2012).

132. Kamalasanan, K. et al. Patchy, anisotropic microspheres with soft protein islets. *Angew Chem Int Ed Engl* **50**, 8706-8708 (2011).

133. Feng, L., Dreyfus, R., Sha, R.J., Seeman, N.C. & Chaikin, P.M. DNA Patchy Particles. *Adv Mater* **25**, 2779-2783 (2013).

134. Wang, Y.F. et al. Colloids with valence and specific directional bonding. *Nature* **491**, 51-U61 (2012).

135. Sudimack, J. & Lee, R.J. Targeted drug delivery via the folate receptor. *Adv Drug Deliver Rev* **41**, 147-162 (2000).

136. Sugahara, K.N. et al. Coadministration of a Tumor-Penetrating Peptide Enhances the Efficacy of Cancer Drugs. *Science* **328**, 1031-1035 (2010).

137. Cheng, Z.L., Al Zaki, A., Hui, J.Z., Muzykantov, V.R. & Tsourkas, A. Multifunctional Nanoparticles: Cost Versus Benefit of Adding Targeting and Imaging Capabilities. *Science* **338**, 903-910 (2012).

138. Moghimi, S.M., Hunter, A.C. & Andresen, T.L. Factors Controlling Nanoparticle Pharmacokinetics: An Integrated Analysis and Perspective. *Annu Rev Pharmacol* **52**, 481-503 (2012).

139. Champion, J.A. & Mitragotri, S. Role of target geometry in phagocytosis. *P Natl Acad Sci USA* **103**, 4930-4934 (2006).

140. Champion, J.A., Katare, Y.K. & Mitragotri, S. Particle shape: A new design parameter for micro- and nanoscale drug delivery carriers. *J Control Release* **121**, 3-9 (2007).

141. Bachelder, E.M., Beaudette, T.T., Broaders, K.E., Dashe, J. & Frechet, J.M.J. Acetal-derivatized dextran: An acid-responsive biodegradable material for therapeutic applications. *J Am Chem Soc* **130**, 10494-+ (2008).

142. Simone, E.A. et al. Endothelial targeting of polymeric nanoparticles stably labeled with the PET imaging radioisotope iodine-124. *Biomaterials* **33**, 5406-5413 (2012).

143. Montdargent, B. & Letourneur, D. Toward new biomaterials. *Infect Cont Hosp Ep* **21**, 404-410 (2000).

144. Baldwin, A.D. & Kiick, K.L. Polysaccharide-Modified Synthetic Polymeric Biomaterials. *Biopolymers* **94**, 128-140 (2010).

145. Cohen, J.A. et al. Acetal-Modified Dextran Microparticles with Controlled Degradation Kinetics and Surface Functionality for Gene Delivery in Phagocytic and Non-Phagocytic Cells. *Adv Mater* **22**, 3593-+ (2010).

146. Broaders, K.E., Cohen, J.A., Beaudette, T.T., Bachelder, E.M. & Frechet, J.M.J. Acetalated dextran is a chemically and biologically tunable material for particulate immunotherapy. *P Natl Acad Sci USA* **106**, 5497-5502 (2009).

147. Mahmoud, E.A., Sankaranarayanan, J., Morachis, J.M., Kim, G. & Almutairi, A. Inflammation Responsive Logic Gate Nanoparticles for the Delivery of Proteins. *Bioconjugate Chem* **22**, 1416-1421 (2011).

148. Gao, W.W., Chan, J.M. & Farokhzad, O.C. pH-Responsive Nanoparticles for Drug Delivery. *Mol Pharmaceut* **7**, 1913-1920 (2010).

149. Yang, Y. et al. Development of highly porous large PLGA microparticles for pulmonary drug delivery. *Biomaterials* **30**, 1947-1953 (2009).

150. Impellitteri, N.A., Toepke, M.W., Levengood, S.K.L. & Murphy, W.L. Specific VEGF sequestering and release using peptide-functionalized hydrogel microspheres. *Biomaterials* **33**, 3475-3484 (2012).

151. Duncanson, W.J. et al. Targeted binding of PLA microparticles with lipid-PEG-tethered ligands. *Biomaterials* **28**, 4991-4999 (2007).

152. Sill, T.J. & von Recum, H.A. Electro spinning: Applications in drug delivery and tissue engineering. *Biomaterials* **29**, 1989-2006 (2008).

153. Hinterwirth, H. et al. Quantifying Thiol Ligand Density of Self-Assembled Monolayers on Gold Nanoparticles by Inductively Coupled Plasma-Mass Spectrometry. *Acs Nano* **7**, 1129-1136 (2013).

154. H. Liu, T.L.D., Y. Cheng, F. Lu, S. Srinivasan, J.-J. Zhu, C. Burda Control of surface ligand density of PEGylated gold nanoparticles for optimized cancer cell uptake. *Part Part Syst Char* (2014).

155. Li, Y.P. et al. PEGylated PLGA nanoparticles as protein carriers: synthesis, preparation and biodistribution in rats. *J Control Release* **71**, 203-211 (2001).

156. Peppas, N.A., Hilt, J.Z., Khademhosseini, A. & Langer, R. Hydrogels in biology and medicine: From molecular principles to bionanotechnology. *Adv Mater* **18**, 1345-1360 (2006).

157. Ling, V. Multidrug resistance: Molecular mechanisms and clinical relevance. *Cancer Chemoth Pharm* **40**, S3-S8 (1997).

158. Livingston, D.M. & Silver, D.P. Cancer - Crossing over to drug resistance. *Nature* **451**, 1066-1067 (2008).

159. Devalapally, H., Duan, Z.F., Seiden, M.V. & Amiji, M.M. Modulation of drug resistance in ovarian adenocarcinoma by enhancing intracellular ceramide using tamoxifen-loaded biodegradable polymeric nanoparticles. *Clin Cancer Res* **14**, 3193-3203 (2008).

160. Zimmermann, G.R., Lehar, J. & Keith, C.T. Multi-target therapeutics: when the whole is greater than the sum of the parts. *Drug Discov Today* **12**, 34-42 (2007).

161. Tran, M.A., Smith, C.D., Kester, M. & Robertson, G.P. Combining nanoliposomal ceramide with sorafenib synergistically inhibits melanoma and breast cancer cell survival to decrease tumor development. *Clin Cancer Res* **14**, 3571-3581 (2008).

162. Colson, Y.L. & Grinstaff, M.W. Biologically Responsive Polymeric Nanoparticles for Drug Delivery. *Adv Mater* **24**, 3878-3886 (2012).

163. Kost, J. & Langer, R. Responsive polymeric delivery systems. *Adv Drug Deliver Rev* **46**, 125-148 (2001).

164. Esser-Kahn, A.P., Odom, S.A., Sottos, N.R., White, S.R. & Moore, J.S. Triggered Release from Polymer Capsules. *Macromolecules* **44**, 5539-5553 (2011).

165. Motornov, M., Roiter, Y., Tokarev, I. & Minko, S. Stimuli-responsive nanoparticles, nanogels and capsules for integrated multifunctional intelligent systems. *Prog Polym Sci* **35**, 174-211 (2010).

166. Saltzman, W.M. & Langer, R. Transport Rates of Proteins in Porous Materials with Known Microgeometry. *Biophys J* **55**, 163-171 (1989).

167. Rothstein, S.N. & Little, S.R. A "tool box" for rational design of degradable controlled release formulations. *J Mater Chem* **21**, 29-39 (2011).

168. Siegel, R.A., Kost, J. & Langer, R. Mechanistic Studies of Macromolecular Drug Release from Macroporous Polymers .1. Experiments and Preliminary Theory Concerning Completeness of Drug Release. *J Control Release* **8**, 223-236 (1989).

169. Yoshida, M. & Lahann, J. Smart nanomaterials. *Acs Nano* **2**, 1101-1107 (2008).

170. Stuart, M.A.C. et al. Emerging applications of stimuli-responsive polymer materials. *Nat Mater* **9**, 101-113 (2010).

171. Sun, A. & Lahann, J. Dynamically switchable biointerfaces. *Soft Matter* **5**, 1555-1561 (2009).

172. Nandivada, H., Ross, A.M. & Lahann, J. Stimuli-responsive monolayers for biotechnology. *Prog Polym Sci* **35**, 141-154 (2010).

173. Tomatsu, I., Peng, K. & Kros, A. Photoresponsive hydrogels for biomedical applications. *Adv Drug Deliver Rev* **63**, 1257-1266 (2011).

174. Li, Y.Y. et al. Stimulus-responsive polymeric nanoparticles for biomedical applications. *Sci China Chem* **53**, 447-457 (2010).

175. Mayer, G. & Heckel, A. Biologically active molecules with a "light switch". *Angew Chem Int Edit* **45**, 4900-4921 (2006).

176. Roy, D., Cambre, J.N. & Sumerlin, B.S. Future perspectives and recent advances in stimuli-responsive materials. *Prog Polym Sci* **35**, 278-301 (2010).

177. Kim, J. & Hayward, R.C. Mimicking dynamic in vivo environments with stimuli-responsive materials for cell culture. *Trends Biotechnol* **30**, 426-439 (2012).

178. Pelliccioli, A.P. & Wirz, J. Photoremovable protecting groups: reaction mechanisms and applications. *Photoch Photobio Sci* **1**, 441-458 (2002).

179. Yu, H.T., Li, J.B., Wu, D.D., Qiu, Z.J. & Zhang, Y. Chemistry and biological applications of photo-labile organic molecules. *Chem Soc Rev* **39**, 464-473 (2010).

180. Zhao, H., Sterner, E.S., Coughlin, E.B. & Theato, P. o-Nitrobenzyl Alcohol Derivatives: Opportunities in Polymer and Materials Science. *Macromolecules* **45**, 1723-1736 (2012).

181. Pillai, V.N.R. Photo-Removable Protecting Groups in Organic-Synthesis. *Synthesis-Stuttgart*, 1-26 (1980).

182. Reuter, S., Gupta, S.C., Chaturvedi, M.M. & Aggarwal, B.B. Oxidative stress, inflammation, and cancer How are they linked? *Free Radical Bio Med* **49**, 1603-1616 (2010).

183. Kondo, T., Hirose, M. & Kageyama, K. Roles of Oxidative Stress and Redox Regulation in Atherosclerosis. *J Atheroscler Thromb* **16**, 532-538 (2009).

184. Barnham, K.J., Masters, C.L. & Bush, A.I. Neurodegenerative diseases and oxidative stress. *Nat Rev Drug Discov* **3**, 205-214 (2004).

185. Tsutsui, H., Kinugawa, S. & Matsushima, S. Oxidative stress and heart failure. *Am J Physiol-Heart C* **301**, H2181-H2190 (2011).

186. Giustarini, D., Dalle-Donne, I., Tsikas, D. & Rossi, R. Oxidative stress and human diseases: Origin, link, measurement, mechanisms, and biomarkers. *Crit Rev Cl Lab Sci* **46**, 241-281 (2009).

187. Vo, C.D., Kilcher, G. & Tirelli, N. Polymers and Sulfur: what are Organic Polysulfides Good For? Preparative Strategies and Biological Applications. *Macromol Rapid Comm* **30**, 299-315 (2009).

188. Yui, N., Okano, T. & Sakurai, Y. Inflammation Responsive Degradation of Cross-Linked Hyaluronic-Acid Gels. *J Control Release* **22**, 105-116 (1992).

189. Pasut, G. & Veronese, F.M. PEG conjugates in clinical development or use as anticancer agents: An overview. *Adv Drug Deliver Rev* **61**, 1177-1188 (2009).

190. Zhang, F., Kang, E.T., Neoh, K.G., Wang, P. & Tan, K.L. Surface modification of stainless steel by grafting of poly(ethylene glycol) for reduction in protein adsorption. *Biomaterials* **22**, 1541-1548 (2001).

191. Bjugstad, K.B., Lampe, K., Kern, D.S. & Mahoney, M. Biocompatibility of poly(ethylene glycol)-based hydrogels in the brain: An analysis of the glial response across space and time. *J Biomed Mater Res A* **95A**, 79-91 (2010).

192. Mangold, C., Wurm, F. & Frey, H. Functional PEG-based polymers with reactive groups via anionic ROP of tailor-made epoxides. *Polym Chem-Uk* **3**, 1714-1721 (2012).

193. Li, Z.Y. & Chau, Y. Synthesis of Linear Polyether Polyol Derivatives As New Materials for Bioconjugation. *Bioconjugate Chem* **20**, 780-789 (2009).

194. Donahue, A., Dubno, J.R. & Beck, L. Guest Editorial: Accessible and Affordable Hearing Health Care for Adults with Mild to Moderate Hearing Loss. *Ear Hearing* **31**, 2-6 (2010).

195. Altschuler, R.A. et al. Protection and Repair of Audition. *Principles of Tissue Engineering, 3rd Edition*, 995-1008 (2007).

196. Raphael, Y. & Altschuler, R.A. Structure and innervation of the cochlea. *Brain Res Bull* **60**, 397-422 (2003).

197. Henderson, D., Bielefeld, E.C., Harris, K.C. & Hu, B.H. The role of oxidative stress in noise-induced hearing loss. *Ear Hearing* **27**, 1-19 (2006).

198. Ylikoski, J., Liang, X.Q., Virkkala, J. & Pirvola, U. Blockade of c-Jun N-terminal kinase pathway attenuates gentamicin-induced cochlear and vestibular hair cell death. *Hearing Res* **166**, 33-43 (2002).

199. Kawamoto, K. et al. Antioxidant gene therapy can protect hearing and hair cells from ototoxicity. *Mol Ther* **9**, 173-181 (2004).

200. Song, B.B., Anderson, D.J. & Schacht, J. Protection from gentamicin ototoxicity by iron chelators in guinea pig in vivo. *J Pharmacol Exp Ther* **282**, 369-377 (1997).

201. Sha, S.H., Qiu, J.H. & Schacht, J. Aspirin to prevent gentamicin-induced hearing loss. *New Engl J Med* **354**, 1856-1857 (2006).

202. Seidman, M.D., Shivapuja, B.G. & Quirk, W.S. The Protective Effects of Allopurinol and Superoxide-Dismutase on Noise-Induced Cochlear Damage. *Otolaryng Head Neck* **109**, 1052-1056 (1993).

203. Yamasoba, T., Schacht, J., Shoji, F. & Miller, J.M. Attenuation of cochlear damage from noise trauma by an iron chelator, a free radical scavenger and glial cell line-derived neurotrophic factor in vivo. *Brain Res* **815**, 317-325 (1999).

204. Pourbakht, A. & Yamasoba, T. Ebselen attenuates cochlear damage caused by acoustic trauma. *Hearing Res* **181**, 100-108 (2003).

205. Kopke, R.D. et al. Reduction of noise-induced hearing loss using L-NAC and salicylate in the chinchilla. *Hearing Res* **149**, 138-146 (2000).

206. Mikuriya, T. et al. Geranylgeranylacetone, a heat shock protein inducer, prevents acoustic injury in the guinea pig. *Brain Res* **1065**, 107-114 (2005).

207. Altschuler, R.A. et al. Rescue and regrowth of sensory nerves following deafferentation by neurotrophic factors. *Ann Ny Acad Sci* **884**, 305-311 (1999).

208. Shoji, F. et al. Glial cell line-derived neurotrophic factor has a dose dependent influence on noise-induced hearing loss in the guinea pig cochlea. *Hearing Res* **142**, 41-55 (2000).

209. Yagi, M. et al. Spiral ganglion neurons are protected from degeneration by GDNF gene therapy. *Jaro* **1**, 315-325 (2000).

210. Shoji, F. et al. Differential protective effects of neurotrophins in the attenuation of noise-induced hair cell loss. *Hearing Res* **146**, 134-142 (2000).

211. Yamagata, T. et al. Delayed neurotrophic treatment preserves nerve survival and electrophysiological responsiveness in neomycin-deafened guinea pigs. *J Neurosci Res* **78**, 75-86 (2004).

212. Probst, F.J. et al. Correction of deafness in shaker-2 mice by an unconventional myosin in a BAC transgene. *Science* **280**, 1444-1447 (1998).

213. Izumikawa, M. et al. Auditory hair cell replacement and hearing improvement by Atoh1 gene therapy in deaf mammals. *Nat Med* **11**, 271-276 (2005).

214. Sage, C. et al. Proliferation of functional hair cells in vivo in the absence of the retinoblastoma protein. *Science* **307**, 1114-1118 (2005).

215. Gantz, B.J., Turner, C., Gfeller, K.E. & Lowder, M.W. Preservation of hearing in cochlear implant surgery: Advantages of combined electrical and acoustical speech processing. *Laryngoscope* **115**, 796-802 (2005).

216. Blessington, A. et al. The effects of low-dose gamma irradiation and storage time on carotenoids, antioxidant activity, and phenolics in the potato cultivar Atlantic. *Am J Potato Res* **84**, 125-131 (2007).

217. Eshraghi, A.A. & van de Water, T.R. Cochlear implantation trauma and noise-induced hearing loss: Apoptosis and therapeutic strategies. *Anat Rec Part A* **288A**, 473-481 (2006).

218. Kanzaki, S. et al. Glial cell line-derived neurotrophic factor and chronic electrical stimulation prevent VIII cranial nerve degeneration following denervation. *J Comp Neurol* **454**, 350-360 (2002).

219. Sinha, V.R. & Trehan, A. Biodegradable microspheres for protein delivery. *J Control Release* **90**, 261-280 (2003).

220. Chung, H.J., Kim, H.K., Yoon, J.J. & Park, T.G. Heparin immobilized porous PLGA microspheres for angiogenic growth factor delivery. *Pharm Res-Dordr* **23**, 1835-1841 (2006).

221. Cho, M., Lee, Y., Choi, W., Chung, H.M. & Yoon, J. Study on Fe(VI) species as a disinfectant: Quantitative evaluation and modeling for inactivating Escherichia coli. *Water Res* **40**, 3580-3586 (2006).

222. Almodovar, J., Bacon, S., Gogolski, J., Kisiday, J.D. & Kipper, M.J. Polysaccharide-Based Polyelectrolyte Multi layer Surface Coatings can Enhance Mesenchymal Stem Cell Response to Adsorbed Growth Factors. *Biomacromolecules* **11**, 2629-2639 (2010).

223. Tan, J. et al. Nanoporous Peptide Particles for Encapsulating and Releasing Neurotrophic Factors in an Animal Model of Neurodegeneration. *Adv Mater* **24**, 3362-3366 (2012).

224. Nagrath, S. et al. Isolation of rare circulating tumour cells in cancer patients by microchip technology. *Nature* **450**, 1235-U1210 (2007).

225. Went, P.T. et al. Frequent EpCam protein expression in human carcinomas. *Hum Pathol* **35**, 122-128 (2004).

226. Balzar, M., Winter, M.J., de Boer, C.J. & Litvinov, S.V. The biology of the 17-1A antigen (Ep-CAM). *J Mol Med-Jmm* **77**, 699-712 (1999).